12-2015

A 3D Biomechanical Model for Analysis of Upper Jaw Protrusion in Carassius Auratus (Goldfish)

Seldon Tenzin Tselung
txs9649@rit.edu

z

A 3D BIOMECHANICAL MODEL FOR ANALYSIS OF UPPER JAW PROTRUSION IN CARASSIUS AURATUS (GOLDFISH)

By: Seldon Tenzin Tselung

Advisor: Dr. Steven W. Day

Department of Mechanical Engineering

Kate Gleason College of Engineering

Rochester Institute of Technology

IN PARTIAL FULFILLMENT OF THE REQUIREMENT FOR THE DEGREE OF MASTER OF SCIENCE IN MECHANICAL ENGINEERING

DECEMBER, 2015

A 3D BIOMECHANICAL MODEL FOR ANALYSIS OF UPPER JAW PROTRUSION IN CARASSIUS AURATUS (GOLDFISH)

By: Seldon Tenzin Tselung

A Thesis Submitted in Partial Fulfillment of the Requirements of the Degree of Master of Science in Mechanical Engineering

Committee Approval:

Dr. Steven W. Day
Thesis Advisor
Department of Mechanical Engineering, Rochester Institute of Technology

---

Dr. Agamemnon Crassidis
Department Representative, Thesis Committee Member
Department of Mechanical Engineering, Rochester Institute of Technology

---

Dr. L. Patricia Hernandez
Thesis Committee Member
Department of Biological Sciences, the George Washington University

---

Dr. Mario W. Gomes
Thesis Committee Member
Department of Mechanical Engineering, Rochester Institute of Technology

ACKNOWLEDGEMENTS

I thank my academic and thesis advisor Dr. Steven W. Day for giving me the opportunity to choose my own research topic and gain research experience under his guidance. I am grateful for his patience and support throughout this project. I thank Dr. L. Patricia Hernandez for giving me the opportunity to work with her and for being ever so co-operative and helpful with sharing her expertise. This project would not have been possible without her. I thank the rest of my thesis committee and mechanical engineering office staff members for all their help and co-operation. I thank MSC Software's support team for all their help. Last but not least, I would like to thank my family members for their unconditional love and support.

DEDICATION

This work is dedicated to the scientific community and those interested in this subject.

ABSTRACT

This thesis studies upper jaw protrusion in carassius auratus (goldfish), a type of Cypriniformes. The presence of a unique sesamoid bone called kinethmoid, suspended by a network of ligaments, allows for more flexibility and longer periods of sustained suction flow speeds in Cypriniformes. Previous researchers used XROMM software to visualize highly accurate (±0.1 mm) re-animations of a carp's 3D bones in vivo and EMG graphs to visualize muscle activation patterns. Based on those results, this thesis takes a reverse approach by building a working 3D model of a goldfish's mouth and simulating it using Adams, a multibody dynamics software program. Since all buccal (mouth) parts act in synchrony during each feeding session, this simulation process allows us to vary one parameter at a time and observe how changes in each parameter affect the overall feeding process. Individual bone measurements taken in the lab were translated into a 3D model using Solidworks. The model consisted of five main bones, two maxillary muscles, A1α and A1β; and a network of ligaments that were modelled as linear springs. Four parameters were tested against mouth opening results. They were A1α, A1β, initial kinethmoid position and initial dentary position. The initial position of the dentary was a primary influence in opening the mouth regardless of the amount of A1 maxillary forces applied. At a minimum dentary angle of 49°, the mouth opened for as little as 1 dyne of A1β force. Also, increasing values of A1β as opposed to changing kinethmoid's starting position had a greater effect on dentary rotation. A1α was the main driver in rotating the kinethmoid while increasing initial kinethmoid position from 130° to 150° increased the total rotational displacement of the kinethmoid by about 45°. All angles are measured counterclockwise to the part's anteroposterior axis. Both actions led to protruding the premaxilla forward and opening of the mouth. The

kinematic patterns were on par with past experimental results, thereby validating the approach taken to creating a realistic 3D model.

TABLE OF CONTENTS

LIST OF FIGURES

LIST OF TABLES

NOMENCLATURE

pmx	Premaxilla
max	Maxilla
pal-ncr	Palatine-neurocranium
dent	Dentary
kin	Kinethmoid
sub-max	Submaxillary
EMG	Electromyography
TTPG	Time to peak gape
DOF	Degrees of freedom
com	Center of mass

GLOSSARY

Anteroposterior	axis running from the anterior to the posterior end of a fish
Cypriniformes:	order of ray-finned fish that possesses a kinethmoid, but lack teeth. They have pharyngeal teeth in the throat.
Gape:	the width of the mouth when opened, as of birds, fishes, etc.
Hyoid:	a horseshoe-shaped bone that supports the tongue and related structures
Kinethmoid:	small median unpaired dermal sesamoid bone.
Operculum:	flap that covers, supports and protects the gill opening in many fishes.
Perciformes:	largest order of ray-finned fish that makes up about 41% of all bony fish. It is also highly diverse containing over 10,000 species.
Teleost:	a class of ray-finned fish that possesses a moving maxilla and premaxilla. They protrude their jaws outwards from the mouth to catch their prey.

CHAPTER 1

1.0 INTRODUCTION

1.1 General

With today's efficient and powerful software programs, making dynamical models of multi-body systems is very practical. Researchers or designers may use models to analyze behavior provided the model is acceptably accurate. The objective of this thesis is to use a commercially available multi-body dynamics software program called AdamsView, typically used for industrial mechanical design and analysis, to model and investigate a complex 3D biomechanical system. Specifically, the thesis presents a functional 3D dynamical model of the buccal system in goldfish. Key anatomical features are included so that the effect of variations of these (initial kinethmoid position, initial dentary position, muscle inputs) on kinematics can be studied. The purpose of this thesis is two-fold.

First, to study Goldfish's mouth opening through this model. The importance of studying the suction feeding process in fish lies in the understanding of the adaptation process of a species' morphological structures to its natural habitat. This process is the primary mode of feeding in ray-finned fishes and previous studies have aimed at calculating the mechanical advantage of the lower jaw system, which was then related to suction performance (Wainwright et al., 2007). Cypriniformes exhibit two types of upper jaw protrusion, namely, open mouth protrusion and closed mouth protrusion. Cypriniformes also exhibit more flexibility when compared to other fish groups lacking a kinethmoid. Flexibility is defined as the ability of an organism to alter its behavior across experimental treatments and the cause of inflexibility could be either mechanical limitations imposed by the anatomy of the fish or regulations taking place at the neural level (Wainwright et al., 2008). In the case of Cypriniformes, a special group of ray-finned fishes

characterized by their possession of a unique sesamoid bone called kinethmoid; the mechanics of the suction feeding process is more complex. This complexity could be responsible for more flexibility and longer periods of sustained flow speeds in Cypriniformes as noticed in goldfish and carp (Staab et al., 2012b). A biomechanical model of upper jaw protrusion in goldfish might help us better understand the mechanics of suction feeding process in Cypriniformes and the purpose behind this complex morphological arrangement.

The second purpose of this thesis is to establish this 3D model as a viable model for complex biological systems. It will allow future researchers to compare similarities and differences between different types of cypriniform fishes and draw performance relations based on various parameters.

1.2 Literature Search

Feeding is essential to animals for survival. Suction feeding is the feeding mode for Teleosts. This particular group of ray finned fishes possesses a moving maxilla and premaxilla as shown in Figure 1. Suction feeding involves rapid cranial expansion that brings about hydrodynamic loading that results in a sharp pressure drop inside the buccal cavity (Lauder 1980; Carroll, 2004). This drop in pressure is accompanied by fluid entering the mouth. Rapid buccal (mouth) expansion, which is the interest area of this project, is characterized by the gape and outward protrusion of the jaws.

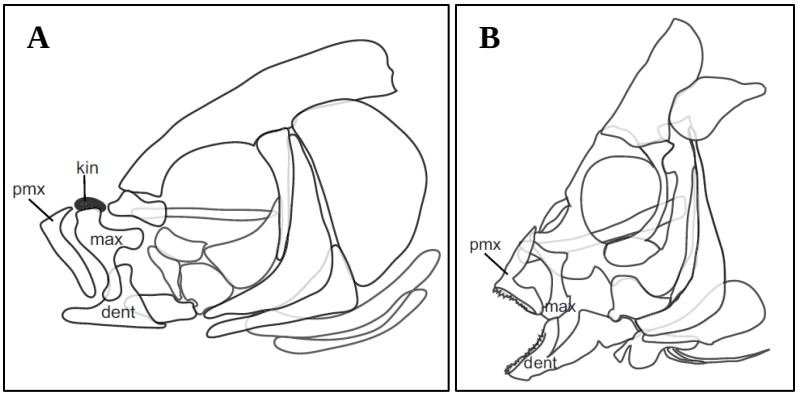

Figure 1: Goldfish's (left) and Bluegill Sunfish's (right) cranial anatomy (from Staab et al., 2012b) where: pmx: premaxilla, kin: kinethmoid, max: maxilla, dent: dentary

Jaw protrusion increases suction forces exerted on the prey in perciformes such as bluegill sunfish and bass by 35% of the total force (Holzman et al., 2008) and in goldfish representative of Cypriniformes by 10% of the total force (Staab et al., 2012b). This increase in suction force shown is due to increasing local acceleration of water located near the prey (Holzman et al., 2008). While both groups experience similar effects due to the jaw protrusion process, they exhibit different sets of kinematic patterns owing to their differences in cranial system anatomy. Figure 1 shows that the most striking difference between them is the presence of a kinethmoid in goldfish, which is clearly lacking in bluegill sunfish.

In the past, the modeling of lower jaw movement began with incorporating lever principles as shown in Figure 2. Anker (1974) proposed that lower jaw depression in teleost could be modeled with a four-bar linkage system. This research was followed by Muller (1987) who also used the same system to model hyoid depression and abduction.

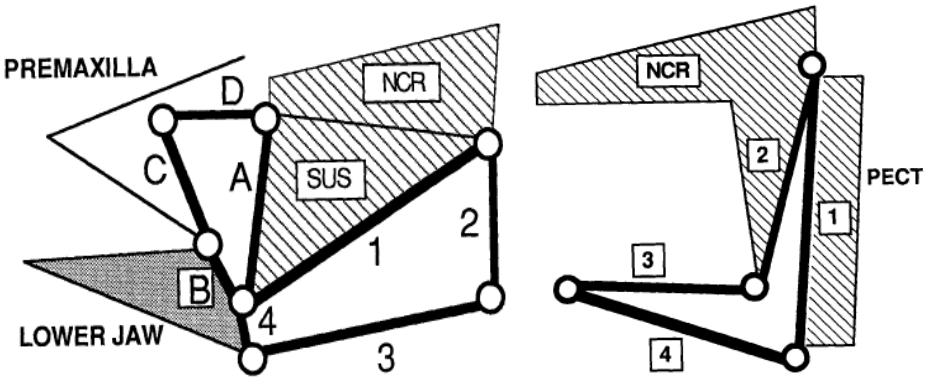

Figure 2: (Left) Anker's lower jaw model (Anker '74) (Right) Muller's hyoid linkage model (from Muller '87)

However, Anker's model of jaw depression via opercular levation was inaccurate (Westneat, 1990). Westneat presented the most comprehensive model involving the use of a software program called Mandib Lever 2.0 that incorporated lever theory along with muscle properties to analyze lower jaw motion in C. Trilobatus, a labrid fish. The model consisted of the lower jaw, A2 muscle and A3 muscle. The program calculated dynamic power output and allowed the computational mechanical analysis of the lower jaw and the jaw muscles of a fish in the family Labridae (Westneat, 2003).

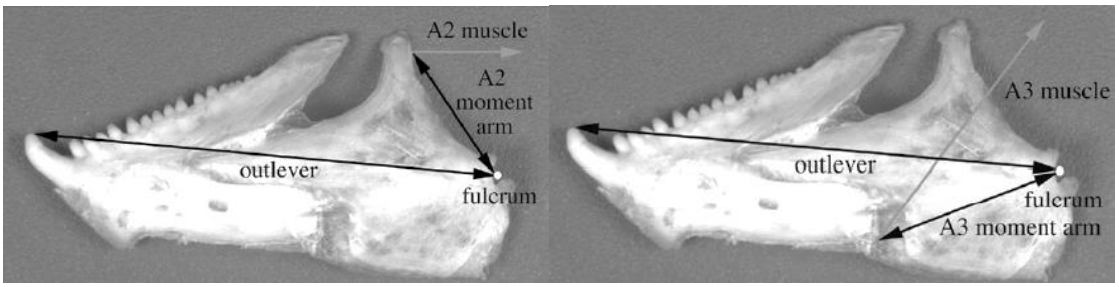

Figure 3: Line of action of A2 muscle (Left) and A3 muscle (Right) on the lower jaw (from Westneat, 2003).

Figure 3 shows how line of action of muscle forces plays a vital role in the lower jaw analysis since it directly affects the output force at the tip of the lower jaw. This model yielded simulation results similar to that of actual fish feeding events in the case of a lower jaw closing angular velocity of about 1.5 degrees/millisecond. But the challenge of creating correct models lies in the accurate modeling of muscle contractile properties, which can be highly variable

among species and even in different muscles in the same region of an organism (McMahon, 1984).

While there has been much done in the field of lower jaw modeling of Perciformes, there has been no upper jaw models for Cypriniformes yet due to complexities such as the number of bones, ligaments and muscles involved. The system can no longer be modeled as a four bar linkage system. Apart from a kinethmoid, Cypriniformes typically have a dentary, a maxilla, a premaxilla, and a palatine. The presence of a kinethmoid makes upper jaw protrusion in goldfish a complex process. Premaxillary protrusion in Cypriniformes involves the rotation of the kinethmoid, which in turn protrudes the premaxilla forward. However, there have been different explanations for the cause of the kinethmoid's rotation. For instance, R McNeill Alexander suggested that lower jaw depression brought about premaxillary protrusion (Alexander, 1966). C.M. Ballintijn conducted an electromyographical study of the maxillary muscles of a free swimming carp, a type of Cypriniformes, and concluded that the position of the dentary influenced the maxilla via the dentary-maxillary ligament (Ballintijn et al., 1972). EMG results showed that simulation of A1β muscle in the carp protruded the upper jaw only when the lower jaw was already depressed (Ballintijn et al., 1972). Philip Jay Motta summarized the process into four basic mechanisms (Motta, 1984). They were the type A or "mandibular depression model", type B or "twisting maxilla model", type C or "decoupled model" and type D or "suspensorial abduction model," (Motta, 1984).

Most recently Gidmark used XROMM (x-ray reconstruction of moving morphology) to measure the kinematics of cranial bones in carp. This led to the conclusion that motion of the maxillary bridge, not the lower jaw, drives premaxillary protrusion (Gidmark et al., 2012). He also stated that there are two modes of protrusion processes, open mouth and closed mouth,

possible based on the starting posture of the maxilla as shown in Figure 4 (Gidmark et al., 2012). The same has been observed in goldfish (Staab et al., 2012b).

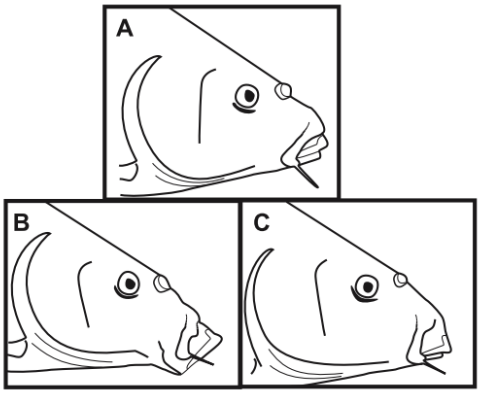

Figure 4: (A) Resting state (B) Open mouth protrusion (C) Closed mouth protrusion of Common Carp (from Gidmark et al., 2012)

This higher flexibility and coordination control owing to the complex morphology allows them to sort food and feed from the bottom (Gidmark et al., 2012). A comparison study of five cypriniform species conducted by Staab, Ferry and Hernandez (2012a) had five different kinethmoid shapes as shown in Figure 5 (Staab et al., 2012a). The study concluded that kinethmoid shape alone does not affect premaxillary protrusion speed (Staab et al., 2012a).

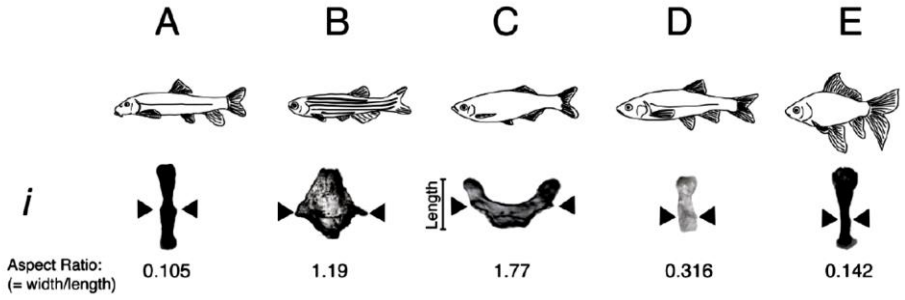

Figure 5: (A) Catostomus insignis, (B) Danio rerio, (C) Devario aequipinnatus, (D) Gila robusta, (E) Carassius auratus. Row (i): The kinethmoid of each species is shown from a dorsal view, anterior at the top. Aspect ratio (width/length) for each kinethmoid (from Staab et al., 2012a)

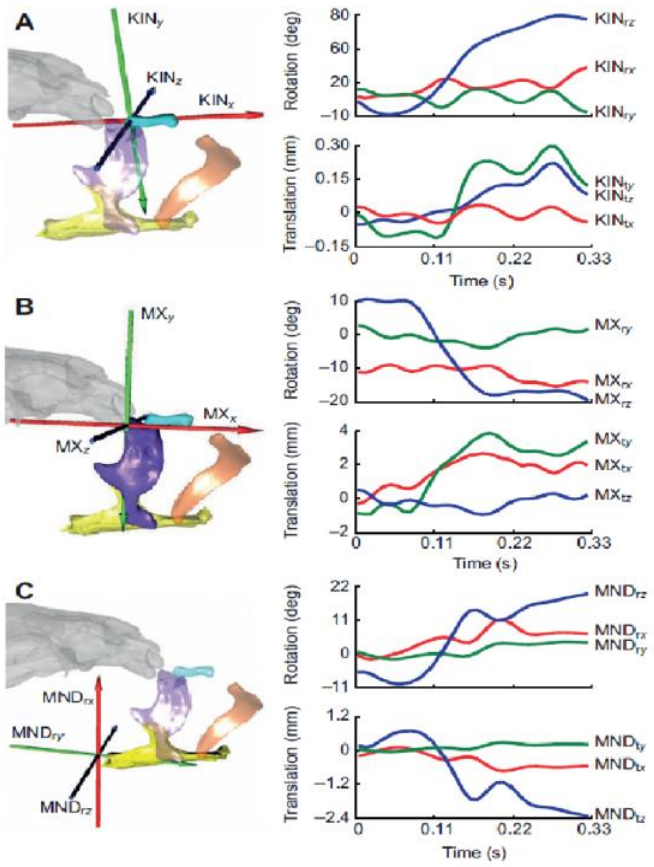

Figure 6: Six DOF bone motion data during an open mouth protrusion (from Gidmark et al., 2012).

So far biomechanical modeling for Cypriniformes has extended to 3D animation of common carp through XROMM techniques. Figure 6 shows accurate kinematic results of the kinethmoid (KIN), the maxilla (MAX) and the mandible (MND) or dentary (DENT) during an open mouth protrusion process. It also gives us an idea of the degrees of freedom of kinethmoid, maxilla and mandible (dentary) joints. For instance, the kinethmoid has 3 DOF because it rotates 90 degrees about its z axis (going into the page) and translates slightly in the y-direction (pointing down) and z-direction. The maxilla has 3 DOF because it rotates 30 degrees about its z axis and translates a distance of about 2.5 mm in the x-direction (pointing to the right) and a distance of about 5 mm in the y-direction. The mandible or the dentary has only 2 DOF because it rotates 30 degrees about its z-axis and translates a distance of about 2.4 mm in the negative z-direction. The

XROMM process, however, does not allow the convenience of changing parameters to predict kinematic results (Gidmark et al., 2012). This is why building a 3D interactive simulation model will help in changing such parameters so that we might be able to explain how changes in kinethmoid shape, starting position of the mandible and/or change in muscle activation patterns affect feeding kinematic results in Cypriniformes.

1.3 Objective

The objective of this thesis is to use Adams, typically used for industrial mechanical design and analysis, to create and simulate a 3D biomechanical model of goldfish's oral anatomy. Goldfish was chosen as the base model for this project mainly due to its easy availability and close anatomical resemblance to the common carp, whose kinematic and EMG results are already available for reference. Figure 7 shows they both have equal number of bones, two branches of adductor mandibular muscles, A1α and A1β, and a network of ligaments.

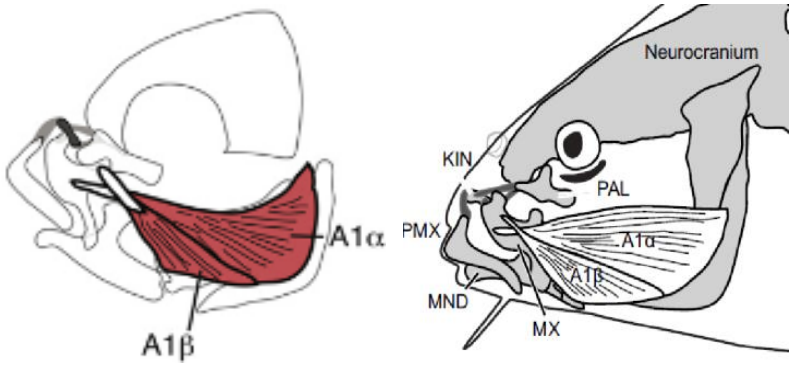

Figure 7: (Left) Skeletal muscular anatomy of Goldfish (Staab et al., 2012a) & (Right) Common Carp (from Gidmark et al., 2012).

Past experiments conducted on goldfish have produced sufficient results such as TTPG and jaw protrusion speed values to help validate our model. Only those experimental results, which come from specimens of similar head length to the 3D model, will be used. This will ensure accuracy and proper validation of the predictor model. This model will aid in studying the mouth opening process by collecting kinematic results due to variations in several parameters such as

the initial resting positions of the kinethmoid and dentary, amount of maxillary forces and timing of muscle activation.

2.0 SPECIMEN AND METHODS

2.1 Goldfish (Carassius Auratus)

Carassius Auratus, a type of Cypriniformes, is characterized by six main bones, namely the maxilla (max), premaxilla (pmx), kinethmoid (kin), palatine (pal), neurocranium (ncr) and dentary (dent) as shown in Figure 8. The maxilla is made up of two halves flexibly inter-connected. Each half also connects on both sides with sub-max cartilaginous rods (Ballintijn, 1972). Palatine connects on both sides to a large condyle, formed by the pre-ethmoid-vomer bones (Ballintijn, 1972). Sub-max rods are connected to condyle bones such that the bones slide along the rods over a great distance (Ballintijn, 1972).

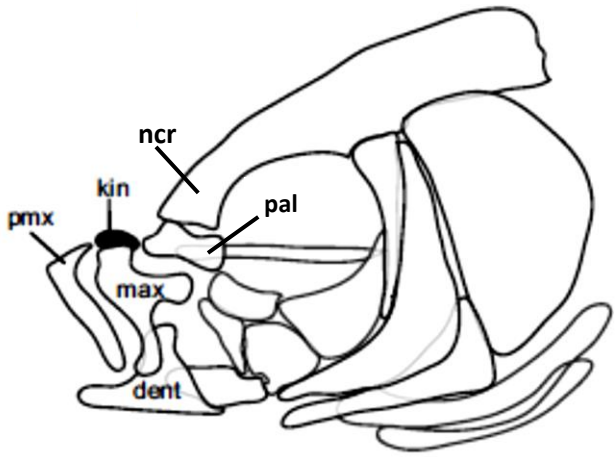

Figure 8: Upper Jaw Anatomy of Goldfish (adapted from Staab et al., 2012b)

These bones are held together by a network of ligaments. Since both goldfish and carp possess the same types of bones, we assumed that goldfish would possess a total of seven types of ligamentous connections like those observed in a carp (Ballintijn, 1972).

2.2 Approach

The process began with gaining familiarity with Adams software program through several tutorials and trials of example models. A double pendulum experiment was carried out in Adams to check if the kinematic and energy results obtained through Adams matched with Matlab's theoretically obtained results. Next, measurements of bones were taken at the lab and a working 3D model of a goldfish's mouth was built using Solidworks. This consisted of key anatomical bones such as a kinethmoid, a dentary, a maxilla, a palatine-neurocranium and a premaxilla. All bones are modeled as rigid bodies with uniform density. In order to analyze the effects of A1 maxillary forces on the kinematics of the jaw protrusion motion, all the physical measurements were obtained or calculated for A1α and A1β. Due to time constraint and lack of resources, the ligaments were modeled as 1D linear springs with certain stiffness values. Once the static model was set up, simulations were run at different conditional parameters to obtain a working model. Specifically, the work performed as part of this thesis includes

1. Quantify anatomy and physiological characteristics as model inputs
    a. Anatomy (See Section 2.3)
        i. Measure skeletal dimensions and joint locations.
        ii. Determine and simplify the types of joints for constraints.
        iii. Build the bones using Solidworks.
    b. Muscles (See Section 2.4)
        i. Determine muscle attachment points for A1α and A1β muscles.
        ii. Determine muscle properties such as cross sectional area, muscle length, muscle density, line of action and muscle mass depending on the type of muscle fibers.

iii. Develop input force functions for each muscle A1α and A1β to apply to the complex linkage system.

c. Ligaments (See Section 2.5)

i. Model ligaments as linear springs with spring constants and damping ratios.

2. Use AdamsView and the gathered parameters to build a 3D working model

a. Validate AdamsView software program. (See Section 2.6)

b. Use morphological data to populate the Goldfish model. (See Section 2.7)

3. Conduct five experimental studies

a. Experiment A: Kinethmoid's ability to achieve static equilibrium state when unattached to the maxillae. (See Section 2.8)

b. Experiment B: Effect of initial kinethmoid positions and initial dentary positions on mouth opening under a constant A1β muscle force. (See Section 2.9)

c. Experiment C: Effect of increasing A1, initial kinethmoid position and initial dentary position on mouth opening. (See Section 2.10)

d. Experiment D: Effect of both A1α and A1β muscles' activation patterns on mouth opening. (See Section 2.11)

e. Experiment E: Effect of adding a fictitious dentary force and changing joint 2 to a spring on mouth opening

2.3 3D Static Model Construction of Goldfish

A stained specimen of HL 3.15 cm shown in Figure 9A was obtained from Dr. L. Patricia Hernandez. Under Dr. Hernandez's guidance, the specimen was carefully placed under a digital microscope and scaled pictures were taken from top and side views. The premaxilla was pulled

slightly with a pair of thumb forceps to observe the kinethmoid's relative positions in both open and closed mouth positions as shown in Figure 9B. The average bone density for goldfish is 0.001 g/mm^3.

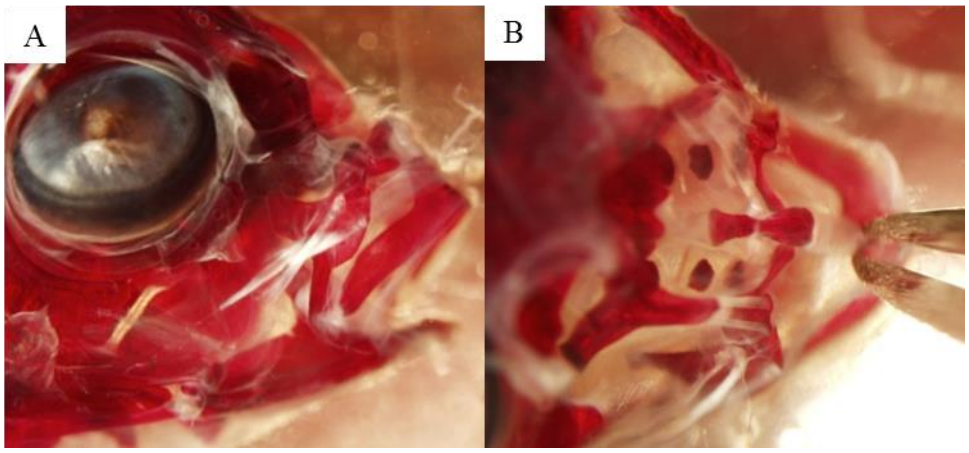

Figure 9: Stained goldfish specimen from side view (A) and top view (B)

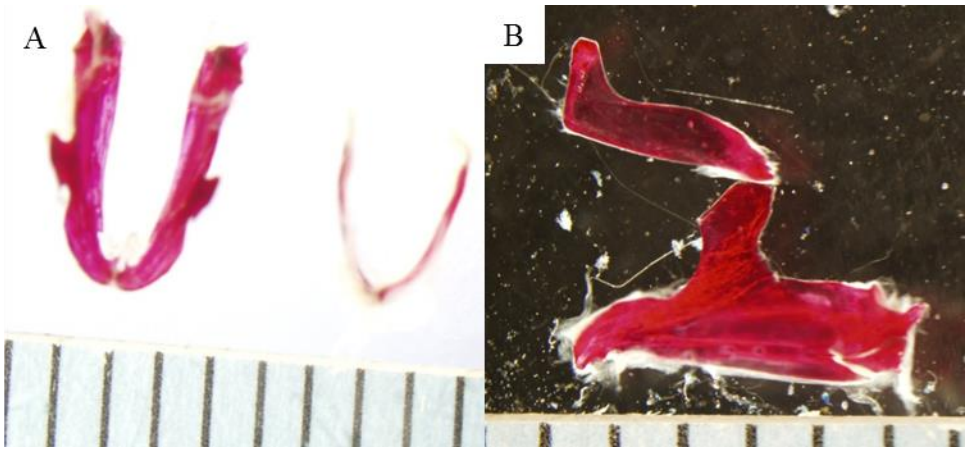

Figure 10: Scaled (mm) views of dent and pmx from top view (A) and side view (B)

Individual pictures of each bone were taken after carefully separating them. The premaxilla appeared as large as the dentary from a lateral view in Figure 10B, but was considerably thinner than the dentary when viewed from the top in Figure 10A. This difference in mass could help in protruding the premaxilla forward. Using ImageJ, approximate scaled measurements (± 0.5 mm) of all the bones, namely, the dentary, maxilla, premaxilla, kinethmoid and pal-ncr were taken (See Appendix B) and their 3D parts were constructed in Solidworks (See Appendix C). These

parts were then imported and consolidated in AdamsView to build a realistic 3D model ready for dynamical analysis.

2.4 Muscle Modeling

Two major muscles, A1αand A1β, are responsible for the upper jaw protrusion movement in goldfish. To simulate the static mouth model, forces exerted by both A1α and A1β have to be determined. Hill's muscle model shown below demonstrates the relationship between muscle contractile velocity and the muscle force output during a contraction (Westneat, 2003).

$$\frac{F}{F_{max}} = (1 - \frac{V}{V_{max}})/(1 + \frac{V}{V_{max} * k}) \quad \ldots \quad \text{(A.V. Hill, 1938)}$$

Where k = -V/Vmax, Vmax is the maximum contraction velocity of muscle and Fmax is the maximum isometric force per unit area of muscle. Though k usually lies within the range 0.15 < k < 0.25 for most muscles, mechanical power output from a muscle has a maximum when the force and speed are between 0.33 and 0.25 their maximal values (McMahon, 1984). Assuming that suction feeding process requires considerable power output, a value of 0.25 shall be used for k. Vmax can range from 3-5 muscle lengths/s in red muscle (Rome et al. 1992) to as high as 8-10 muscle length/s in white muscle of fishes (James et al., 1998). Hill's muscle model only gives us a relationship between contractile velocity ratio and input force ratio as shown below in Figure 11.

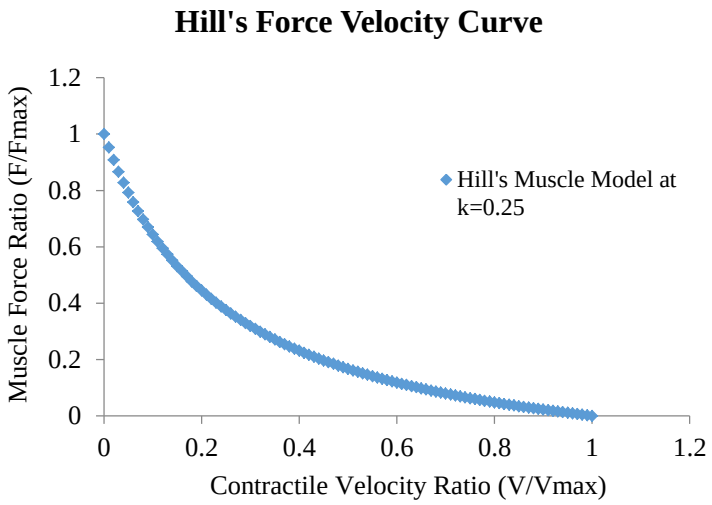

Figure 11: Relationship between contractile force and contractile velocity in isometric and concentric contractions

In order to solve for F, we shall need values for Fmax. Maximum isometric stresses in muscles can range from 100kN/m^2 to 200kN/m^2 in both red fibers (Rome et al. 1992) and white fibers (James et al., 1998) of vertebrates. Fmax is then calculated by multiplying maximum stress values with the physiological cross-sectional areas (PCSA).

$$PCSA = [muscles\ mass * \cos\theta] / [muscle\ density * fiber\ length],$$

where θ is the mean fiber angle relative to a muscle's line of action. Clear lines of action of A1α and A1β muscles are visible in Figure 12.

Figure 12: Lines of action of muscles A1α and A1β

Using ImageJ software, the maximum inclined fiber angles relative to the line of action were measured for both muscles (Figure 13). These values were then averaged to obtain mean values.

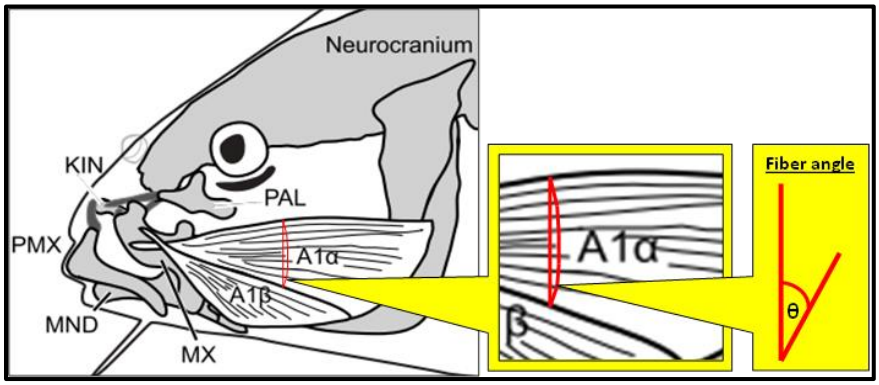

Figure 13: Mean muscle fiber angle calculation

A1α and A1β are both red muscle fibers with mean fiber angle of 9.77° and 7.14°, respectively. The fiber lengths were assumed to be equal to their muscle lengths. Other morphometric properties such as muscle length, muscle density and muscle mass were obtained from Dr. P. Hernandez. Table 1 summarizes these properties along with the calculated PCSA values for both muscles A1α and A1β. Using this data, muscle force values at each contractile velocity ratio were calculated for the range of maximum stress (Figures 14 and 15). The muscle force output from A1α is almost twice that of A1β because PCSA values have a direct proportional relationship to muscle force output. This muscle output ratio was also validated by Dr. P. Hernandez.

Acting muscles	A1α	A1β
Muscle length (cm)	0.818	0.455
Muscle density (g/cm^3)	1.056	1.056
Muscle mass (g)	0.036	0.010
Mean fiber angle (rad)	0.171	0.125

PCSA (cm^2)	0.042	0.021

Table 1: Morphometric data used in muscle force calculation

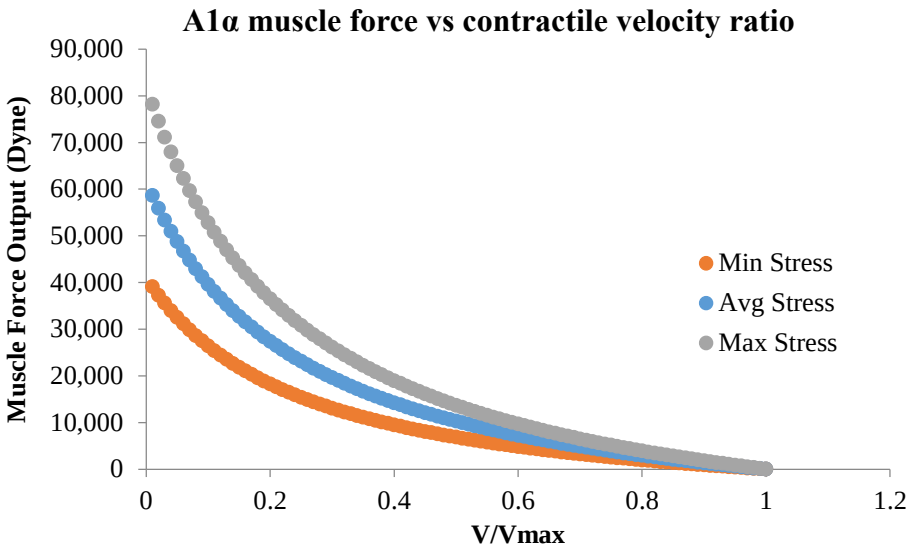

Figure 14: A1α output force vs contractile velocity ratio for min, max and avg. stress values, which come from red muscle fibers' information noted in the literature section.

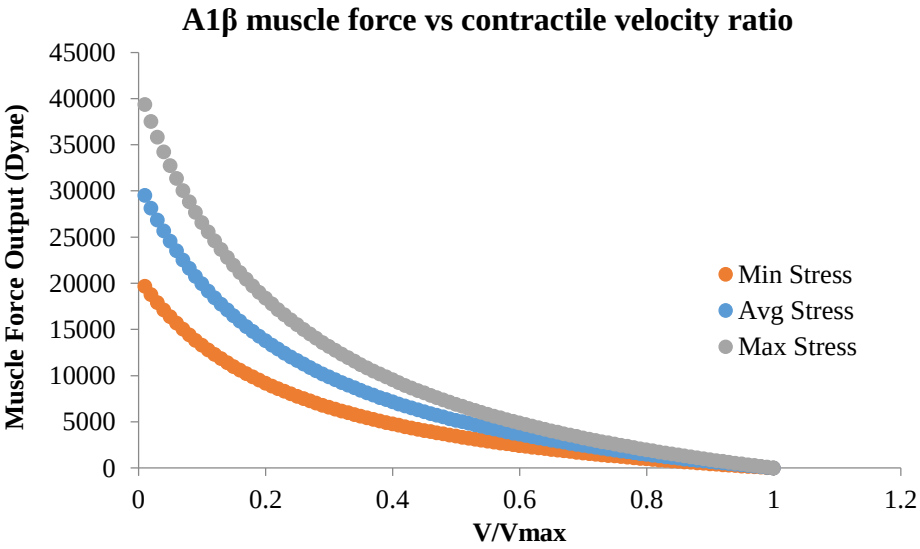

Figure 15: A1β output force vs contractile velocity ratio for min, max and avg. stress values, which come from red muscle fibers' information noted in the literature section.

In order to simulate the 3D static model, forces from both A1α and A1β have to be applied in a proper sequence. This sequence comes from EMG results obtained from previous experiments of mouth opening and closing during feeding in carp (Ballintijn et. al., 1972). EMG is the

electrical activity induced by depolarization of the muscle fibers and as such merely indicates the number of active fibers and firing frequency (Oatis, 2009). Since carp and goldfish share common oral anatomical features, EMG results obtained by Ballintijn such as the one shown in Figure 16 will be used for proper sequential application of muscle forces in goldfish.

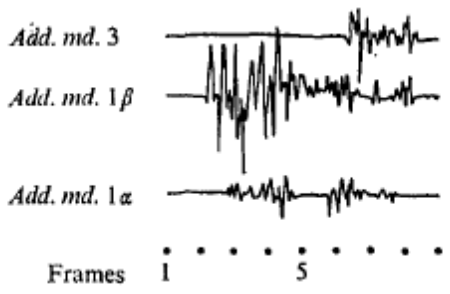

Figure 16: Extending the mouth opening downwards to suck in food followed by mouth closing (from Ballintijn, 1972)

Each frame in Figure 16 is $1/20^{th}$ of a second. While A1β muscles act on the maxilla throughout the duration of the open mouth protrusion process, A1α muscles seem to act in pulses.

In order to simulate the system correctly, muscle force graphs (Figures 14 and 15) and EMG results collected from a carp (Figure 16) are combined and translated into impulse force functions for A1α. Example functions for A1α and A1β are shown in equations 1 and 2 respectively, and Figure 17 below.

$$F_{A1\alpha}(t) = \text{step (time,0.08,0,0.09,C) + step (time,0.18,0,0.19,-C) + step (time,0.23,0,0.24,C) + step (time,0.33,0,0.34,-C) … (1),}$$

$$F_{A1\beta}(t) = \text{step (time ,0 , C , 0.4 , C) … (2),}$$

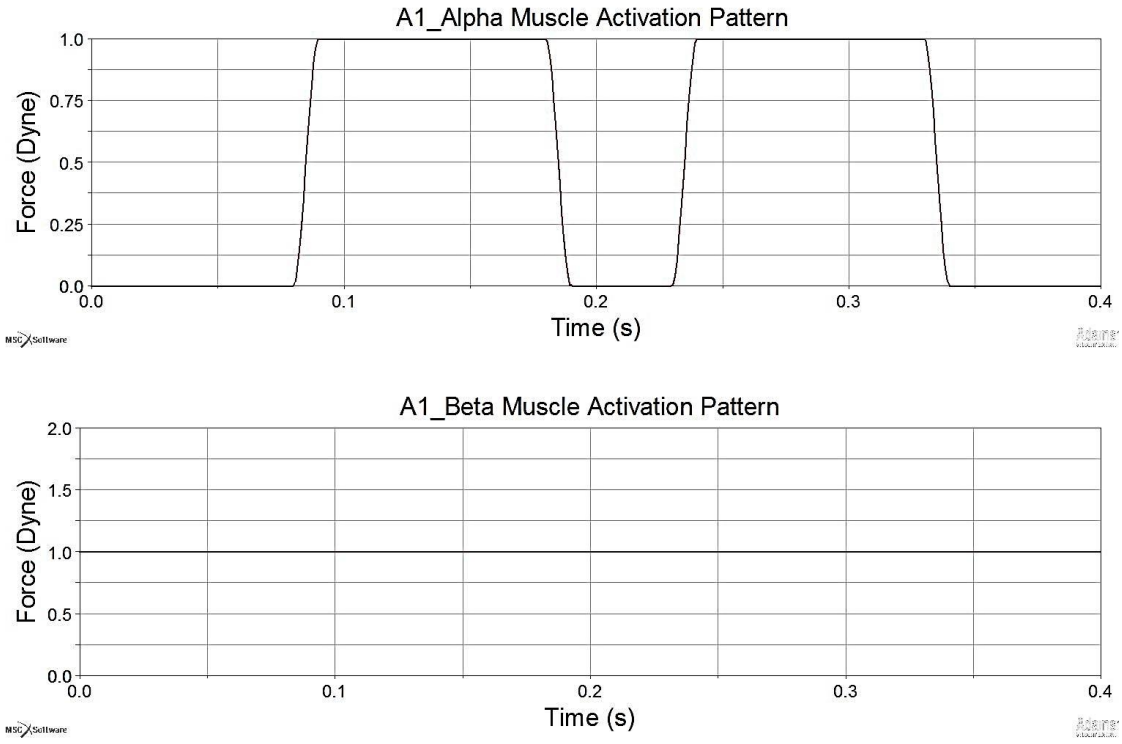

Figure 17: Impulse function input for A1α (top) and constant function input for A1β (bottom) in Adams

Where C represents constant muscle output force values chosen from Figures 14 and 15, and the total duration of force application is 0.4 secs in this equation. However, it is important to note that the duration of mouth opening will differ based on prey type, type of protrusion, muscle efficiency and type of species. Since we only have EMG graphs for feeding in carps, this may not be the exact pattern for goldfish. It is, however, the best initial reference.

2.5 Ligament Modeling

Ligament 1 runs from the ventral point of the premaxilla to the ventral tip of the maxilla. It allows the premaxilla's ventral tip to lie in the corner of the hook of the maxilla to lying at the tip of the hook of the maxilla (Ballintijn, 1972). Ligament 2 is a bony ligament between the maxilla and the coronary process of the dentary that communicates the movements of the lower jaw to the maxilla. Ligament 3 connects the dorsal (upper) lateral part of the maxilla to the palatine (Ballintijn, 1972). Ligament 4 is short and stiff connecting the rostral tip of the kinethmoid to the

dorsal process of the premaxilla (Ballintijn, 1972). Ligament 5 is a broad, flat ligament connecting the caudal point of the rostral bone to the anterior end of the cranium (Ballintijn, 1972). Ligament 6 connects the ventral (under) part of the kinethmoid to the medial part of the maxilla at a quarter of the height of the ventral part of the rostral bone (Ballintijn, 1972). Ligament 7 connects the kinethmoid to the palatines through the sub-max rod at halfway along the kinethmoid (Ballintijn, 1972). All these ligaments present in a carp are shown in Figure 18.

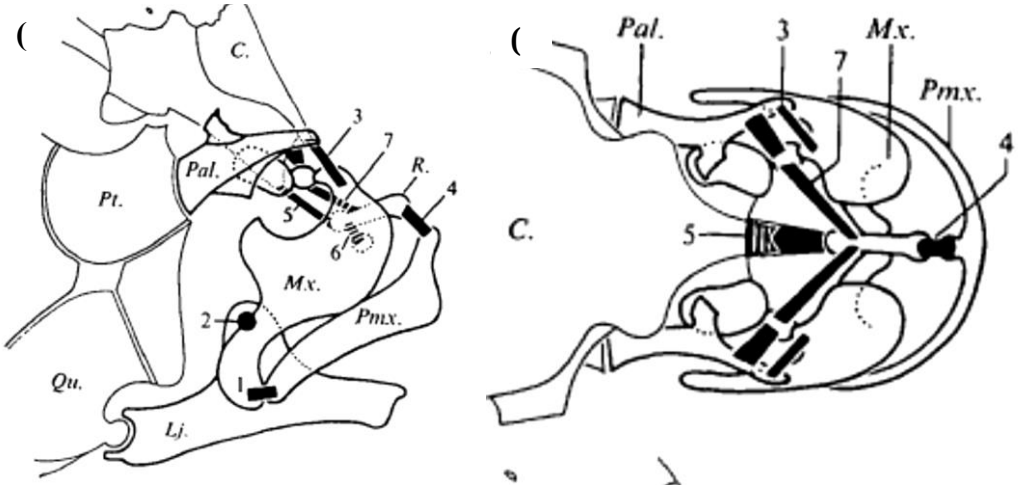

Figure 18: Ligaments of a carp; (a) side view (b) top view (Adapted from Ballintijn, 1972)

Ligaments 1, 3, 6 and 7 are present on both sides of the mouth so they are denoted by 'R' for right side and 'L' for left side. Ligament 2 is simplified to a pin joint. All ligaments are modeled as springs with arbitrary stiffness values, represented by k, and damping ratios, represented by c as summarized in Table 2.

Bone connections	Ligament	k (dyne/mm)	c (dyne-sec/mm)
Pmx-Max	1L	1,000	1.05
Pmx-Max	1R	1,000	1.05
Dent-Max	Pin Joint	n/a	n/a
Dent-Max	Pin Joint	n/a	n/a
Pal-Max	3L	100	1.05
Pal-Max	3R	100	1.05

Kin-Pmx	4	30,000,000	1.05
Kin-Pal	5	100	1.05
Kin-MaxR	6L	10,000	1.05
Kin-MaxL	6R	10,000	1.05
Kin-Pal	7L	1,000	1.05
Kin-Pal	7R	1,000	1.05

Table 2: Stiffness and damping coefficient values chosen for all ligaments modeled as linear springs in AdamsView

2.6 Validating AdamsView software program

In order to use Adams software for our simulations, it is important to validate it first. This was achieved by running a double pendulum simulation in Adams (See Appendix A for settings) and plotting the results against theoretical results solved in Matlab (See Appendix A for Matlab code). The model consisted of two cylindrical rods connected to each other by a frictionless pin joint. The other end of the first cylinder was connected to ground by a frictionless pin joint as shown in Figure 19. Their initial positons were θ_1= 90° and θ_2=135° from – y axis going anti-clockwise. Both their initial angular velocities were at 0 rad/sec.

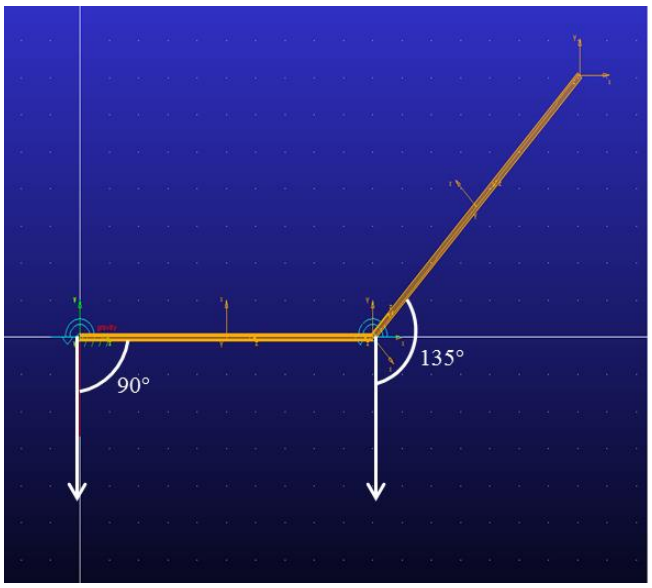

Figure 19: Double pendulum system set up in Adams

After running Adams simulation for 3 seconds, we compared its kinematic and energy results to those of Matlab results as shown in Figures 20 and 21, respectively. Kinematic and energy

results obtained from Adams simulation were equal and/or close to those obtained through Matlab. The maximum difference between both program results was about 1e-4%.

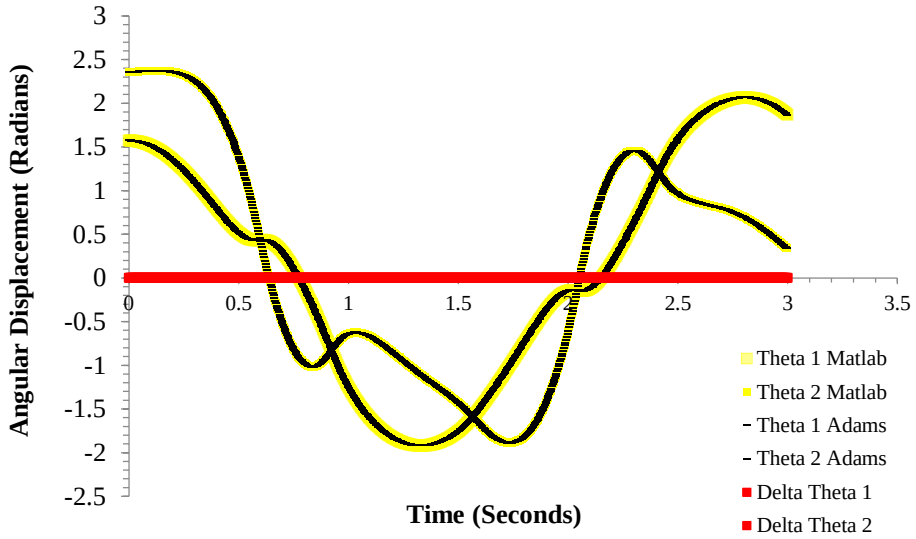

Figure 20: Angular displacement for links 1and 2 from Matlab overlap those obtained through AdamsView. The yellow squares represent Matlab results while the black lines represent AdamsView results. The red squares represent the differences between results from the two programs.

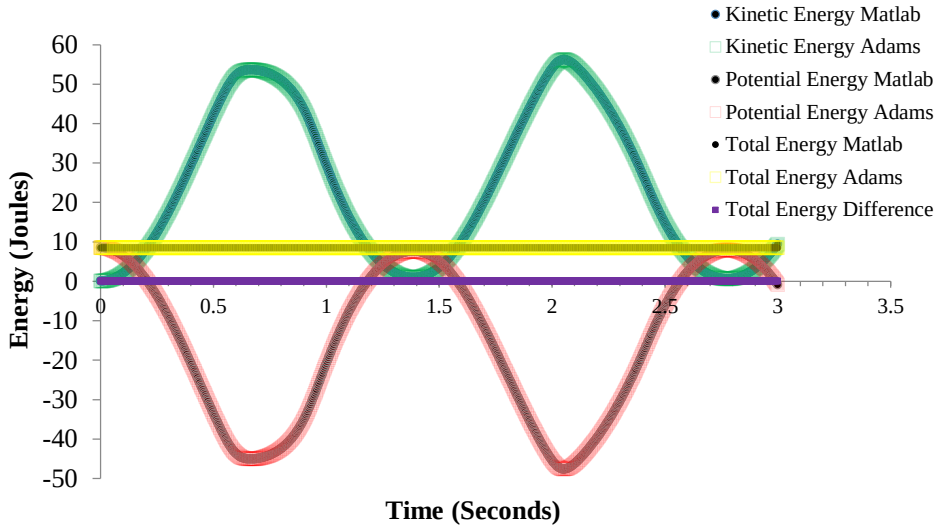

Figure 21: Kinetic, potential and total energy results from AdamsView overlap those obtained through Matlab. The green, yellow and red squares represent kinetic, total and potential energies respectively and are obtained through AdamsView. The black dots represent energy results obtained through Matlab.

2.7 Simulation in MSC Software's AdamsView

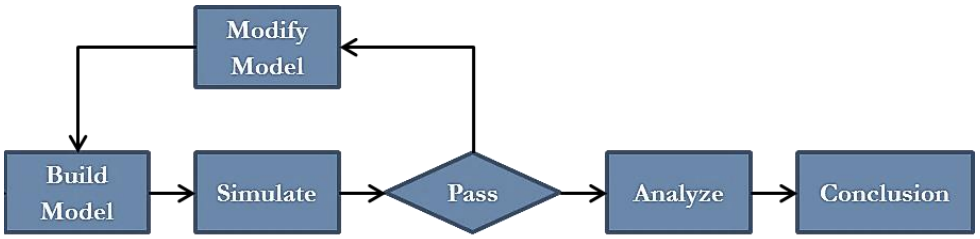

Figure 22: Flowchart representing key steps involved in Adams simulations

Figure 22 summarizes the key steps needed to complete Adams simulation analysis. Parasolid cad models of bones were imported into AdamsView and connected by springs, which represented ligaments. Closed mouth position measurements were obtained from observational hand drawings of a stained goldfish specimen under a microscope (Figure 23). Figure 24 shows this position in AdamsView where the dentary is at an angle of 53.44° +/- 0.25° from the horizontal x-axis. This dentary angle is the starting reference for simulations and will be optimized depending on the kinematic results obtained. AdamsView guidelines are shown in Appendix F.

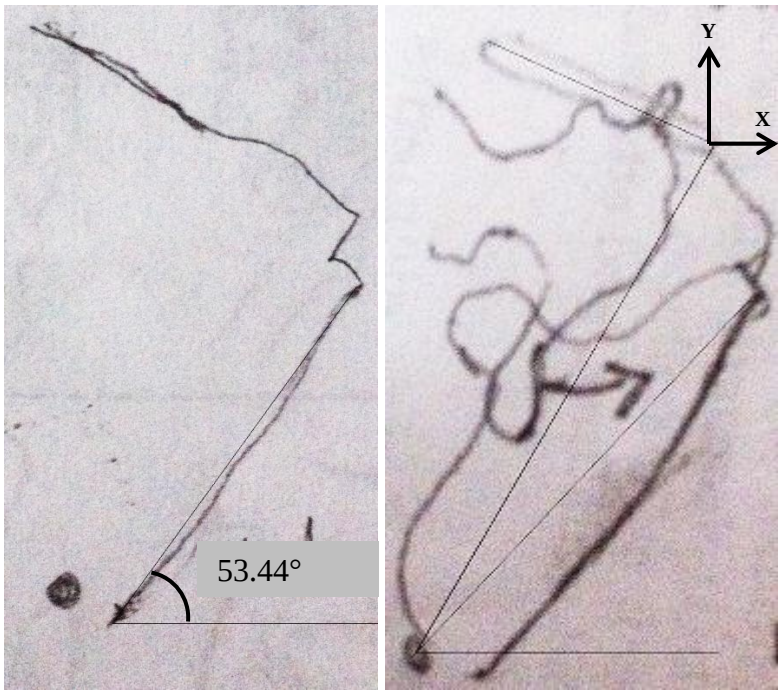

Figure 23: Sketched resting position of a goldfish observed under a microscope

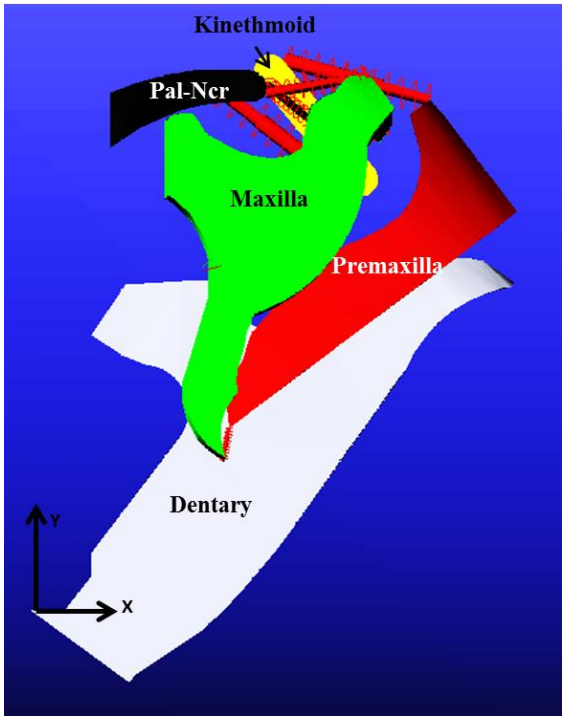

Figure 24: Reference position of goldfish in AdamsView where dentary is at 53.44 degrees from horizontal x-axis

A gravitational force of 9.81 m/s^2 acting in the –y direction was in effect throughout all the simulations. The simulation environment did not mimic the presence of any fluid. Hence, there were no fluid forces acting on the 3D model. Also, constraints due to the presence of skin were neglected in this thesis. Due to these reasons, very low maxillary muscle force values were chosen to open the mouth.

2.8 Experiment A: Kinethmoid's resting position under suspension

The first thing we want to understand is how the kinethmoid stays suspended in its resting position. This will help explain how the parts move when external forces are applied on the system. The purpose of this experiment is to see the effects of varying kinethmoid positions and orientations on the final resting state of the kinethmoid. We learned that the ventral translation of the maxilla has a direct influence on the kinethmoid's rotation (Gidmark et al., 2012). Assuming

that the maxilla is protruding the mouth to open, it is reasonable to say that the maxilla has little or no effect on the kinethmoid during its resting position. This simplifies the first analysis model to a system of four bodies, namely, the dentary, the premaxilla, the kinethmoid and the pal-ncr as shown in Figure 25. Because the premaxilla is connected to the maxilla during the resting phase, we can assume that ligament 2 prevents the premaxilla from moving in the x, y and z directions, but it does allow for rotation about its z axis. Since the dentary and premaxilla are held at fixed angles during a closed mouth position as shown in Figure 23, the model is further simplified by reducing the pmx's DOF to zero. Since a goldfish's head anatomy is symmetrical, the kinethmoid's DOF can be reduced to three parameters, namely, kin(x), kin(y) and kin(θ_z). To further simplify our analysis, the kinethmoid's orientations and positions about its com will be limited to a specific area called the region of mobility as shown in Figure 25. Given the geometric constraints of the head shape such as the fixed distance between the neurocranium and premaxilla, and the presence of ligament connections, kin(θ_Z) can physically attain a maximum of 160° from x-axis for resting state as shown in Figure 23. From lab observations, it is known that the minimum angle of starting position cannot possibly be less than 90°. For kin(θ_Z) = 90°, we get the maximum range of x values where -1.75 mm < com(x) < -0.425 mm, and for kin(θ_Z) = 160°, we get a maximum range of y values -3.875 mm < com(y) < -3.4 mm. These values are again based on geometric constraints of the parts surrounding the kinethmoid. To see the effects of varying kinethmoid orientation on its angular displacement values, a constant com (x, y) location for the kinethmoid is chosen as (-1.09, -3.64) in mm and kin(θ_Z) values range between 90° and 150°. At this com location, it was not physically possible for the kinethmoid to be at 160° without increasing the length of the ligament; hence the maximum kin(θ_Z) value was reduced from 160° to 150°. The simulations are run for 0.4 seconds and the results are shown in

Figure 26. To test for kinethmoid's stability at different positions, the system is simulated between its minimum and maximum angles of 90° and 150° until it showed static equilibrium at certain positions.

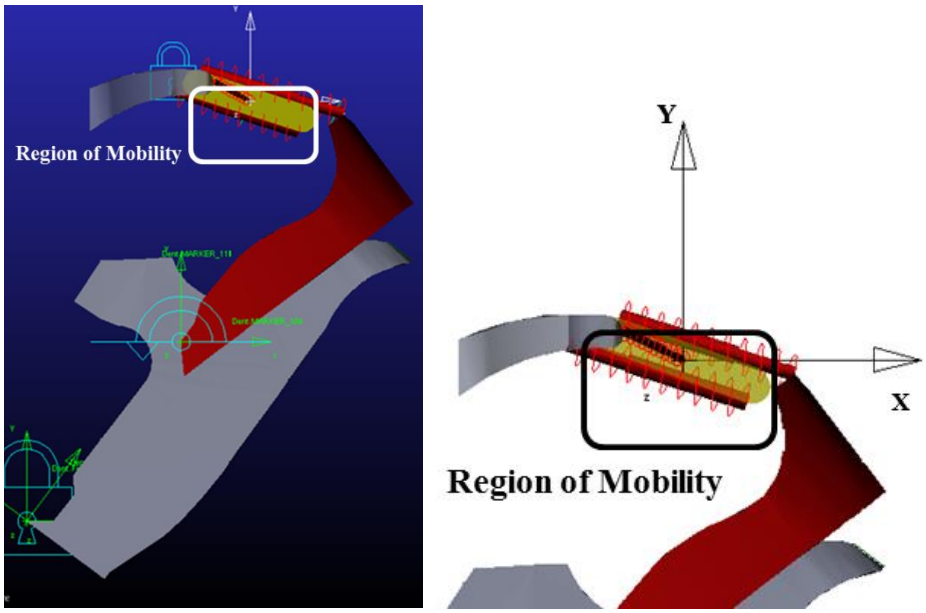

Figure 25: Simpler model showing the region of mobility to analyze kinethmoid's behavior in suspension

2.9 Experiment B: Effect of initial kinethmoid positions and initial dentary positions on mouth opening under constant A1β muscle force

In order to simulate mouth opening process, it is important to build a complete working model. It is known that the two maxilla bones are connected to the kinethmoid through its median processes, which pull on the kinethmoid causing rotation (Ballintijn, 1972). Unlike the first experiment, this one will include all the bones and ligaments as shown in Figure 24. This model is assuming that the joints between dentary and ground and between maxillae and dentary are pin joints. EMG results, obtained by Ballintijn, show that stimulation of A1β in the carp will only protrude the upper jaw when the lower jaw is already depressed. It was also concluded that as long as the lower jaw is at least minimally depressed, the line of action of this muscle is fully capable of causing protrusion (Ballintijn, 1972). This means that the lower jaw should be at a

certain position for the mouth to open according to his hypothesis. To test this, the dentary is depressed at various angles beginning with the reference resting angle of 53.44° as calculated from Figure 23, followed by 51.5°, 50°, 49° and 48°. For each initial dentary position, constant A1β maxillary force of 1 dyne is applied on both sides of the mouth and the 3D model is simulated for 0.1 seconds. Previous results showed that the kinethmoid's orientation could range from 90° to 150°, which will be taken into account during these simulations. All the results are shown in Figures 29 through 33. Once an ideal angle of mandibular depression is observed, the kinethmoid's behavior at this ideal angle for varying initial kinethmoid positions will be collected. This is shown in Figure 34.

2.10 Experiment C: Effect of increasing A1β, initial kinethmoid position and initial dentary position on mouth opening

This experiment aims at understanding the effects of increasing A1β force, initial kinethmoid position and initial dentary position on mouth opening. Specifically the model is simulated for 0.1 secs at kin(θ_Z) values of 90°, 120° and 150°, and dent(θ_Z) values of 53.44° and 50° with increasing values of A1β. These five parameters give us a total of six cases which are shown in Figures 35 through 40. In all cases, A1β values are increased to show a change of direction in dentary motion if possible.

2.11 Experiment D: Effect of both A1α and A1β muscles' activation patterns on mouth opening

In order to open the mouth like in suction feeding, both A1α and A1β muscles have to contract to protrude the upper lip (Ballintijn et al, 1972). A1α acts on both sides of the mouth, but in a more horizontal fashion as shown in Figure 12. EMG results obtained for carp's feedings show different activation patterns for A1α and A1β (Ballintijn et. al, 1972). Four common

parameters will be measured to analyze open mouth protrusion in Goldfish. They are dentary rotation, kinethmoid rotation, gape and protrusion distance. The distance between a point on the tip of the premaxilla and another on the tip of the mandible measures gape (Nicholas, 2012). Protrusion distance is taken as the distance between the anterior tip of the premaxilla and the anterior tip of the neurocranium (Nicholas, 2012). The initial dentary position is set at 49° to allow mouth opening and the initial kinethmoid positions are 130° and 150°. The model is simulated with a constant input of A1β, while A1α is applied at different time intervals as step functions. Because the kinethmoid rotated at a steady rate at higher kinethmoid positions, this experiment aims to look at initial kinethmoid positions of 130° and 150°. From muscle modeling in section 2.4, it was determined that A1α should be double of A1β. At an initial kinethmoid position of 130°, A1α and A1β were 5 dynes and 10 dynes, respectively, and at an initial kinethmoid position of 150°, A1α and A1β were 12 dynes and 24 dynes, respectively. All the results are shown in Figures 41 through 46.

2.12 Experiment E: Effect of a fictitious dentary force F on mouth opening

This experiment builds upon the previous model, where the dentary was positioned at 49° and the kinethmoid was positioned at 150°. Because there is a very small muscle called the intermandibularis, which connects to the rami of the lower jaw (Ballintijn et al, 1972), the fictitious dentary force in this model will represent the intermandibularis force that may or may not affect the kinematic results of mouth opening. The first test will see the effects of this fictitious force F acting alone on the 3D model. The second test will see the effects of A1 maxillary forces combined with dentary force F.

3.0 RESULTS

3.1Experiment A: Kinethmoid's resting position under suspension

Figure 26 shows the kinethmoid's angular displacement as a function of its changing initial angular position, but fixed location (x,y) in space. When the kinethmoid is simulated at an initial kin(θ_Z) of 120°, its position and orientation barely fluctuate. This means that at a certain com position and orientation, the kinethmoid is able to achieve static equilibrium. As initial kin(θ_Z) is increased or decreased from 120°, the kinethmoid oscillates away from its initial orientation and position. Therefore, for these unstable orientations, the system is simulated several times within the region of mobility till it demonstrates static behavior. Figure 27 shows that for each initial kin(θ_Z) value between 90° and 150°, the system achieved static equilibrium at their specific com positions. Figure 28 gives a visual representation of the kinethmoid's initial resting positions ranging from 90° to 150° that were used to test for its static equilibrium positions.

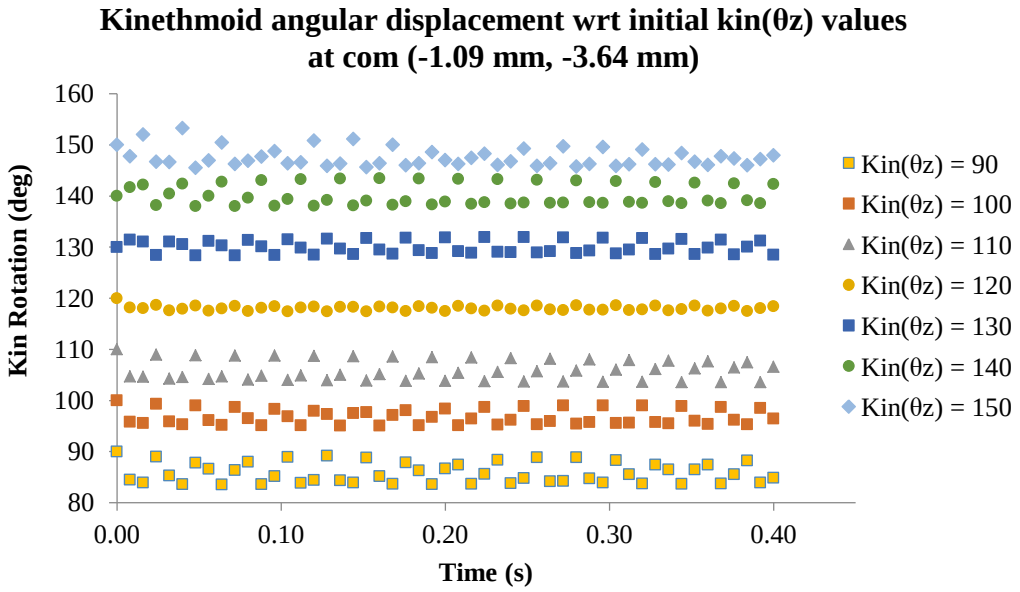

Figure 26: The effect of varying initial kin(θz) positions on its static equilibrium

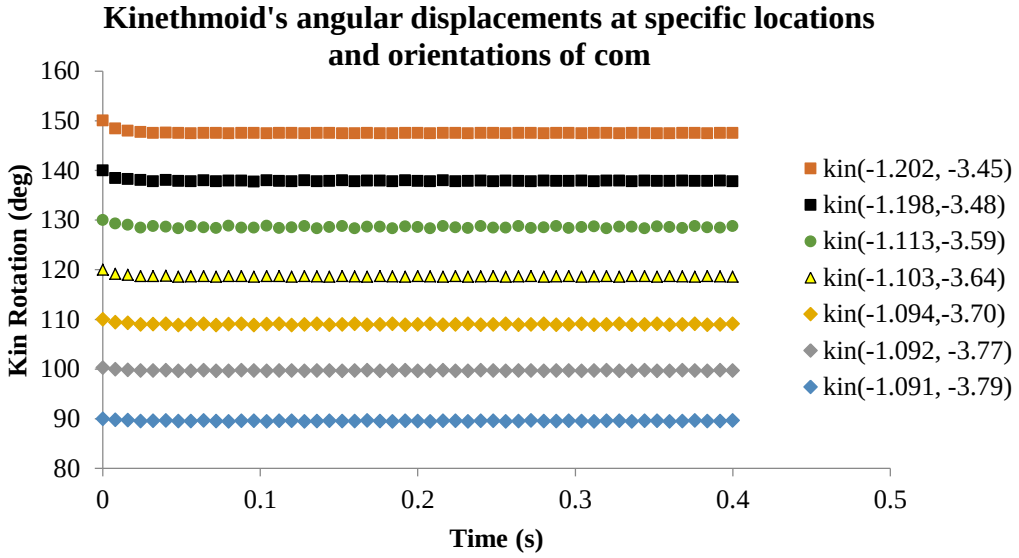

Figure 27: Kinethmoid's state of static equilibrium at specific initial kin(θz) and kin(com) locations.

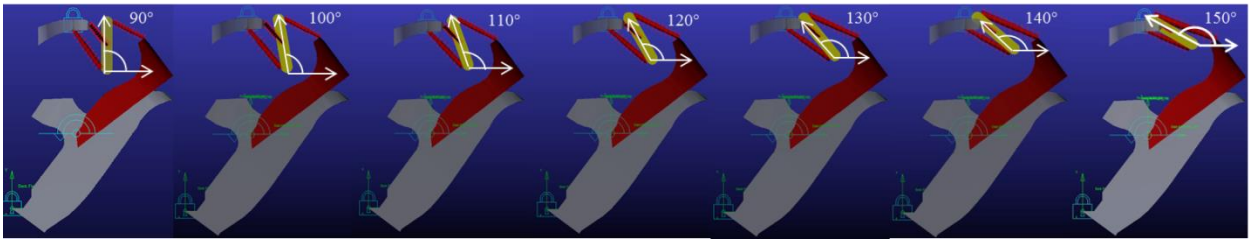

Figure 28: Images of kinethmoid's static positions specified in Figure 27.

3.2 Experiment B: Effect of initial kinethmoid positions and initial dentary positions on mouth opening under constant A1β muscle force

Figures 29 through 33 show the effect of a constant A1β, range of initial kinethmoid positions and decreasing initial dentary positions on dentary's motion. The results are consistent for initial dentary values of 53.44°, 51.5° and 50° in figures 29, 30 and 31, respectively, where the dentary rotates in the positive z-direction. In figures 32 and 33, the dentary rotates in the negative z-direction. Figure 34 shows the kinethmoid's angular displacements for all initial kinethmoid positions with initial dentary position of 49°.

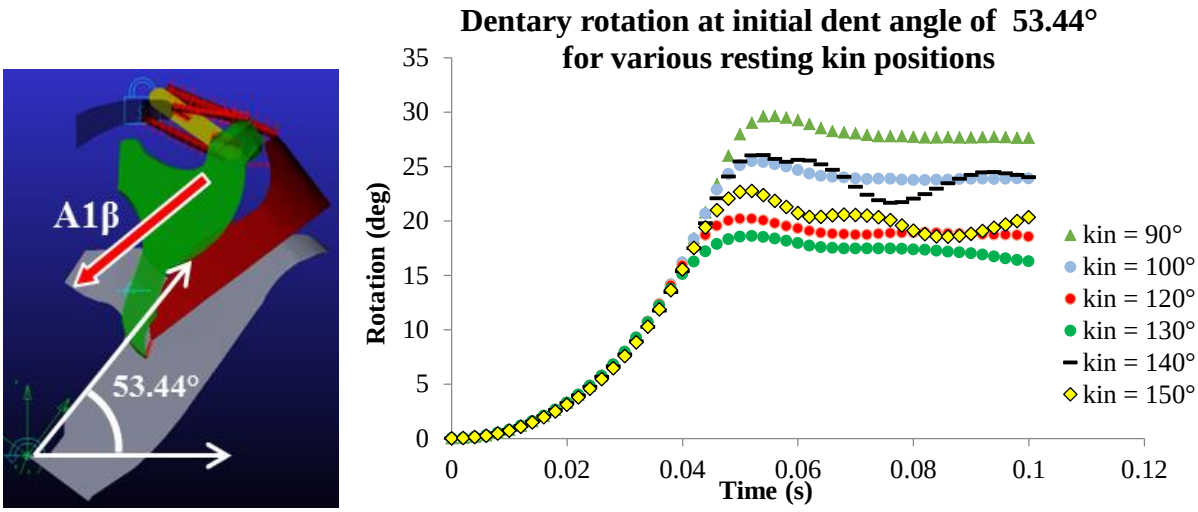

Figure 29: Effect of A1β and initial dentary position of 53.44° on dentary rotation with respect to each kinethmoid position

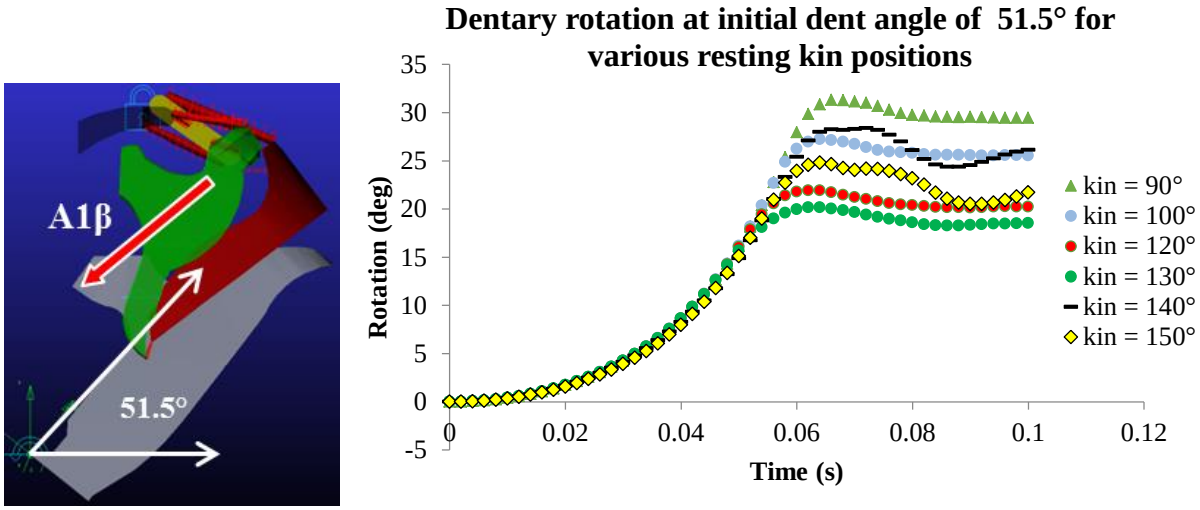

Figure 30: Effect of A1β and initial dentary position of 51.5° on dentary rotation with respect to each kinethmoid position.

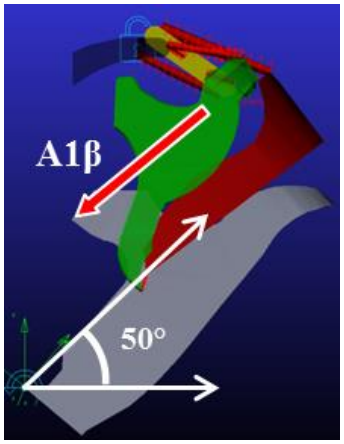

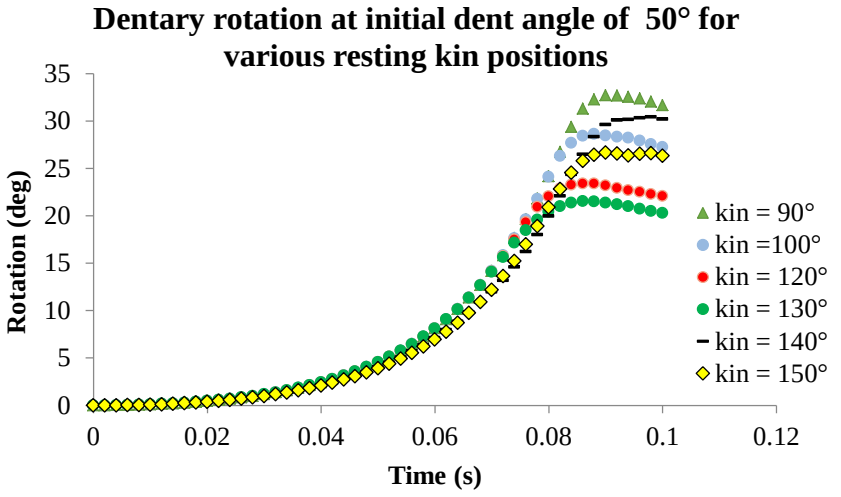

Figure 31: Effect of A1β and initial dentary position of 50° on dentary rotation with respect to each kinethmoid position

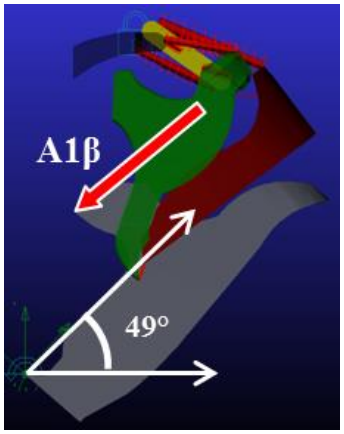

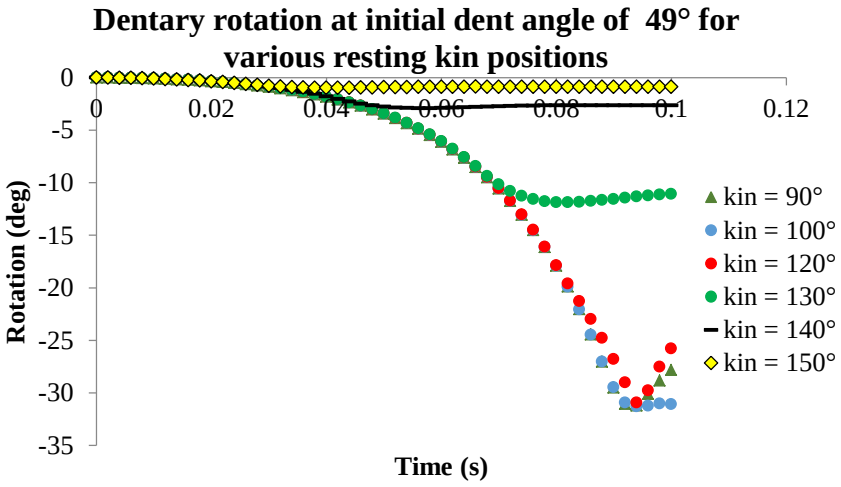

Figure 32: Effect of A1β and initial dentary position of 49° on dentary rotation with respect to each kinethmoid position

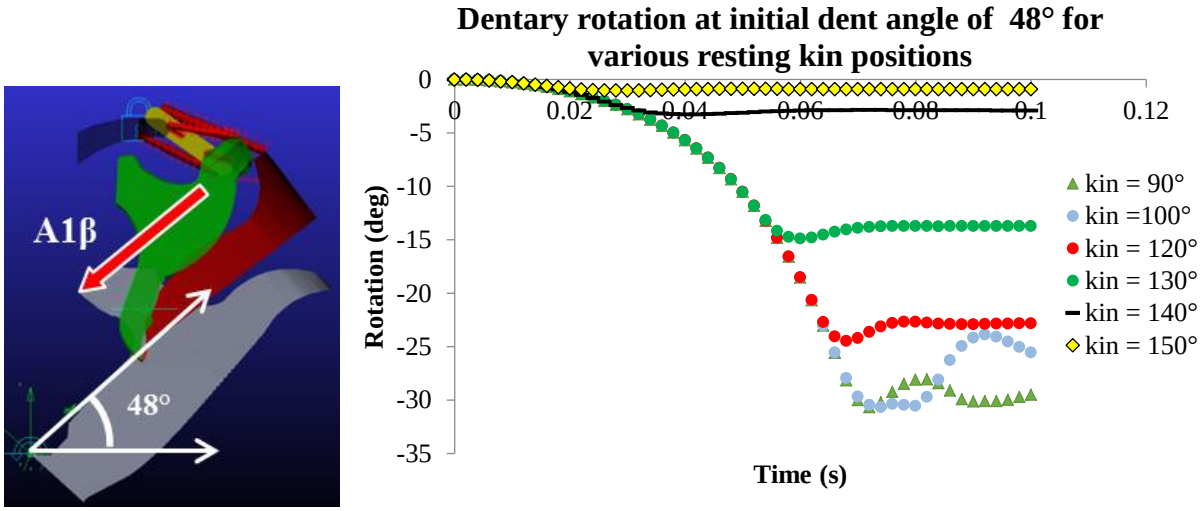

Figure 33: Effect of A1β and initial dentary position of 48° on dentary rotation with respect to each kinethmoid position

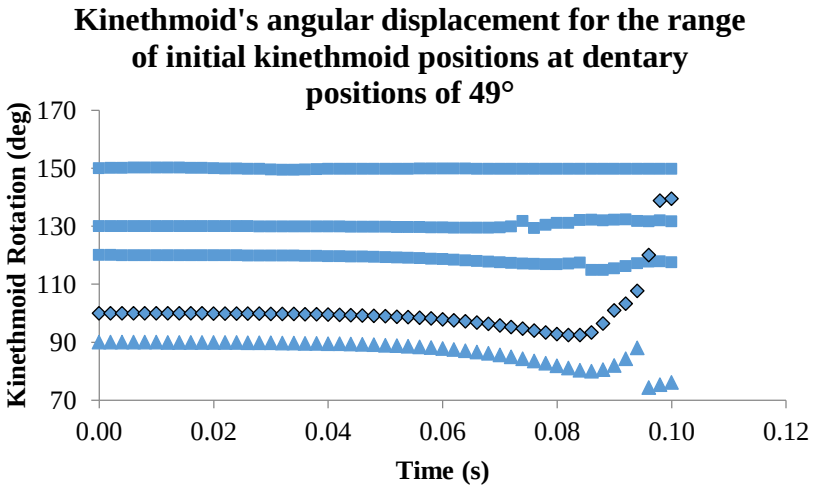

Figure 34: Effect of A1β, initial kinethmoid positions on kinethmoid rotation at initial dentary positions of 49°

3.3 Experiment C: Effect of increasing A1β, initial kinethmoid position and initial dentary position on mouth opening

Figures 35 and 38 represent the cases where the initial kinethmoid angle is at 90° for initial dentary angles of 53.44° and 50°, respectively. Figures 36 and 39 represent the cases where the initial kinethmoid angle is at 120° for initial dentary angles of 53.44° and 50°, respectively, and Figures 37 and 40 represent the cases where the initial kinethmoid angle is at 150°.

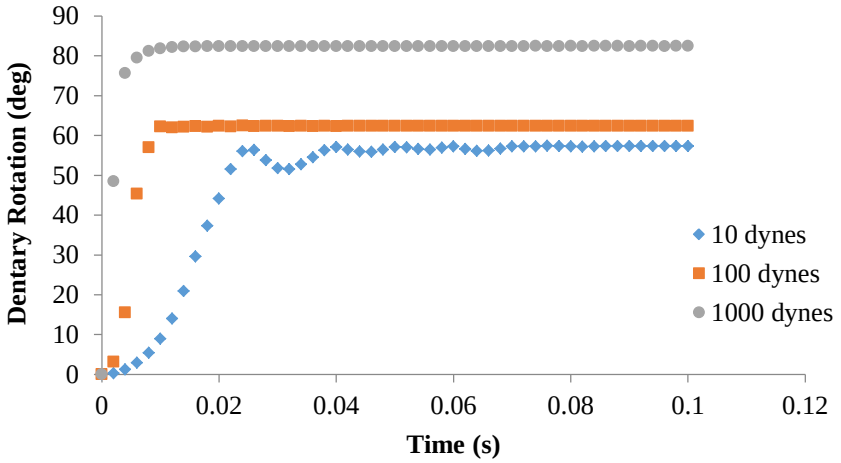

Figure 35: Effect of increasing A1β force on dentary opening at initial dent position of 53.44° and initial kin position of 90°

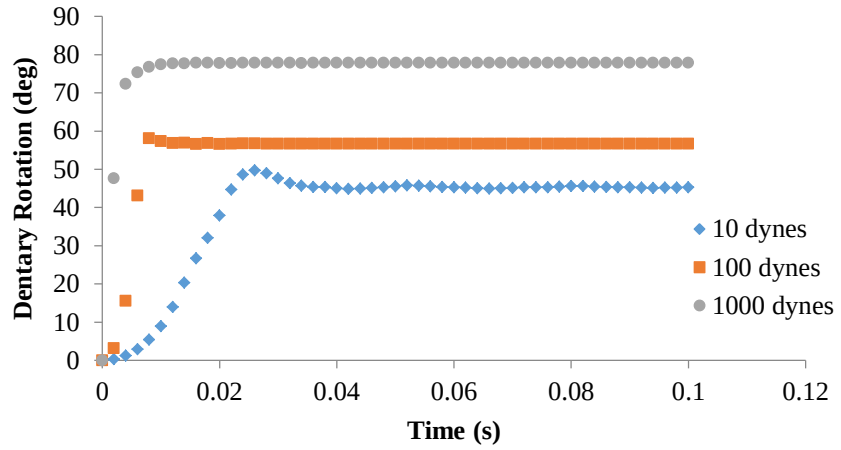

Figure 36: Effect of increasing A1β force on dentary opening at initial dent position of 53.44° and initial kin position of 120°

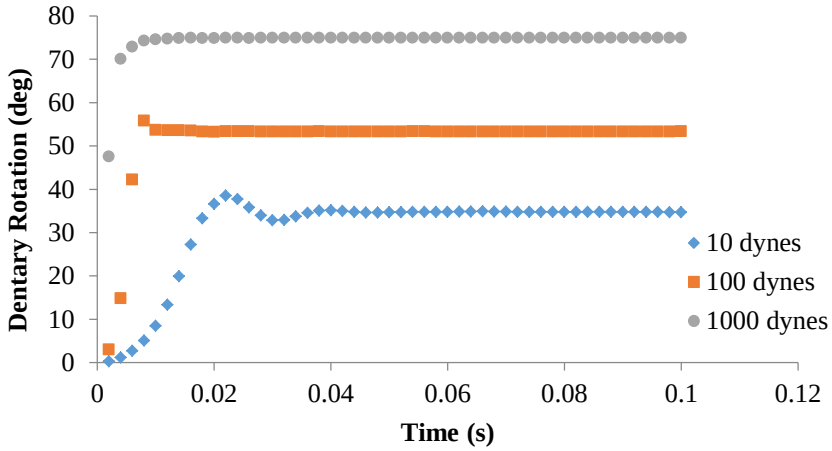

Figure 37: Effect of increasing A1β force on dentary opening at initial dent position of 53.44° and initial kin position of 150°

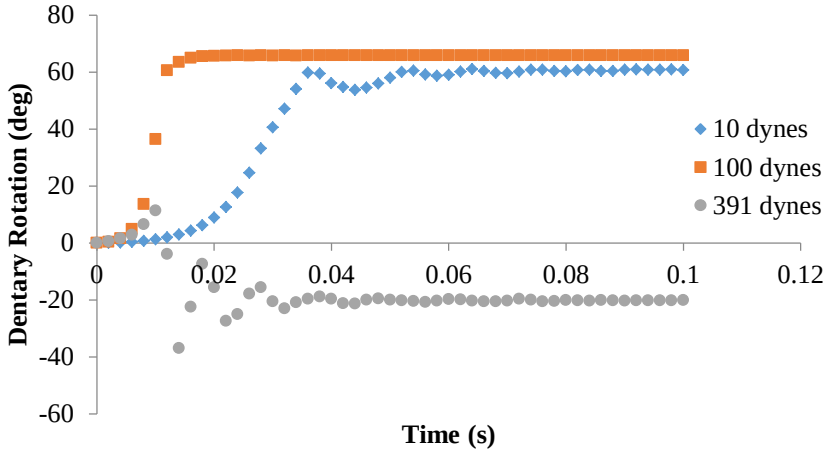

Figure 38: Effect of increasing A1β force on dentary opening at initial dent position of 50° and initial kin position of 90°

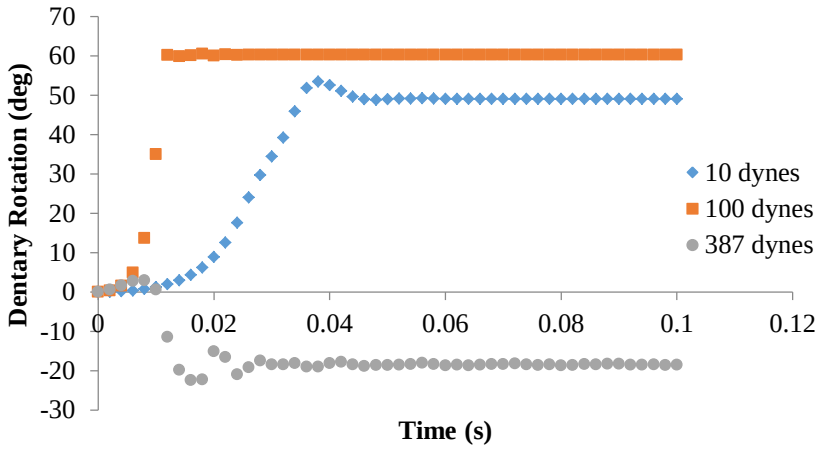

Figure 39: Effect of increasing A1β force on dentary opening at initial dent position of 50° and initial kin position of 120°

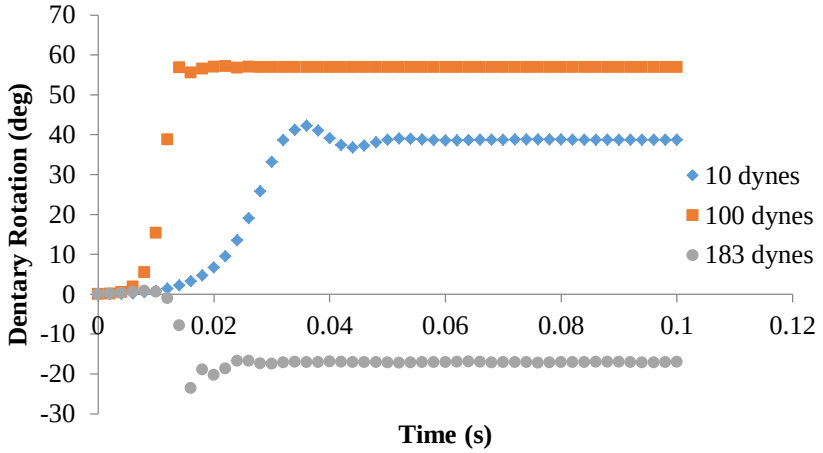

Figure 40: Effect of increasing A1β force on dentary opening at initial dent position of 50° and initial kin position of 150°

3.4 Experiment D: Effect of both A1α and A1β muscles' activation patterns on mouth opening

Figures 41 and 44 show the dentary's rotation as a result of A1 maxillary muscles applied at different time intervals. The initial dentary position is at 49° for both cases while the initial kinethmoid position is at 130° in Figure 41 and 150° in Figure 44.

Figures 42 and 45 show the kinethmoid's rotation as a result of A1 maxillary muscles applied at time intervals where the dentary had rotated counterclockwise previously. This narrows down the list of time intervals at which A1α can rotate the kinethmoid clockwise.

Figures 43 and 46 then show kinethmoid's rotation, dentary's rotation, gape and protrusion for the case where previously the kinethmoid had just begun to rotate clockwise in repeating patterns.

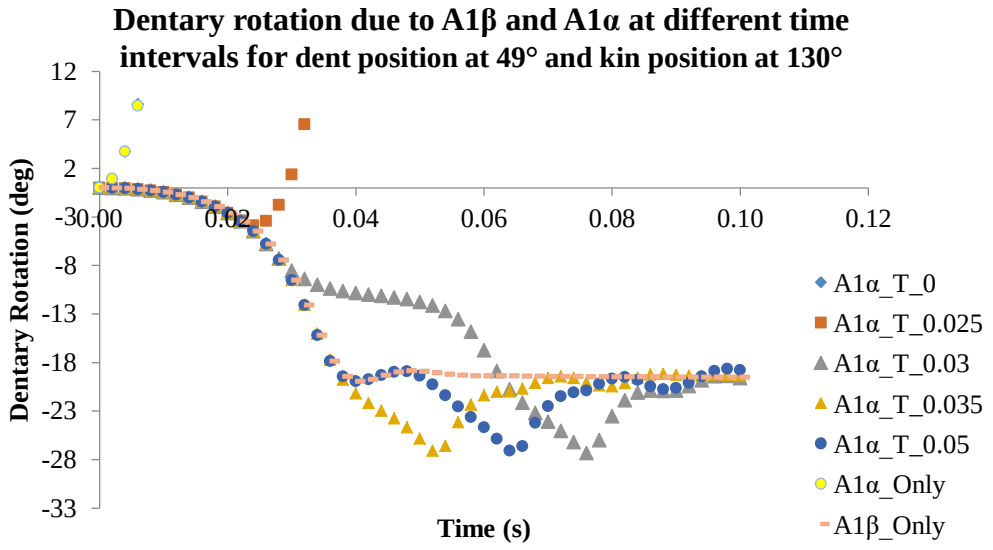

Figure 41: Effect of A1α = 10 dynes and A1β = 5 dynes on dentary opening during open mouth process

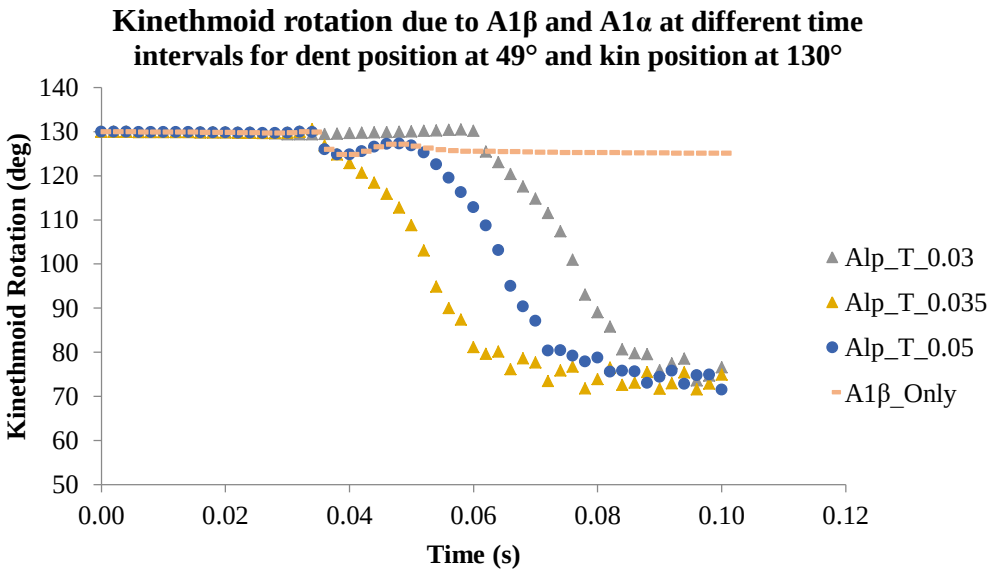

Figure 42: Effect of A1α = 10 dynes and A1β = 5 dynes on kinethmoid rotation during open mouth process

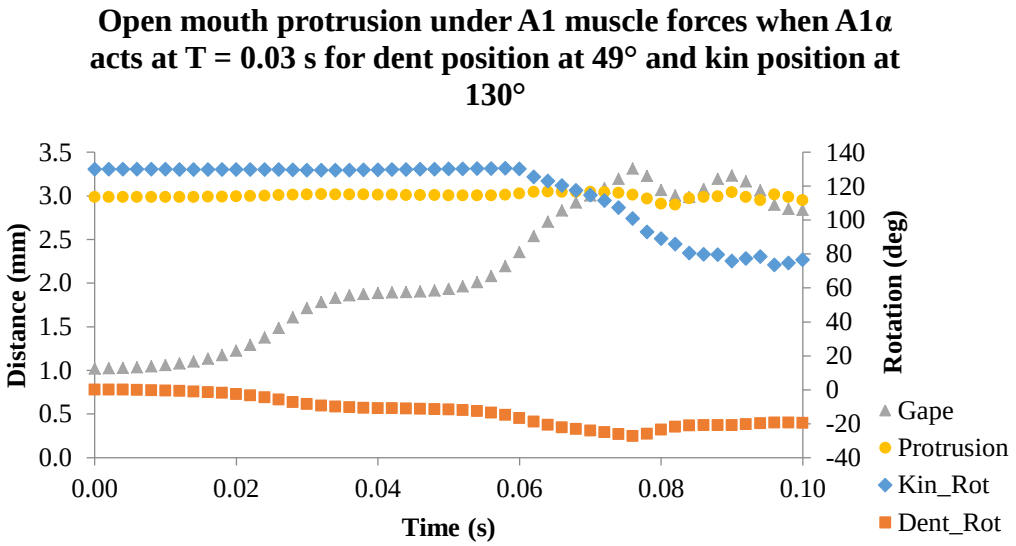

Figure 43: Gape, protrusion, kinethmoid rotation and dentary rotation when A1α acts upon the maxilla at 0.03 seconds after A1β acts.

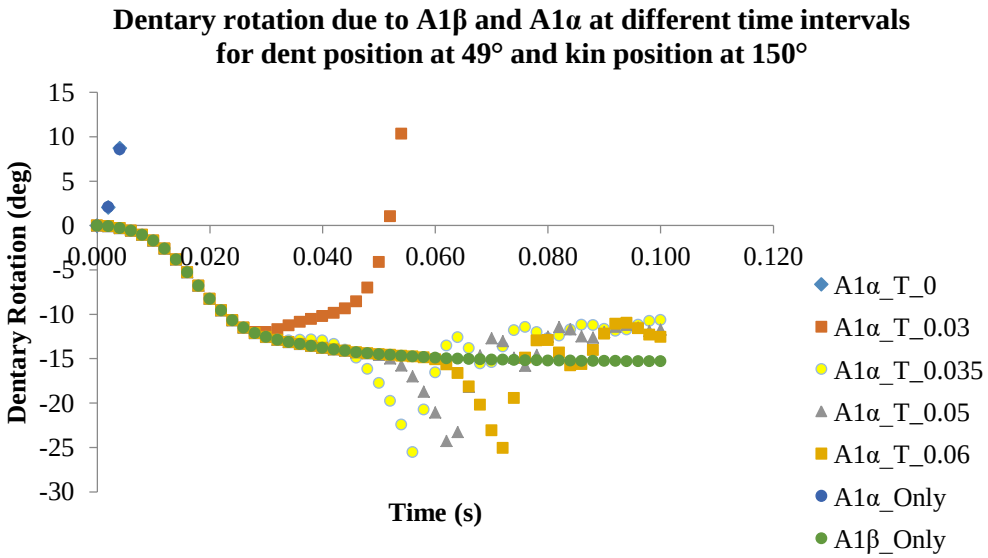

Figure 44: Effect of A1α = 24 dynes and A1β = 12 dynes on dentary opening during open mouth process

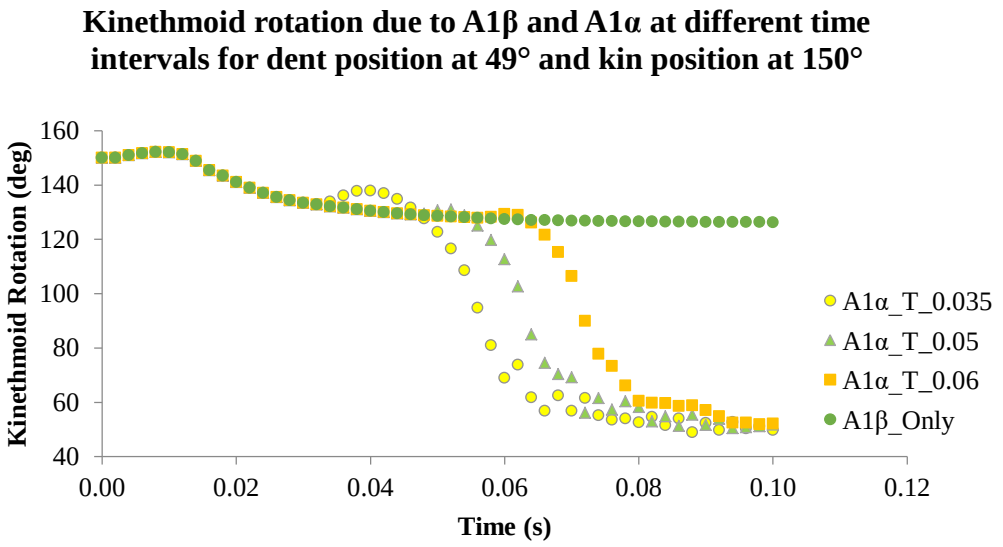

Figure 45: Effect of A1α = 24 dynes and A1β = 12 dynes on kinethmoid rotation during open mouth process

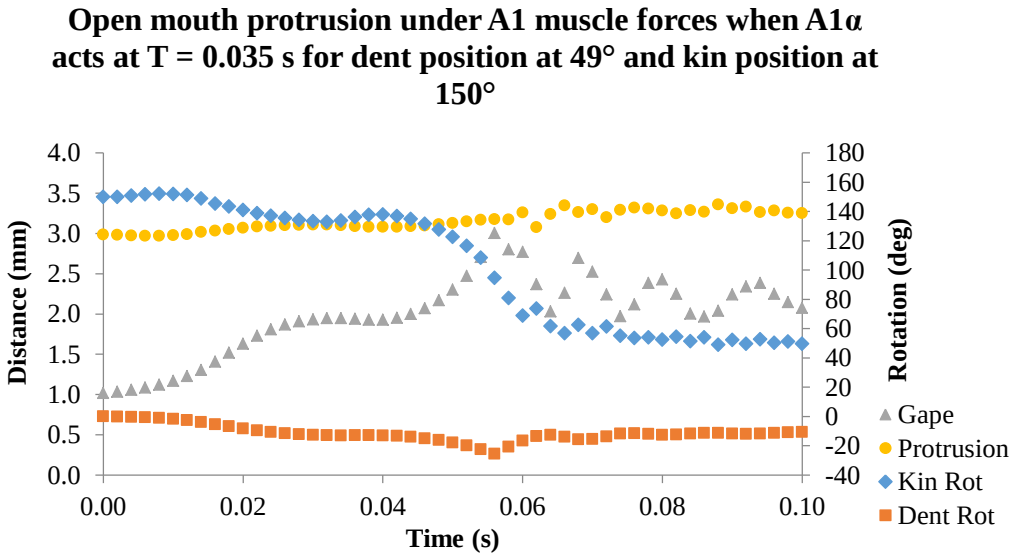

Figure 46: Gape, protrusion, kinethmoid rotation and dentary rotation when A1α acts upon the maxilla at 0.035 seconds after A1β acts.

3.5 Experiment E: Effect of a fictitious dentary force F on mouth opening

Figure 47 and 48 show the effects of fictitious force F on the kinethmoid and dentary rotations. In the model only force F of 30 dynes is acting at the tip of the dentary. The positive values indicate rotation in the clockwise direction. See CD for simulation.

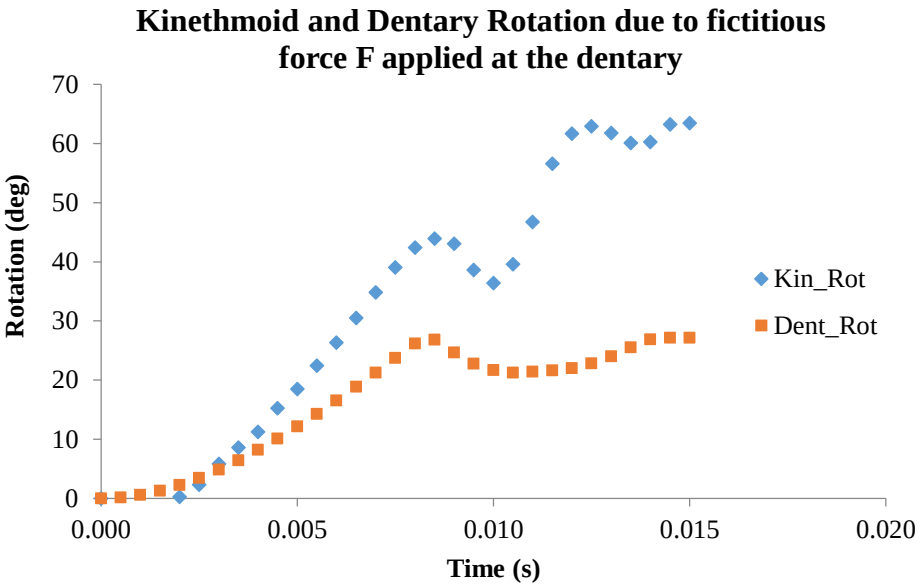

Figure 47: Kinethmoid and Dentary Rotation due to application of a fictitious force F at the dentary

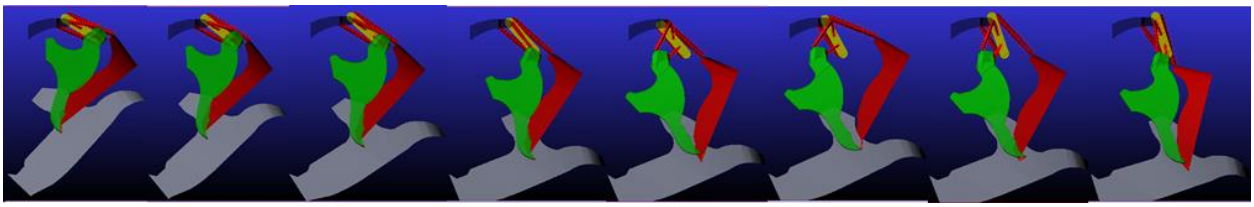

Figure 48: Animation frames for Experiment E test 1 simulation

Figure 49 shows the effects of fictitious force F on the kinethmoid and dentary rotations. In the model maxillary forces, A1αand A1β, and a fictitious force F of 10 dynes are acting. The simulation is only carried out for 0.05 secs because the mouth opens fairly quickly due to the additional force input. See CD for simulation.

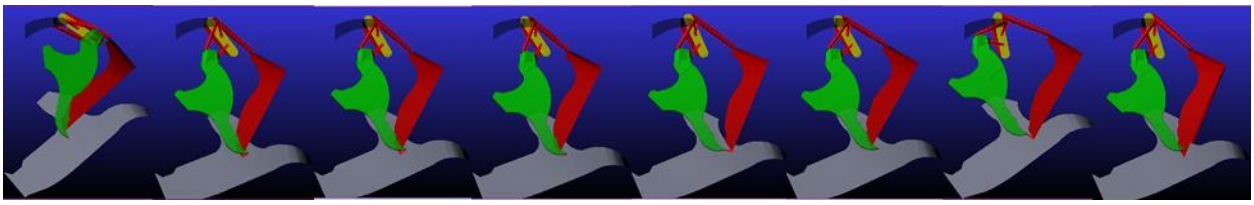

Figure 49: Animation frames for experiment E test 2 simulations

4.0 DISCUSSIONS

While the 3D model was built as accurately as possible given the tools and conditions, it is important to note that there were uncertainties involved with dimensional measurements of the bones. For instance, measurements were collected using ImageJ from images taken of the bones. These images don't give the exact 3D profile of the bones and as such they were protruded straight out in the z direction, but more accurate in the XY plane. The estimated protrusion or the thickness of the bones along with +/- 0.5 mm uncertainty from the measuring scale affects moment of inertia of each individual bone. This in turn affects the angular velocity with which these bones rotate about their axis of rotation and they rotate about 3 axes. While the results obtained from the simulations are not precise, the accuracy of the trends is not affected. In the future, we could scan the bones for more accurate 3D dimensions so that these uncertainties are almost negligible.

4.1 Experiment A: Kinethmoid's resting position under suspension

Figures 26 and 27 clearly show that the kinethmoid is capable of achieving static equilibrium states under gravity without being attached to the maxillae. This means that while the kinethmoid is connected to the maxillae, it does not have to rely on them simply for support. This could mean that the importance of maxillary attachment to the kinethmoid lies in rotating the kinethmoid. This is a new finding about the kinethmoid, which would not have been discovered without the help of multibody dynamics software programs. While the kinethmoid approached stability for all initial kin(θ_Z) values in figure 27 , the deviation from its initial kin(θ_Z) increased as the initial kin(θ_Z) value increased. Since the rotation of the kinethmoid is the most important prerequisite to protruding the premaxilla, it would make sense for the kinethmoid to be less

stable in order to allow ease of rotation. If this is the case, then the experiments conducted later in the research should favor a greater initial kinethmoid position.

4.2 Experiment B: Effect of initial kinethmoid positions and initial dentary positions on mouth opening under constant A1β muscle force

In figures 29, 30 and 31, the dentary rotates counterclockwise (+ deg) for starting positions of 53.44°, 51.5° and 50°. While the graphs show that the mouth adducts to 35 degrees in some cases, it is important to remember that this is happening due to a lack of mandibularis muscles in the model that connect to the dentary. At these initial dentary angles, no amount of variation in initial kinethmoid position will abduct the dentary for A1β force equal to 1 dyne. An interesting change is observed between figures 31 and 32 where the dentary finally begins to abduct, a motion necessary for mouth opening. Figures 32 and 33 show that initial dentary positions of 49° or less facilitate mouth opening because the dentary rotates clockwise (- deg) for the range of initial kinethmoid positions and a minimum value of A1β. When the dentary's starting angle decreases from 49° to 48°, its angular speed increases while its maximum displacement value decreases ever so slightly. These results are very similar to the ones concluded by Ballintijn where he states that stimulation of A1β when the dentary is abducted results in protrusion of the upper lip, the farther the lower jaw is abducted, the more pronounced is the effect and when the dentary is adducted, A1β stimulation has no visible effect (Ballintijn et al., 1972). All graphs, in figures 29 through 33, show that initial kinethmoid positions do not affect the rate at which the dentary rotates, however, they increase the maximum displacement obtained by the dentary. In figures 32 and 33, decreasing initial kinethmoid positions produces greater dentary angular displacements. Figure 34 shows that for lower values of initial kin(θ_z), the kinethmoid rotates slightly clockwise followed by a counterclockwise angular displacement. This is contradictory to

past experiment results obtained through XROMM for a carp, where the kinethmoid rotates counterclockwise initially then rotates clockwise to protrude the premaxilla forward (Gidmark et. al, 2012). Because lower values of initial kin(θ_z) causes kinematic patterns opposite of the ones obtained in past experiments, higher kin(θ_z) values seem to produce favorable results.

4.3 Experiment C: Effect of increasing A1β, initial kinethmoid position and initial dentary position on mouth opening

In figures 35, 36 and 37 where the initial dentary angle is at 53.44°, increasing A1β force is increased from 1 dyne to 1000 dynes or increasing initial kinethmoid position did not abduct the dentary at all. This confirms that the dentary is a major, if not the primary, cause of dentary abduction. It sets the line of action of A1β, which is why increasing this force only increases dentary angular displacement in the counterclockwise direction. Increasing initial kinethmoid positions from 90° to 150° in figures 35, 36 and 37 resulted in decreasing angular displacements of the dentary. This could be due to greater force required to rotate the kinethmoid since the maxilla is connected to the kinethmoid about its ventral end.

In figures 38, 39 and 40, when the initial dentary angle is lowered to 50°, the mouth opens for all initial kinethmoid positions as long as a specific amount of A1β force is applied on the maxilla. In Figure 38, the dentary abducts for A1β values equal to or greater than 391 dynes. In Figure 39, the dentary abducts for A1β values equal to or greater than 387 dynes and in Figure 40, the dentary abducts for A1β values equal to or greater than 183 dynes. As the initial kin(θ_z) increased from 90° to 150°, once again the dentary's angular displacement decreased. But what is interesting is that with increasing initial kin(θ_z), the amount of A1β force required to open the mouth decreased from 391 dynes to 183 dynes. This means that at higher initial kin(θ_z) values, the system uses less energy to open the mouth.

4.4 Experiment D: Effect of both A1α and A1β muscles' activation patterns on mouth opening

Figure 41 shows the dentary's angular displacement when A1α and A1β muscles are applied to it. When only A1β of 5 dynes is applied on the maxilla, the dentary abducts as it can be predicted from results 3.2. When only A1α of 10 dynes is applied on the dentary, the dentary adducts instead. This is clearly due to a difference in point of application and line of action of A1α muscle. When both A1α and A1β are applied, the dentary adducts again. Only when A1α is applied at a time interval of 0.03 seconds after A1β activates, the dentary begins to abduct. This means that the importance of A1α's activation time lies in the position of the dentary if it is to open the mouth. All following activation times seem to abduct the dentary. Only those conditions that initiated dentary abduction were used to obtain kinethmoid's angular displacement as shown in Figure 42. It is clear the while A1β abducts the dentary; it only rotates the kinethmoid by about 3°. A1α, on the other hand, brings about 55° of rotation for activation times of 0.03 seconds or greater. Figure 43 shows the gape and protrusion when A1α activates at 0.03 seconds. The gape increases from about 1 mm to 3.3 mm, thereby opening for about 2.3 mm. The model attains maximum gape in 76 milliseconds, right about when the dentary abducts to its maximum limit. It then adducts due to spring force from the ligaments. The premaxilla protrudes about 0.05 mm and most of the protrusion happens after the kinethmoid begins to rotate.

Figure 44 shows the effects of A1 muscles on the dentary's angular displacements when the dentary is at 49° and the kinethmoid at 150°. Here, since the initial kinethmoid increases from 130° to 150°, greater A1β force is needed to adduct the dentary. For only A1β force of 12 dynes, the dentary abducted just as observed before. When only A1α of 24 dynes is applied on the dentary or when both A1α and A1β are applied, the dentary adducts in both cases again. Only

when A1α is applied at a time interval of 0.035 seconds after A1β activates, the dentary begins to abduct again and all following activation times also do the same. Only those conditions that initiate dentary abduction are used to obtain kinethmoid's angular displacements as shown in Figure 45. Once again, while A1β abducts the dentary, it only rotates the kinethmoid by about 25°. A1α, on the other hand, brings about 100° of kinethmoid rotation for activation times of 0.035 seconds or greater. Figure 46 shows the gape and protrusion when A1α activates at 0.035 seconds. The gape increases from about 1 mm to 3 mm, thereby opening for a total of 2 mm. The model attains maximum gape in 56 milliseconds, which is also when the dentary abducts to its maximum limit. It then adducts due to spring force from the ligaments. The premaxilla protrudes about 0.358 mm and most of the protrusion happens after the kinethmoid begins to rotate.

Simulation results obtained in figures 44 and 45 for kinethmoid and dentary rotations, respectively, compared with XROMM results shown in Figure 6 show at the very least a high correlation between dentary and kinethmoid rotations. An interesting behavior is seen in Figure 6 for MNDrz where the dentary abducts only to slightly adduct and abduct again while the kinethmoid continues to rotate clockwise. This same behavior is visible in figures 44 and 45. However, unlike XROMM results where it is hard to predict what may have caused that behavior, in our case, this behavior is due to the activation of A1α muscle acting on the maxilla. This shows that simulating models can help explain the mechanics of suction feeding in Cypriniformes.

4.5 Experiment E: Effect of a fictitious dentary force F on mouth opening

Experiment E was carried out to see if the mouth could be opened by applying a fictitious dentary force on the model. Both figures 47 and 48 show that this fictitious force F is in fact able to open the mouth but it does it differently. Figure 47 shows that both kinethmoid and dentary

rotate clockwise with kin(θ_Z) maximum value of 63.2° and dent(θ_Z) maximum value of 26.8°. These values can change with increasing or decreasing F value. Therefore, more than the numbers, it is important here to observe that the motions of both bones are correlated. In this test, the kinethmoid rotated only about 63° for a dentary rotation of about 26°. Whereas in figures 44 and 45, where maxillary forces act together to open the mouth, the kinethmoid rotates about 81° for a dentary rotation of about 25°. This shows that this fictitious force is capable of rotating the dentary but it produces less kinethmoid rotation. This could be due to the maxilla's connection to the palatine through ligament 3 which allows A1α to pull on the maxilla horizontally aiding in higher kinethmoid rotation. When fictitious force acts alone on the model, the only motion that the maxilla is allowed to pursue is in the ventral direction and this does not allow the kinethmoid to rotate as much.

Adding both maxillary forces and fictitious force in test 2 shows that the mouth opens faster and the premaxilla protrudes further as seen in figure 49. Maximum protrusion occurs under the influence of A1α muscle once again.

5.0 CONCLUSIONS AND RECOMMENDATIONS

5.1 Conclusions

It was interesting to find that the kinethmoid was able to stay suspended under gravity at various kinethmoid positions while only being attached to three parts, the neurocranium, the palatines and the premaxilla. This allowed the kinethmoid to be at various starting positions even though an attempt to capture starting positions of the kinethmoid in vivo has not been undertaken so far. Understanding that ligaments involved here may not support the kinethmoid like springs do, there is a possibility that the main function of the maxilla in the mouth is to rotate the kinethmoid. For this thesis, four parameters such as initial kinethmoid position, initial dentary

position, and A1α and A1β muscles were chosen and analyzed. Maxillary forces produced by A1α and A1β are known to abduct the dentary and protrude the mouth open, but proper sequential activation was key to understanding mouth opening process. The first main observation was that the starting position of the dentary initiated mouth opening. Figures 29 through 33 showed that until the dentary attained an angle of 50°, the other three parameters failed to open the mouth. At 50°, the dentary abducted for higher values of A1β as shown in Figure 31 but at 49°, the dentary abducted for all values of initial kinethmoid positions and A1β as shown in Figure 32. This angle can be called the ideal dentary angle. Keeping the dentary at a constant position, increasing values of A1β as opposed to changing kinethmoid's starting position had a greater effect on dentary rotation. However, the kinethmoid's initial position and A1α had a greater effect on premaxillary protrusion. From Figures 42 and 45, it is clear that the kinethmoid rotates in the clockwise direction only when A1α is activated. Only when the kinethmoid rotated, the premaxilla protruded forward. Also, increasing the initial kinethmoid position from 130° to 150° increased the total rotational displacement of the kinethmoid from about 55° to about 100°. This increased rotational displacement of the kinethmoid had a direct effect on its premaxillary protrusion distance, which increased from about 0.05 mm to 0.358 mm, and gape, which decreased from 2.3 mm to 2 mm. This clearly shows that the initial position of the kinethmoid influences both premaxillary protrusion and gape.

These results mark just the beginning of the efficiency of Adams for future kinematic research questions. While the relationship between the four parameters and mouth opening is complex due to several other parameters acting synchronously, this was the first attempt to build a realistic 3D model using physical measurements, past EMG and XROMM kinematic results as

guides. XROMM method is limited as it is currently time-consuming and can only be applied to larger fishes.

5.2 Recommendations

The current model is far from perfect due to several errors that could have accumulated as a result of assumptions and simplifications, which can be divided into three main categories. They are joints, ligaments and muscle inputs.

Joints

The first assumption was that the bones of a goldfish's mouth would share the same relations as the bones of a carp's mouth. Because there has been more research on carp's mouth's parts, it was convenient to translate those relations into the current goldfish model since physically the two species share the same number of mouth parts, ligaments and maxillary muscles. This means that joint properties might not necessarily be the same. The dentary is connected to the maxilla by a ligament that though translates the movement between maxilla and dentary, is also slack enough to permit the downward extension movement without influencing the position of the lower jaw, unless the extension is very great (Ballintijn, 1972). Due to the maxilla's ability to rotate about global z-axis and to move some distance in the y direction, the ligament could be modeled as a sliding pin joint in future studies. This is to allow for the possibility of closed mouth protrusions where the maxillary forces protrude the premaxilla forward without abducting the dentary. In the future, an attempt to calculate the exact distance of vertical mobility or to collect accurate joint kinematics will help produce an accurate model.

Ligaments

Due to time constraint and lack of resources, the ligaments were modeled as linear springs with varying stiffness values and damping ratios. While springs contract and extend from

original length, ligaments slack in the presence of compressive force and slightly give under tensile forces. Also, varying proportions of elastin to collagen fibers among ligaments lead to different mechanical properties for each ligament. Tensile tests should be conducted on each ligament to obtain load-deformation curves, which will help model ligaments more accurately. Large differences in stiffness values and damping ratios do impact kinematic results so using exact values will help reduce errors.

Muscle

Muscle activation patterns observed in EMG graphs for a carp may or may not be the same for goldfish. While the dentary was lowered as a result of A1β activity in this model, in reality there are other muscles that also control dentary motion. They are the mandibularis muscles, which are A2, A3 and Aω for carps. More information is needed for these muscles in Goldfish.

REFERENCES

Anker, G.Ch. 1974. Morphology and kinetics of the stickleback, *Gasterosteus aculeatus*. Trans. Zool. Soc. (London) 32: 311-416.

Ballintijn, C.M., Van den Burg, A., and Egberink, B.P. 1972. An electromyographic study of the adductor mandibulae complex of a free-swimming carp (Cyprinus Carpio L .) during feeding. *Journal of Experimental Biology* 57: 261–283.

Carroll, A. M. 2004. Muscle Activation and Strain during Suction Feeding in the Largemouth Bass Micropterus Salmoides. *Journal of Experimental Biology* 207: 983-91.

Danos, N., and K. L. Staab. 2010. Can Mechanical Forces Be Responsible for Novel Bone Development and Evolution in Fishes? *Journal of Applied Ichthyology* 26: 156–161.

Gidmark, N. J., Staab, K. L., Brainerd, E. L., & Hernandez, L. P. (2012). Flexibility in starting posture drives flexibility in kinematic behavior of the kinethmoid-mediated premaxillary protrusion mechanism in a cyprinid fish, Cyprinus carpio. *Journal of Experimental Biology*, *215*, 2262–72.

Hill, A.V., 1938. The heat of shortening and the dynamic constants of muscle. Proc. R. Soc. B. 141: 104-117.

Holzman, Roi, Steven W. Day, Rita S. Mehta, and Peter C. Wainwright. 2008. Jaw Protrusion Enhances Forces Exerted on Prey by Suction Feeding Fishes. *Journal of the Royal Society Interface* 5, 1445-457.

Lauder, By George V. 1980. The Suction Feeding Mechanism in Sunfishes (Lepomis): An Experimental Analysis. *Journal of Experimental Biology*: 49–72.

McMahon, T.A., 1984. Muscles, Reflexes, and Locomotion. Princeton University Press , Princeton, NJ.

Muller, M. 1987. Optimization principles applied to the mechanism of neurocranium levation and mouth bottom depression in bony fishes (Halecostomi). Journal of Theoretical Biology 126: 343-368.

Potthoff, T. 1984. Clearing and Staining Techniques. In: Moser, H.G., Richards, W.J., Cohen, D.M., Fahay, M.P., Kendall Jr., A.W., Richardson, S.L. (Eds.), Ontogeny and Systematics of Fishes, vol. 1. American Society of Ichthyologists and Herpetologists, pp. 35-37, Spec. Publ.

Rome, L.C., Sosnicki, A., Choi, I.H. 1992. The Influence of Temperature on muscle function in the fast swimming scup II. The mechanics of red muscle. J. Exp. Biol. 163, 281-295.

Spector, S. A., P. F. Gardiner, R. F. Zernicke, R. R. Roy and V. R. Edgerton. 1980. Muscle architecture and force-velocity characteristics of cat soleus and medial gastrocnemius: implications for motor control. Journal of Neurophysiology 44:951-960

Staab, Katie Lynn, Lara a Ferry, and L Patricia Hernandez. 2012a. Comparative Kinematics of Cypriniform Premaxillary Protrusion. *Zoology (Jena, Germany)* 115: 65–77.

Staab, Katie Lynn, Roi Holzman, L Patricia Hernandez, and Peter C Wainwright. 2012b. Independently Evolved Upper Jaw Protrusion Mechanisms Show Convergent Hydrodynamic Function in Teleost Fishes. *The Journal of Experimental Biology* 215: 1456–63.

Wainwright, P.C., A. M. Carroll, D. C. Collar, S. W. Day, T. E. Higham, and R. A. Holzman. 2007. Suction Feeding Mechanics, Performance, and Diversity in Fishes. *Integrative and Comparative Biology* 47: 96-106.

Wainwright, P. C., R. S. Mehta, and T. E. Higham. 2008. Stereotypy, Flexibility and Coordination: Key Concepts in Behavioral Functional Morphology. *Journal of Experimental Biology* 211: 3523-528.

Westneat, M. W. 1990. Feeding Mechanics of Teleost Fishes (Labridae ; Perciformes): A Test of Four-Bar Linkage Models. Journal of Morphology 205: 269-295.

Westneat, M. W. 2003. A Biomechanical Model for Analysis of Muscle Force, Power Output and Lower Jaw Motion in Fishes. *Journal of Theoretical Biology* 223: 269–281.

Wu, Kao-yi, and Shih-chieh Shen. 2004. Review of the Teleostean Adductor Mandibulae and Its Significance to the Systematic Positions of the Polymixiiformes, Lampridiformes, and Triacanthoidei. 43: 712–736.

Basmajian JV, DeLuca CJ, Muscles Alive. Their function revealed by electromyography. Baltimore: Williams & Wilkins, 1985.

APPENDIX

Appendix A (Adams Validation)

Adams Settings for double pendulum simulation

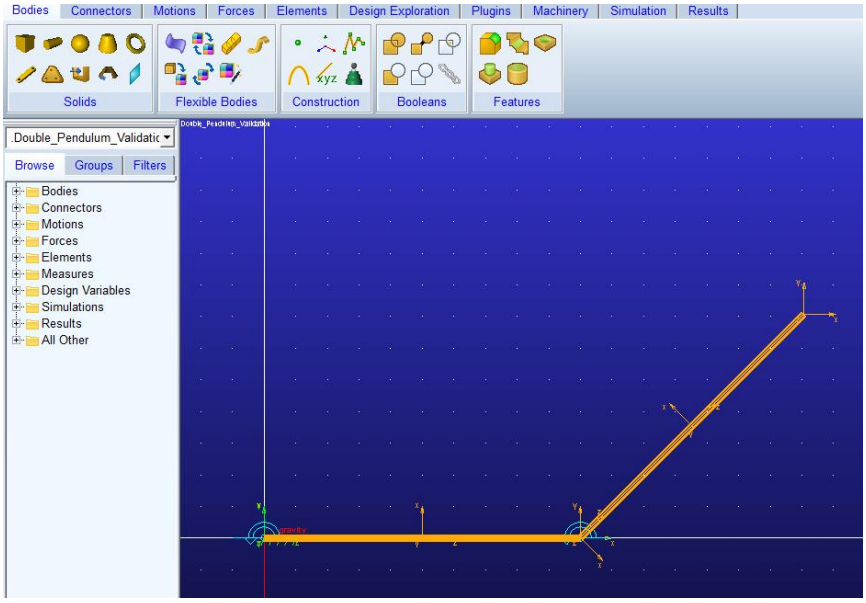

Object Name : .Double_Pendulum_Validation.Link1
Object Type : Part
Parent Type : Model
Adams ID : 2
Active : NO_OPINION
Global :
Location: 0.0, 0.0, 0.0 (meter, meter, meter)
Orientation: 0.0, 0.0, 0.0 (rad)
Ground Part : False
Material : .Double_Pendulum_Validation.steel
Material Density : 7801.0 (7801.0(kg/meter**3)) kg/meter**3
Calculated Mass : 2.4507564291 kg
Calculated Volume : 3.1415926536E-004 meter**3
Center Marker : Link1.cm
Inertia Marker : None
Mass Inertia Tensor:
IXX : 0.2042909713 kg-meter**2
IYY : 0.2042909713 kg-meter**2
IZZ : 1.2253782145E-004 kg-meter**2
IXY : 0.0 kg-meter**2
IZX : 0.0 kg-meter**2
IYZ : 0.0 kg-meter**2
No Initial Velocities
Exact Coordinates : None

Object Name : .Double_Pendulum_Validation.Link2
Object Type : Part
Parent Type : Model
Adams ID : 5
Active : NO_OPINION
Global :
Location : 0.0, 0.0, 0.0 (meter, meter, meter)
Orientation : 0.0, 0.0, 0.0 (rad)
Ground Part : False
Material : .Double_Pendulum_Validation.steel
Material Density : 7801.0 (7801.0(kg/meter**3)) kg/meter**3
Calculated Mass : 2.4507564291 kg
Calculated Volume : 3.1415926536E-004 meter**3
Center Marker : Link2.cm
Inertia Marker : None
Mass Inertia Tensor :
IXX : 0.2042909713 kg-meter**2
IYY : 0.2042909713 kg-meter**2
IZZ : 1.2253782145E-004 kg-meter**2
IXY : 0.0 kg-meter**2
IZX : 0.0 kg-meter**2
IYZ : 0.0 kg-meter**2
No Initial Velocities
Exact Coordinates : None

Object Name : .Double_Pendulum_Validation.JOINT_1
Object Type : Revolute Joint
Parent Type : Model
Adams ID : 1
Active : NO_OPINION
I Marker : .Double_Pendulum_Validation.Link1.MARKER_3
J Marker : .Double_Pendulum_Validation.ground.MARKER_4
Initial Conditions
Angular Displacement : 0.0 rad
Angular Velocity : 0.0 rad/sec

Object Name : .Double_Pendulum_Validation.JOINT_2
Object Type : Revolute Joint
Parent Type : Model
Adams ID : 2
Active : NO_OPINION
I Marker : .Double_Pendulum_Validation.Link2.MARKER_10
J Marker : .Double_Pendulum_Validation.Link1.MARKER_11
Initial Conditions
Angular Displacement : 0.0 rad
Angular Velocity : 0.0 rad/sec

Matlab Analysis Code

```
%This program will simulate a double pendulum system. One end of Cylinder 1
is connected to a fixed reference point by a pin joint and its other end is
connected to Cylinder 2 by a pin joint.

% Double pendulum simulation with differentiated constraints
% written by: Mario W. Gomes
% date: Dec. 13, 2012

clear all;
clf reset;
format compact;
format long;

global m1 m2 l1 l2 d1 d2 I1 I2 g;

%time span for integration
t0 = 0;
tf = 3;

%state vector
%theta1
%theta2
%theta1dot
%theta1dot

%system parameters
l1 = 1; %length of link 1 in [m]
l2 = 1; %length of link 2 in [m]
d1 = 0.01; %radius of cylinder in [m]
d2 = 0.01; %radius of cylinder in [m]
m1 = 2.4507564291; %mass of link 1 in [kg]
m2 = 2.4507564291; %mass of link 2 in [kg]
g = 9.80665; %gravity [m/s^2]
I1 = 1/12*m1*(3*(d1^2)+(l1^2)); %moment of inertia of cylinder about cm
I2 = 1/12*m2*(3*(d2^2)+(l2^2)); %moment of inertia of cylinder about cm

%initial conditions
th1_0 = pi/2; %link 1 is horizontal at 90 deg from vertical counterclockwise
th2_0 = 3/4*pi; %link 2 is at 45 deg counterclockwise from horizontal
th1d_0 = 0;
th2d_0 = 0;

IC = [th1_0; ...
      th2_0;...
      0.0;
      0.0]; %[th1 th2 th1d th2d]

options = odeset('RelTol',1e-7,'AbsTol',1e-7);

time_vect = linspace(0,tf,900);

[time, state] = ode45(@deriv4, time_vect ,IC,options);
```

```
% draw animation
figure(1)

th1 = state(:,1);
th2 = state(:,2);
th1d = state(:,3);
th2d = state(:,4);

link1 = line([0  l1*sin(th1(1))],[0 -l1*cos(th1(1))]);
link2 = line([l1*sin(th1(1))  l1*sin(th1(1))+l2*sin(th2(1))],[-l1*cos(th1(1))
-l1*cos(th1(1))-l2*cos(th2(1))]);

wid = l1+l2;
axis([-wid wid -wid wid]);
axis square;
grid on;
for i = 2:length(th1)
    set(link1,'xdata',[0  l1*sin(th1(i))],'ydata',[0 -l1*cos(th1(i))]);
    set(link2,'xdata',[l1*sin(th1(i))
l1*sin(th1(i))+l2*sin(th2(i))],'ydata',[-l1*cos(th1(i)) -l1*cos(th1(i))-
l2*cos(th2(i))]);
    drawnow;
end

%make energy plot
figure(2)
for ind=1:length(th1),
    %unit vectors
    i = [1 0 0]';
    j = [0 1 0]';
    k = [0 0 1]';
    u1 = [sin(th1(ind)) -cos(th1(ind)) 0]';
    u2 = [cos(th1(ind)) sin(th1(ind)) 0]';
    u3 = [sin(th2(ind)) -cos(th2(ind)) 0]';
    u4 = [cos(th2(ind)) sin(th2(ind)) 0]';
    %angular velocities
    w1 = th1d(ind)*k;
    w2 = th2d(ind)*k;
    %position vectors
    r_a_o = l1*u1;
    r_cm1_o = l1/2*u1;
    r_cm2_a = l2/2*u3;
    r_cm2_o = r_a_o + r_cm2_a;

    v1_A = sqrt((l1/2*th1d(ind)*cos(th1(ind))).^2 +
(l1/2*th1d(ind)*sin(th1(ind))).^2);
    v1 = norm(cross(w1,r_cm1_o),2);
    v2 = norm(cross(w1,r_a_o) + cross(w2,r_cm2_a),2);

    KE(ind) = 1/2*m1*v1^2 + 1/2*I1*th1d(ind)^2 + 1/2*m2*v2^2 +
1/2*I2*th2d(ind).^2;
    PE(ind) = m1*g*dot(r_cm1_o,j) + m2*g*dot(r_cm2_o,j);
    Tot_eng(ind) = KE(ind) + PE(ind);
end
```

```
plot(time, Tot_eng);
xlabel('time [s]');
ylabel('Total System Energy [J]');

%make phase plane plot
figure(3)
plot(th1, th2);
xlabel('theta1 [rad]');
ylabel('theta2 [rad]');
```

```
function [statedot] = deriv4(time,state)
%DERIV this function calcuates the derivative of the state vector

%state = [th1 th2 th1d th2d]
global m1 m2 l1 l2 d1 d2 I1 I2 g;

th1 = state(1);
th2 = state(2);
th1d = state(3);
th2d = state(4);

%[th1dd, th2dd, Rx, Ry, Fx, Fy];

b = -eqnn(state,0,0,0,0,0,0)';
eq(:,1) = eqnn(state,1,0,0,0,0,0)'+b;
eq(:,2) = eqnn(state,0,1,0,0,0,0)'+b;
eq(:,3) = eqnn(state,0,0,1,0,0,0)'+b;
eq(:,4) = eqnn(state,0,0,0,1,0,0)'+b;
eq(:,5) = eqnn(state,0,0,0,0,1,0)'+b;
eq(:,6) = eqnn(state,0,0,0,0,0,1)'+b;

z = inv(eq)*b;

statedot = [th1d;...
            th2d;...
            z(1);...
            z(2)];

end
```

```
function [ eqn ] = eqnn(state, th1dd, th2dd, Rx, Ry, Fx, Fy)
%UNTITLED Summary of this function goes here
%   Detailed explanation goes here
global m1 m2 l1 l2 I1 I2 g;
i = [1 0 0]';
j = [0 1 0]';
k = [0 0 1]';

th1 = state(1);
th2 = state(2);
th1d = state(3);
th2d = state(4);
```

```
%unit vectors
u1 = [sin(th1) -cos(th1) 0]';
u2 = [cos(th1) sin(th1) 0]';
u3 = [sin(th2) -cos(th2) 0]';
u4 = [cos(th2) sin(th2) 0]';

%constraint forces
F = Fx*i + Fy*j;
R = Rx*i + Ry*j;

%angular velocities
w1 = th1d*k;
w2 = th2d*k;

%angular accels
alph1 = th1dd*k;
alph2 = th2dd*k;

%position vectors
r_a_o = l1*u1;
r_cm1_o = l1/2*u1;
r_cm2_a = l2/2*u3;
r_o_cm1 = -r_cm1_o;
r_a_cm1 = l1/2*u1;
r_a_cm2 = -l2/2*u3;

%Linear acceleration vectors of points
a_cm1A = cross(w1,cross(w1,r_cm1_o)) + cross(alph1,r_cm1_o);
a_cm1 = -l1/2*th1d^2*u1 + th1dd*l1/2*u2;
a_a = -l1*th1d^2*u1 + th1dd*l1*u2;
a_cm2A = a_a + cross(w2,cross(w2,r_cm2_a)) + cross(alph2,r_cm2_a);
a_cm2 = a_a -l2/2*th2d^2*u3 + th2dd*l2/2*u4;

%Linear Momentum Balance for Link 1
LinM1 = R + F -m1*g*j - m1*a_cm1;
eqn(1) = LinM1(1);
eqn(2) = LinM1(2);
%Angular Momentum Balance for Link 2
AngM1_cm1 = cross(r_o_cm1,R) + cross(r_a_cm1,F) - I1*alph1;
eqn(3) = AngM1_cm1(3);

%Linear Momentum Balance for Link 2
LinM2 =  -F - m2*g*j - m2*a_cm2;
eqn(4) = LinM2(1);
eqn(5) = LinM2(2);
%Angular Momentum Balance for Link 2
AngM2_cm2 = cross(r_a_cm2,-F) - I2*alph2;
eqn(6) = AngM2_cm2(3);

end
```

Appendix B (Images)

Kinethmoid (Left) and Maxillae (Right)

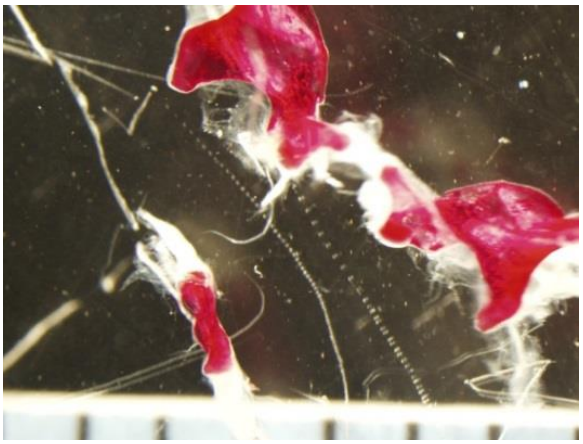

Premaxilla (Upper) and Dentary (Lower)

Dentary (Left) and Premaxilla (Right)

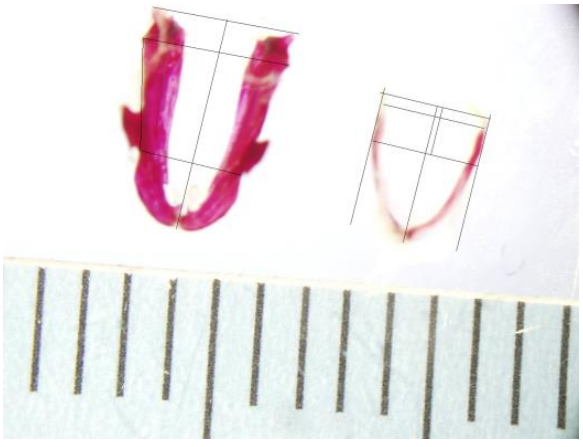

Appendix C (Solidworks CAD Drawings and Adams Model)

Dentary

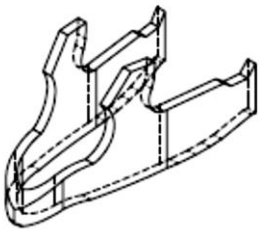

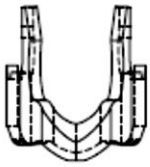

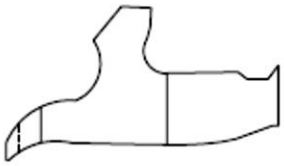

Premaxilla

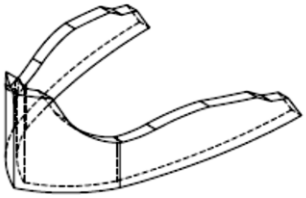

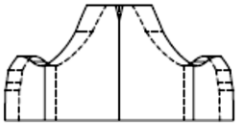

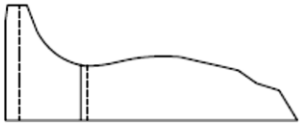

Left and Right Maxilla

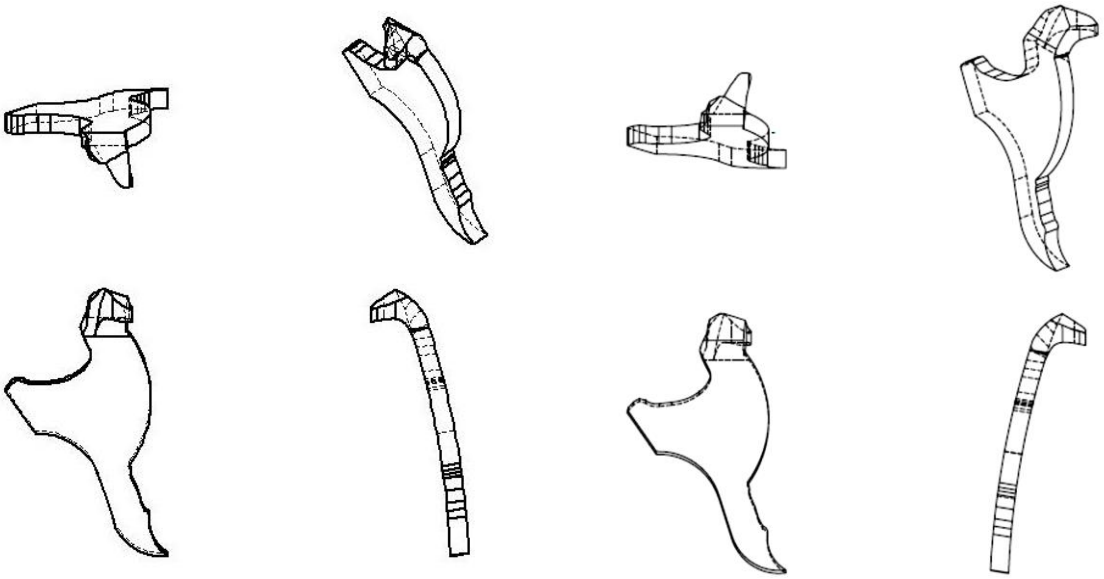

Palatine Neurocranium

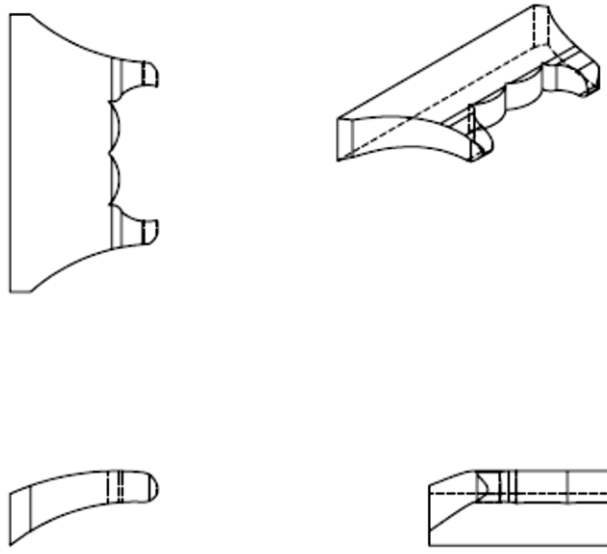

Appendix D (Experimental Data)

2.3 Muscle Modeling

Figure 11

V/Vmax	F/Fmax
0	1.000
0.010	0.952
0.020	0.907
0.030	0.866
0.040	0.828
0.050	0.792
0.060	0.758
0.070	0.727
0.080	0.697
0.090	0.669
0.100	0.643
0.110	0.618
0.120	0.595
0.130	0.572
0.140	0.551
0.150	0.531
0.160	0.512
0.170	0.494
0.180	0.477
0.190	0.460
0.200	0.444
0.210	0.429
0.220	0.415
0.230	0.401
0.240	0.388
0.250	0.375
0.260	0.363
0.270	0.351
0.280	0.340
0.290	0.329
0.300	0.318
0.310	0.308
0.320	0.298
0.330	0.289
0.340	0.280
0.350	0.271
0.360	0.262
0.370	0.254
0.380	0.246
0.390	0.238
0.400	0.231
0.410	0.223
0.420	0.216
0.430	0.210
0.440	0.203
0.450	0.196
0.460	0.190
0.470	0.184
0.480	0.178
0.490	0.172
0.500	0.167
0.510	0.161
0.520	0.156
0.530	0.151
0.540	0.146
0.550	0.141
0.560	0.136
0.570	0.131
0.580	0.127
0.590	0.122
0.600	0.118
0.610	0.113
0.620	0.109
0.630	0.105
0.640	0.101
0.650	0.097
0.660	0.093
0.670	0.090
0.680	0.086
0.690	0.082
0.700	0.079
0.710	0.076
0.720	0.072
0.730	0.069
0.740	0.066
0.750	0.063
0.760	0.059
0.770	0.056
0.780	0.053
0.790	0.050
0.800	0.048
0.810	0.045
0.820	0.042
0.830	0.039
0.840	0.037
0.850	0.034
0.860	0.032
0.870	0.029
0.880	0.027
0.890	0.024
0.900	0.022
0.910	0.019
0.920	0.017
0.930	0.015
0.940	0.013
0.950	0.010
0.960	0.008
0.970	0.006
0.980	0.004
0.990	0.002
1.000	0.000

Figure 14

V/Vmax	F @ Smax=100 kN/m2	F @ Smax=150 kN/m2	F @ Smax=200 kN/m2
0	41062.370	61593.555	82124.740
0.010	39088.218	58632.327	78176.436
0.020	37260.299	55890.448	74520.598
0.030	35562.946	53344.418	71125.891
0.040	33982.651	50973.977	67965.302
0.050	32507.710	48761.565	65015.419
0.060	31127.926	46691.889	62255.852
0.070	29834.378	44751.568	59668.757
0.080	28619.228	42928.842	57238.455
0.090	27475.557	41213.335	54951.113
0.100	26397.238	39595.857	52794.476
0.110	25378.826	38068.239	50757.652
0.120	24415.463	36623.195	48830.927
0.130	23502.804	35254.206	47005.608
0.140	22636.948	33955.422	45273.895
0.150	21814.384	32721.576	43628.768
0.160	21031.946	31547.919	42063.891
0.170	20286.766	30430.149	40573.532
0.180	19576.246	29364.369	39152.493
0.190	18898.023	28347.034	37796.045
0.200	18249.942	27374.913	36499.885
0.210	17630.039	26445.059	35260.079
0.220	17036.515	25554.773	34073.031
0.230	16467.721	24701.582	32935.443
0.240	15922.144	23883.215	31844.287
0.250	15398.389	23097.583	30796.778
0.260	14895.174	22342.760	29790.347
0.270	14411.313	21616.969	28822.625
0.280	13945.711	20918.566	27891.421
0.290	13497.353	20246.030	26994.706
0.300	13065.300	19597.949	26130.599
0.310	12648.677	18973.015	25297.353
0.320	12246.672	18370.008	24493.344
0.330	11858.529	17787.794	23717.059
0.340	11483.544	17225.316	22967.088
0.350	11121.059	16681.588	22242.117
0.360	10770.458	16155.687	21540.916
0.370	10431.167	15646.750	20862.333

0.380	10102.647	15153.970	20205.293
0.390	9784.393	14676.589	19568.786
0.400	9475.932	14213.897	18951.863
0.410	9176.818	13765.226	18353.635
0.420	8886.632	13329.949	17773.265
0.430	8604.982	12907.473	17209.964
0.440	8331.495	12497.243	16662.991
0.450	8065.823	12098.734	16131.645
0.460	7807.634	11711.451	15615.268
0.470	7556.617	11334.925	15113.233
0.480	7312.477	10968.715	14624.954
0.490	7074.935	10612.403	14149.871
0.500	6843.728	10265.593	13687.457
0.510	6618.606	9927.909	13237.211
0.520	6399.330	9598.996	12798.661
0.530	6185.678	9278.516	12371.355
0.540	5977.434	8966.150	11954.867
0.550	5774.396	8661.594	11548.792
0.560	5576.371	8364.557	11152.743
0.570	5383.177	8074.765	10766.353
0.580	5194.637	7791.956	10389.274
0.590	5010.587	7515.880	10021.174
0.600	4830.867	7246.301	9661.734
0.610	4655.327	6982.990	9310.654
0.620	4483.822	6725.733	8967.644
0.630	4316.215	6474.323	8632.430
0.640	4152.375	6228.562	8304.749
0.650	3992.175	5988.262	7984.350
0.660	3835.496	5753.244	7670.992
0.670	3682.223	5523.335	7364.447
0.680	3532.247	5298.370	7064.494
0.690	3385.461	5078.192	6770.923
0.700	3241.766	4862.649	6483.532
0.710	3101.064	4651.597	6202.129
0.720	2963.264	4444.896	5926.528
0.730	2828.275	4242.413	5656.551
0.740	2696.014	4044.021	5392.028
0.750	2566.398	3849.597	5132.796
0.760	2439.349	3659.023	4878.697
0.770	2314.790	3472.186	4629.581
0.780	2192.651	3288.976	4385.302

0.790	2072.860	3109.290	4145.720
0.800	1955.351	2933.026	3910.702
0.810	1840.059	2760.089	3680.118
0.820	1726.922	2590.383	3453.844
0.830	1615.880	2423.820	3231.761
0.840	1506.876	2260.314	3013.752
0.850	1399.854	2099.780	2799.707
0.860	1294.759	1942.139	2589.519
0.870	1191.542	1787.313	2383.084
0.880	1090.151	1635.227	2180.303
0.890	990.540	1485.809	1981.079
0.900	892.660	1338.990	1785.320
0.910	796.468	1194.703	1592.937
0.920	701.921	1052.881	1403.842
0.930	608.976	913.464	1217.952
0.940	517.593	776.389	1035.186
0.950	427.733	641.600	855.466
0.960	339.358	509.038	678.717
0.970	252.433	378.649	504.865
0.980	166.920	250.380	333.840
0.990	82.787	124.181	165.574
1.000	0.000	0.000	0.000

Figure 15

V/Vmax	F @ Smax=100 kN/m2	F @ Smax=150 kN/m2	F @ Smax=200 kN/m2
0	20672.005	31008.008	41344.010
0.010	19678.159	29517.238	39356.318
0.020	18757.931	28136.896	37515.861
0.030	17903.433	26855.150	35806.866
0.040	17107.866	25661.800	34215.733
0.050	16365.337	24548.006	32730.675
0.060	15670.714	23506.070	31341.427
0.070	15019.504	22529.256	30039.008
0.080	14407.761	21611.642	28815.522
0.090	13832.003	20748.005	27664.007
0.100	13289.146	19933.719	26578.292
0.110	12776.448	19164.671	25552.895
0.120	12291.463	18437.194	24582.925
0.130	11832.003	17748.004	23664.006
0.140	11396.105	17094.158	22792.211
0.150	10982.003	16473.004	21964.006

0.160	10588.100	15882.150	21176.200
0.170	10212.955	15319.432	20425.910
0.180	9855.258	14782.887	19710.517
0.190	9513.821	14270.731	19027.641
0.200	9187.558	13781.337	18375.116
0.210	8875.480	13313.221	17750.961
0.220	8576.683	12865.025	17153.366
0.230	8290.335	12435.503	16580.671
0.240	8015.675	12023.513	16031.351
0.250	7752.002	11628.003	15504.004
0.260	7498.669	11248.003	14997.337
0.270	7255.079	10882.618	14510.157
0.280	7020.681	10531.022	14041.362
0.290	6794.965	10192.447	13589.929
0.300	6577.456	9866.184	13154.912
0.310	6367.716	9551.574	12735.432
0.320	6165.335	9248.002	12330.670
0.330	5969.933	8954.899	11939.865
0.340	5781.154	8671.731	11562.308
0.350	5598.668	8398.002	11197.336
0.360	5422.165	8133.248	10844.331
0.370	5251.356	7877.034	10502.712
0.380	5085.970	7628.954	10171.939
0.390	4925.751	7388.627	9851.502
0.400	4770.463	7155.694	9540.925
0.410	4619.880	6929.820	9239.760
0.420	4473.792	6710.688	8947.584
0.430	4332.001	6498.002	8664.002
0.440	4194.320	6291.480	8388.640
0.450	4060.572	6090.859	8121.145
0.460	3930.593	5895.889	7861.185
0.470	3804.223	5706.335	7608.446
0.480	3681.316	5521.974	7362.632
0.490	3561.731	5342.596	7123.461
0.500	3445.334	5168.001	6890.668
0.510	3332.001	4998.001	6664.002
0.520	3221.611	4832.417	6443.222
0.530	3114.052	4671.078	6228.104
0.540	3009.216	4513.824	6018.432
0.550	2907.001	4360.501	5814.001
0.560	2807.309	4210.964	5614.619

0.570	2710.049	4065.074	5420.099
0.580	2615.133	3922.700	5230.266
0.590	2522.477	3783.715	5044.954
0.600	2432.001	3648.001	4864.001
0.610	2343.628	3515.443	4687.257
0.620	2257.288	3385.932	4514.576
0.630	2172.910	3259.364	4345.819
0.640	2090.427	3135.641	4180.855
0.650	2009.778	3014.667	4019.557
0.660	1930.902	2896.352	3861.803
0.670	1853.740	2780.609	3707.479
0.680	1778.237	2667.356	3556.474
0.690	1704.341	2556.511	3408.682
0.700	1632.000	2448.001	3264.001
0.710	1561.167	2341.751	3122.334
0.720	1491.794	2237.691	2983.588
0.730	1423.837	2135.756	2847.674
0.740	1357.253	2035.879	2714.506
0.750	1292.000	1938.000	2584.001
0.760	1228.040	1842.060	2456.080
0.770	1165.334	1748.000	2330.667
0.780	1103.845	1655.767	2207.690
0.790	1043.539	1565.308	2087.077
0.800	984.381	1476.572	1968.762
0.810	926.340	1389.510	1852.680
0.820	869.383	1304.075	1738.767
0.830	813.482	1220.223	1626.963
0.840	758.606	1137.909	1517.211
0.850	704.727	1057.091	1409.455
0.860	651.820	977.730	1303.640
0.870	599.857	899.786	1199.715
0.880	548.814	823.221	1097.629
0.890	498.667	748.000	997.334
0.900	449.391	674.087	898.783
0.910	400.966	601.448	801.931
0.920	353.368	530.051	706.735
0.930	306.576	459.865	613.153
0.940	260.571	390.857	521.143
0.950	215.333	323.000	430.667
0.960	170.843	256.265	341.686
0.970	127.082	190.623	254.164

0.980	84.033	126.049	168.065
0.990	41.677	62.516	83.355
1.000	0.000	0.000	0.000

3.1 Results

Figure 26

Time	Kin(θz) = 90°	Kin(θz) = 100°	Kin(θz) = 110°	Kin(θz) = 120°	Kin(θz) = 130°	Kin(θz) = 140°	Kin(θz) = 150°
0.00	90.00	100.00	110.00	120.00	130.00	140.00	150.00
0.01	84.52	95.82	104.73	118.15	131.46	141.71	147.79
0.02	83.92	95.53	104.65	118.03	131.08	142.19	152.05
0.02	89.01	99.31	108.97	118.69	128.45	138.18	146.71
0.03	85.31	95.86	104.29	117.61	131.06	140.48	146.66
0.04	83.60	95.30	104.60	117.91	130.57	142.39	153.27
0.05	87.78	99.03	108.85	118.56	128.36	138.02	145.54
0.06	86.63	96.16	104.18	117.51	131.19	139.99	146.95
0.06	83.53	95.20	104.69	117.98	130.32	142.78	150.49
0.07	86.38	98.71	108.80	118.50	128.39	138.02	146.28
0.08	87.98	96.51	104.10	117.47	131.35	139.66	146.89
0.09	83.61	95.14	104.80	118.07	130.10	143.09	147.74
0.10	85.20	98.34	108.76	118.43	128.45	138.05	148.77
0.10	88.92	96.90	104.03	117.44	131.50	139.41	146.40
0.11	83.86	95.10	104.91	118.17	129.89	143.29	146.59
0.12	84.40	97.94	108.72	118.35	128.51	138.10	150.83
0.13	89.20	97.30	103.96	117.43	131.64	139.22	145.88
0.14	84.37	95.09	105.03	118.26	129.70	143.39	146.36
0.14	83.94	97.53	108.66	118.27	128.59	138.16	151.13
0.15	88.78	97.70	103.90	117.43	131.75	139.07	145.67
0.16	85.19	95.09	105.15	118.34	129.52	143.43	146.38
0.17	83.70	97.14	108.58	118.17	128.68	138.24	150.05
0.18	87.84	98.08	103.85	117.44	131.84	138.95	146.05
0.18	86.29	95.11	105.28	118.42	129.35	143.41	146.37
0.19	83.62	96.78	108.48	118.08	128.78	138.33	148.60
0.20	86.69	98.41	103.80	117.47	131.90	138.85	147.04
0.21	87.45	95.16	105.42	118.49	129.19	143.34	146.25
0.22	83.65	96.46	108.38	117.98	128.89	138.42	147.45
0.22	85.61	98.67	103.75	117.52	131.93	138.78	148.28
0.23	88.39	95.23	105.56	118.53	129.05	143.25	146.06
0.24	83.82	96.19	108.27	117.88	129.02	138.52	146.76

0.25	84.79	98.86	103.71	117.57	131.94	138.72	149.27
0.26	88.88	95.32	105.70	118.56	128.92	143.13	145.87
0.26	84.16	95.95	108.16	117.80	129.16	138.63	146.42
0.27	84.24	98.98	103.68	117.64	131.90	138.67	149.71
0.28	88.84	95.44	105.85	118.58	128.81	143.01	145.80
0.29	84.73	95.76	108.03	117.72	129.32	138.74	146.28
0.30	83.91	99.02	103.65	117.72	131.83	138.64	149.58
0.30	88.31	95.59	106.00	118.57	128.72	142.87	145.90
0.31	85.52	95.60	107.89	117.65	129.49	138.85	146.21
0.32	83.75	98.99	103.63	117.79	131.72	138.61	149.07
0.33	87.46	95.77	106.15	118.56	128.65	142.73	146.21
0.34	86.49	95.48	107.76	117.58	129.67	138.96	146.16
0.34	83.69	98.88	103.61	117.88	131.59	138.59	148.40
0.35	86.47	95.98	106.30	118.53	128.59	142.59	146.72
0.36	87.46	95.38	107.62	117.53	129.86	139.06	146.10
0.37	83.74	98.72	103.59	117.96	131.44	138.58	147.75
0.38	85.57	96.21	106.45	118.50	128.55	142.45	147.33
0.38	88.23	95.31	107.48	117.48	130.05	139.14	146.03
0.39	83.90	98.51	103.58	118.06	131.26	138.57	147.22
0.40	84.86	96.46	106.60	118.44	128.52	142.33	147.93

Figure 27

Kin (θz)	**90°**	**100°**	**110°**	**120°**	**130°**	**140°**	**150°**
Time	**(-1.091, -3.79)**	**(-1.092, -3.77)**	**(-1.094, -3.70)**	**(-1.103, -3.64)**	**(-1.113, -3.59)**	**(-1.198, -3.48)**	**(-1.202, -3.45)**
0.000	90.000	100.281	110.000	120.000	130.000	140.000	150.000
0.008	89.774	99.960	109.461	119.163	129.275	138.417	148.441
0.016	89.694	99.849	109.297	118.969	128.993	138.264	147.988
0.024	89.523	99.683	108.959	118.694	128.424	138.047	147.694
0.032	89.556	99.706	109.072	118.703	128.776	137.802	147.543
0.040	89.624	99.752	109.122	118.741	128.643	138.035	147.573
0.048	89.504	99.646	108.880	118.585	128.322	137.818	147.522
0.056	89.507	99.662	109.030	118.674	128.777	137.804	147.455
0.064	89.618	99.745	109.107	118.709	128.531	138.004	147.523
0.072	89.529	99.659	108.875	118.572	128.354	137.749	147.516
0.080	89.481	99.642	109.021	118.685	128.804	137.882	147.448
0.088	89.604	99.741	109.108	118.692	128.449	137.942	147.508
0.096	89.563	99.679	108.877	118.571	128.416	137.740	147.523
0.104	89.468	99.629	109.015	118.698	128.806	137.952	147.450
0.112	89.579	99.731	109.109	118.678	128.383	137.859	147.496

0.120	89.593	99.700	108.880	118.574	128.491	137.775	147.529
0.128	89.471	99.622	109.010	118.708	128.781	137.980	147.456
0.136	89.547	99.715	109.112	118.663	128.337	137.792	147.485
0.144	89.614	99.719	108.883	118.579	128.571	137.837	147.532
0.152	89.489	99.623	109.006	118.717	128.731	137.957	147.464
0.160	89.512	99.694	109.113	118.648	128.315	137.762	147.476
0.168	89.622	99.734	108.886	118.587	128.649	137.903	147.532
0.176	89.517	99.631	109.001	118.723	128.663	137.898	147.473
0.184	89.485	99.673	109.115	118.633	128.316	137.771	147.468
0.192	89.613	99.743	108.889	118.597	128.714	137.947	147.529
0.200	89.552	99.645	108.996	118.726	128.586	137.834	147.483
0.208	89.469	99.653	109.117	118.619	128.341	137.811	147.463
0.216	89.590	99.746	108.892	118.609	128.760	137.952	147.524
0.224	89.585	99.664	108.991	118.727	128.508	137.791	147.492
0.232	89.467	99.636	109.118	118.606	128.387	137.865	147.459
0.240	89.558	99.741	108.896	118.623	128.782	137.919	147.517
0.248	89.610	99.685	108.986	118.725	128.438	137.780	147.502
0.256	89.481	99.624	109.119	118.596	128.448	137.913	147.457
0.264	89.523	99.728	108.899	118.637	128.778	137.867	147.509
0.272	89.621	99.707	108.981	118.719	128.383	137.799	147.511
0.280	89.507	99.620	109.120	118.588	128.519	137.936	147.458
0.288	89.493	99.709	108.903	118.651	128.747	137.820	147.501
0.296	89.617	99.726	108.976	118.711	128.347	137.840	147.517
0.304	89.540	99.624	109.121	118.582	128.592	137.926	147.460
0.312	89.474	99.686	108.907	118.666	128.697	137.796	147.492
0.320	89.598	99.740	108.972	118.701	128.332	137.884	147.521
0.328	89.574	99.635	109.122	118.578	128.660	137.889	147.465
0.336	89.468	99.664	108.911	118.681	128.634	137.798	147.484
0.344	89.569	99.746	108.967	118.689	128.337	137.914	147.523
0.352	89.601	99.652	109.122	118.578	128.717	137.849	147.472
0.360	89.476	99.644	108.915	118.693	128.561	137.822	147.477
0.368	89.535	99.744	108.963	118.676	128.366	137.922	147.522
0.376	89.617	99.674	109.123	118.580	128.754	137.816	147.479
0.384	89.498	99.630	108.919	118.703	128.490	137.858	147.472
0.392	89.504	99.733	108.959	118.662	128.414	137.904	147.519
0.400	89.618	99.696	109.123	118.585	128.766	137.805	147.486

3.2 Results

Figure 29

	kin = 90°	kin = 100°	kin = 120°	kin = 130°	kin = 140°	kin = 150°
Time	**Dent angle = 53.44°**					
0	0.000	0.000	0.000	0.000	0.000	0.000
0.002	0.030	0.030	0.032	0.030	0.030	0.027
0.004	0.122	0.122	0.124	0.121	0.121	0.110
0.006	0.276	0.276	0.278	0.276	0.273	0.252
0.008	0.495	0.495	0.498	0.495	0.489	0.455
0.01	0.782	0.782	0.784	0.781	0.772	0.724
0.012	1.138	1.138	1.141	1.137	1.124	1.060
0.014	1.566	1.565	1.568	1.565	1.546	1.464
0.016	2.064	2.064	2.067	2.063	2.037	1.935
0.018	2.635	2.634	2.638	2.633	2.599	2.474
0.02	3.281	3.280	3.284	3.279	3.234	3.085
0.022	4.009	4.009	4.013	4.008	3.948	3.775
0.024	4.829	4.829	4.834	4.828	4.748	4.554
0.026	5.751	5.751	5.757	5.749	5.641	5.436
0.028	6.788	6.787	6.793	6.782	6.631	6.433
0.03	7.951	7.950	7.955	7.937	7.721	7.561
0.032	9.256	9.254	9.255	9.225	8.916	8.832
0.034	10.716	10.713	10.705	10.649	10.236	10.258
0.036	12.346	12.340	12.313	12.185	11.741	11.851
0.038	14.160	14.148	14.071	13.729	13.455	13.614
0.04	16.167	16.143	15.898	15.099	15.368	15.529
0.042	18.373	18.323	17.507	16.247	17.480	17.495
0.044	20.774	20.644	18.678	17.192	19.765	19.371
0.046	23.350	22.855	19.531	17.862	22.061	20.959
0.048	25.964	24.294	20.002	18.287	24.051	22.042
0.05	27.934	25.101	20.171	18.539	25.453	22.659
0.052	28.999	25.468	20.192	18.597	26.004	22.726
0.054	29.580	25.373	20.033	18.501	26.035	22.364
0.056	29.624	25.172	19.757	18.343	25.688	21.835
0.058	29.467	24.958	19.507	18.160	25.420	21.264
0.06	29.248	24.645	19.297	17.936	25.594	20.719
0.062	28.890	24.319	19.073	17.708	25.530	20.355
0.064	28.496	24.119	18.886	17.557	25.189	20.361
0.066	28.235	24.042	18.800	17.490	24.691	20.507
0.068	28.118	23.977	18.763	17.455	24.022	20.568

0.07	28.026	23.878	18.716	17.429	23.126	20.543
0.072	27.885	23.830	18.720	17.429	22.379	20.462
0.074	27.775	23.849	18.788	17.444	21.872	20.313
0.076	27.753	23.842	18.858	17.435	21.655	20.049
0.078	27.755	23.776	18.892	17.402	21.722	19.574
0.08	27.704	23.733	18.914	17.367	22.017	19.084
0.082	27.647	23.741	18.918	17.324	22.450	18.755
0.084	27.644	23.754	18.881	17.252	22.952	18.573
0.086	27.665	23.769	18.825	17.161	23.443	18.526
0.088	27.656	23.818	18.786	17.077	23.861	18.607
0.09	27.643	23.859	18.762	16.998	24.209	18.797
0.092	27.670	23.846	18.734	16.879	24.435	19.069
0.094	27.696	23.831	18.708	16.708	24.472	19.361
0.096	27.670	23.857	18.697	16.529	24.364	19.655
0.098	27.632	23.886	18.665	16.372	24.195	19.978
0.1	27.630	23.890	18.544	16.254	24.005	20.329

Figure 30

	kin = 90°	**kin = 100°**	**kin = 120°**	**kin = 130°**	**kin = 140°**	**kin = 150°**
Time	**Dent angle = 51.5°**					
0	0.000	0.000	0.000	0.000	0.000	0.000
0.002	0.017	0.016	0.015	0.016	0.014	0.012
0.004	0.063	0.067	0.061	0.064	0.059	0.050
0.006	0.142	0.145	0.140	0.143	0.135	0.118
0.008	0.253	0.257	0.252	0.254	0.243	0.218
0.01	0.400	0.404	0.398	0.400	0.385	0.350
0.012	0.582	0.587	0.580	0.583	0.563	0.517
0.014	0.803	0.808	0.801	0.804	0.778	0.721
0.016	1.066	1.071	1.063	1.066	1.033	0.963
0.018	1.371	1.377	1.369	1.372	1.330	1.246
0.02	1.723	1.728	1.720	1.723	1.672	1.572
0.022	2.122	2.128	2.119	2.122	2.060	1.941
0.024	2.570	2.577	2.567	2.571	2.496	2.356
0.026	3.072	3.080	3.069	3.073	2.984	2.819
0.028	3.632	3.640	3.628	3.633	3.527	3.335
0.03	4.255	4.264	4.252	4.258	4.130	3.909
0.032	4.950	4.960	4.947	4.953	4.800	4.548
0.034	5.725	5.736	5.722	5.728	5.543	5.263
0.036	6.588	6.600	6.585	6.591	6.364	6.064
0.038	7.552	7.565	7.548	7.553	7.268	6.963
0.04	8.627	8.642	8.621	8.624	8.256	7.973

0.042	9.826	9.842	9.818	9.816	9.325	9.105
0.044	11.164	11.181	11.149	11.136	10.481	10.371
0.046	12.654	12.671	12.628	12.586	11.758	11.785
0.048	14.309	14.326	14.260	14.136	13.225	13.357
0.05	16.143	16.156	16.035	15.664	14.886	15.095
0.052	18.163	18.169	17.863	16.993	16.737	16.994
0.054	20.374	20.358	19.437	18.102	18.780	18.997
0.056	22.775	22.682	20.568	18.989	21.001	20.941
0.058	25.351	24.858	21.372	19.587	23.305	22.696
0.06	27.955	26.212	21.785	19.963	25.383	23.927
0.062	29.845	26.952	21.927	20.153	27.081	24.577
0.064	30.835	27.217	21.918	20.143	28.003	24.810
0.066	31.296	27.116	21.727	20.015	28.257	24.627
0.068	31.260	26.952	21.448	19.851	28.196	24.246
0.07	31.149	26.735	21.210	19.646	28.277	24.033
0.072	31.010	26.403	21.009	19.393	28.395	24.173
0.074	30.683	26.089	20.785	19.155	28.198	24.137
0.076	30.274	25.914	20.578	18.967	27.691	23.926
0.078	29.949	25.852	20.454	18.784	27.008	23.612
0.08	29.762	25.790	20.383	18.579	26.084	23.164
0.082	29.666	25.680	20.289	18.398	25.158	22.520
0.084	29.593	25.599	20.191	18.290	24.592	21.683
0.086	29.532	25.585	20.143	18.257	24.377	21.039
0.088	29.515	25.587	20.138	18.275	24.379	20.661
0.09	29.533	25.555	20.136	18.331	24.544	20.507
0.092	29.530	25.524	20.158	18.404	24.852	20.513
0.094	29.482	25.538	20.215	18.451	25.229	20.660
0.096	29.437	25.570	20.252	18.469	25.630	20.927
0.098	29.432	25.565	20.235	18.490	25.940	21.289
0.1	29.447	25.535	20.220	18.517	26.142	21.710

Figure 31

	kin = 90°	**kin =100°**	**kin = 120°**	**kin = 130°**	**kin = 140°**	**kin = 150°**
Time	**Dent angle = 50°**					
0	0.000	0.000	0.000	0.000	0.000	0.000
0.002	0.004	0.004	0.004	0.004	0.003	0.001
0.004	0.018	0.018	0.017	0.017	0.013	0.005
0.006	0.040	0.040	0.038	0.039	0.031	0.019
0.008	0.070	0.070	0.067	0.068	0.057	0.041
0.01	0.109	0.109	0.106	0.107	0.091	0.073
0.012	0.158	0.158	0.155	0.156	0.134	0.113

0.014	0.216	0.216	0.213	0.214	0.186	0.163
0.016	0.286	0.286	0.283	0.284	0.247	0.223
0.018	0.368	0.368	0.364	0.365	0.319	0.294
0.02	0.462	0.462	0.458	0.460	0.403	0.376
0.022	0.570	0.570	0.566	0.567	0.498	0.470
0.024	0.694	0.694	0.689	0.691	0.607	0.577
0.026	0.834	0.834	0.828	0.830	0.731	0.700
0.028	0.992	0.992	0.986	0.989	0.872	0.838
0.03	1.171	1.171	1.164	1.167	1.030	0.994
0.032	1.372	1.371	1.364	1.367	1.207	1.169
0.034	1.596	1.596	1.588	1.591	1.407	1.366
0.036	1.848	1.847	1.839	1.842	1.630	1.584
0.038	2.127	2.127	2.117	2.121	1.879	1.827
0.04	2.438	2.437	2.427	2.431	2.155	2.097
0.042	2.781	2.781	2.770	2.774	2.461	2.394
0.044	3.162	3.162	3.149	3.154	2.800	2.722
0.046	3.583	3.583	3.569	3.575	3.176	3.083
0.048	4.049	4.049	4.034	4.040	3.590	3.481
0.05	4.565	4.565	4.549	4.555	4.048	3.920
0.052	5.137	5.136	5.119	5.127	4.554	4.405
0.054	5.771	5.770	5.751	5.760	5.114	4.943
0.056	6.474	6.474	6.453	6.463	5.732	5.540
0.058	7.256	7.256	7.233	7.243	6.414	6.206
0.06	8.126	8.126	8.100	8.110	7.164	6.950
0.062	9.093	9.093	9.064	9.074	7.987	7.782
0.064	10.170	10.170	10.136	10.144	8.882	8.711
0.066	11.369	11.368	11.328	11.332	9.845	9.750
0.068	12.702	12.701	12.652	12.646	10.872	10.910
0.07	14.184	14.181	14.120	14.088	11.972	12.203
0.072	15.827	15.821	15.738	15.631	13.203	13.642
0.074	17.642	17.632	17.500	17.156	14.624	15.236
0.076	19.637	19.619	19.327	18.477	16.226	16.992
0.078	21.817	21.782	20.923	19.571	18.011	18.901
0.08	24.186	24.090	22.056	20.430	19.982	20.903
0.082	26.744	26.295	22.844	21.002	22.125	22.823
0.084	29.360	27.689	23.244	21.363	24.363	24.557
0.086	31.286	28.409	23.395	21.531	26.507	25.792
0.088	32.262	28.619	23.396	21.500	28.352	26.430
0.09	32.724	28.469	23.207	21.367	29.633	26.673
0.092	32.684	28.329	22.932	21.202	30.108	26.562
0.094	32.541	28.213	22.701	20.990	30.166	26.352

0.096	32.366	27.935	22.507	20.732	30.344	26.548
0.098	32.041	27.548	22.292	20.493	30.450	26.612
0.1	31.664	27.252	22.078	20.296	30.199	26.349

Figure 32

	kin = 90°	**kin = 100°**	**kin = 120°**	**kin = 130°**	**kin = 140°**	**kin = 150°**
Time	**Dent angle = 49°**					
0.000	0.000	0.000	0.000	0.000	0.000	0.000
0.002	-0.004	-0.004	-0.004	-0.004	-0.005	-0.007
0.004	-0.015	-0.015	-0.015	-0.014	-0.017	-0.023
0.006	-0.033	-0.033	-0.031	-0.030	-0.036	-0.044
0.008	-0.058	-0.058	-0.054	-0.053	-0.063	-0.069
0.010	-0.089	-0.088	-0.084	-0.083	-0.097	-0.100
0.012	-0.127	-0.126	-0.122	-0.121	-0.140	-0.136
0.014	-0.172	-0.171	-0.167	-0.166	-0.192	-0.180
0.016	-0.226	-0.224	-0.220	-0.219	-0.253	-0.230
0.018	-0.288	-0.287	-0.282	-0.281	-0.324	-0.287
0.020	-0.360	-0.359	-0.353	-0.352	-0.406	-0.351
0.022	-0.443	-0.441	-0.435	-0.434	-0.500	-0.423
0.024	-0.537	-0.535	-0.528	-0.527	-0.606	-0.501
0.026	-0.643	-0.641	-0.634	-0.632	-0.727	-0.580
0.028	-0.762	-0.760	-0.753	-0.750	-0.862	-0.655
0.030	-0.897	-0.894	-0.886	-0.884	-1.014	-0.717
0.032	-1.048	-1.045	-1.036	-1.033	-1.185	-0.767
0.034	-1.216	-1.213	-1.203	-1.200	-1.375	-0.804
0.036	-1.404	-1.401	-1.390	-1.386	-1.586	-0.822
0.038	-1.614	-1.610	-1.598	-1.594	-1.820	-0.824
0.040	-1.847	-1.843	-1.830	-1.825	-2.077	-0.817
0.042	-2.107	-2.102	-2.087	-2.082	-2.339	-0.804
0.044	-2.395	-2.390	-2.374	-2.368	-2.560	-0.788
0.046	-2.715	-2.710	-2.691	-2.685	-2.742	-0.770
0.048	-3.070	-3.064	-3.044	-3.036	-2.883	-0.754
0.050	-3.464	-3.457	-3.435	-3.426	-2.985	-0.739
0.052	-3.900	-3.893	-3.868	-3.858	-3.043	-0.724
0.054	-4.383	-4.375	-4.348	-4.337	-3.072	-0.710
0.056	-4.918	-4.909	-4.879	-4.866	-3.079	-0.698
0.058	-5.509	-5.500	-5.466	-5.452	-3.068	-0.689
0.060	-6.164	-6.153	-6.116	-6.100	-3.039	-0.686
0.062	-6.888	-6.876	-6.835	-6.817	-3.003	-0.686
0.064	-7.688	-7.676	-7.631	-7.610	-2.964	-0.688
0.066	-8.573	-8.560	-8.510	-8.486	-2.927	-0.692

0.068	-9.551	-9.537	-9.482	-9.454	-2.888	-0.697
0.070	-10.633	-10.617	-10.557	-10.524	-2.850	-0.703
0.072	-11.829	-11.812	-11.746	-11.705	-2.817	-0.708
0.074	-13.151	-13.133	-13.062	-12.988	-2.789	-0.711
0.076	-14.613	-14.595	-14.521	-14.068	-2.769	-0.712
0.078	-16.231	-16.212	-16.133	-14.779	-2.753	-0.713
0.080	-18.020	-18.000	-17.917	-15.104	-2.737	-0.714
0.082	-19.999	-19.978	-19.886	-15.121	-2.726	-0.715
0.084	-22.183	-22.160	-22.027	-14.961	-2.720	-0.716
0.086	-24.583	-24.551	-23.806	-14.726	-2.717	-0.717
0.088	-27.168	-27.089	-24.805	-14.497	-2.718	-0.719
0.090	-29.614	-29.355	-25.000	-14.312	-2.719	-0.719
0.092	-31.151	-30.823	-24.659	-14.183	-2.719	-0.719
0.094	-31.454	-31.399	-24.129	-14.098	-2.721	-0.717
0.096	-30.841	-31.414	-23.665	-14.052	-2.724	-0.715
0.098	-29.900	-31.202	-23.376	-14.033	-2.730	-0.714
0.100	-29.249	-31.380	-23.266	-14.022	-2.734	-0.713

Figure 33

	kin = 90°	**kin =100°**	**kin = 120°**	**kin = 130°**	**kin = 140°**	**kin = 150°**
Time	**Dent angle = 48°**					
0.000	0.000	0.000	0.000	0.000	0.000	0.000
0.002	-0.013	-0.012	-0.011	-0.011	-0.012	-0.014
0.004	-0.047	-0.046	-0.042	-0.044	-0.045	-0.050
0.006	-0.099	-0.098	-0.095	-0.097	-0.101	-0.103
0.008	-0.173	-0.172	-0.168	-0.170	-0.178	-0.172
0.010	-0.269	-0.268	-0.264	-0.266	-0.279	-0.260
0.012	-0.388	-0.387	-0.383	-0.385	-0.403	-0.365
0.014	-0.532	-0.531	-0.526	-0.529	-0.554	-0.484
0.016	-0.701	-0.701	-0.696	-0.698	-0.731	-0.611
0.018	-0.899	-0.898	-0.892	-0.895	-0.936	-0.731
0.020	-1.125	-1.124	-1.119	-1.122	-1.172	-0.837
0.022	-1.384	-1.383	-1.377	-1.380	-1.441	-0.924
0.024	-1.677	-1.676	-1.669	-1.673	-1.743	-0.982
0.026	-2.008	-2.006	-1.999	-2.003	-2.077	-1.013
0.028	-2.378	-2.377	-2.369	-2.373	-2.409	-1.025
0.030	-2.793	-2.792	-2.783	-2.787	-2.685	-1.024
0.032	-3.256	-3.255	-3.245	-3.250	-2.908	-1.015
0.034	-3.772	-3.770	-3.760	-3.765	-3.080	-0.996
0.036	-4.345	-4.344	-4.332	-4.337	-3.188	-0.970
0.038	-4.982	-4.980	-4.968	-4.978	-3.249	-0.943

0.040	-5.687	-5.686	-5.672	-5.687	-3.277	-0.920
0.042	-6.469	-6.468	-6.453	-6.473	-3.270	-0.902
0.044	-7.335	-7.334	-7.318	-7.341	-3.242	-0.890
0.046	-8.294	-8.292	-8.275	-8.302	-3.201	-0.883
0.048	-9.354	-9.352	-9.333	-9.363	-3.158	-0.880
0.050	-10.526	-10.525	-10.505	-10.535	-3.106	-0.878
0.052	-11.823	-11.823	-11.801	-11.827	-3.057	-0.878
0.054	-13.257	-13.258	-13.235	-13.163	-3.011	-0.880
0.056	-14.843	-14.844	-14.824	-14.166	-2.976	-0.885
0.058	-16.596	-16.600	-16.580	-14.729	-2.945	-0.891
0.060	-18.535	-18.540	-18.521	-14.897	-2.915	-0.898
0.062	-20.676	-20.681	-20.653	-14.786	-2.894	-0.903
0.064	-23.031	-23.032	-22.718	-14.541	-2.879	-0.906
0.066	-25.586	-25.558	-24.047	-14.273	-2.873	-0.907
0.068	-28.144	-27.953	-24.459	-14.051	-2.867	-0.908
0.070	-30.004	-29.669	-24.199	-13.895	-2.862	-0.908
0.072	-30.664	-30.464	-23.646	-13.802	-2.861	-0.909
0.074	-30.216	-30.677	-23.128	-13.752	-2.864	-0.910
0.076	-29.248	-30.373	-22.800	-13.734	-2.870	-0.910
0.078	-28.483	-30.470	-22.674	-13.732	-2.872	-0.908
0.080	-28.082	-30.540	-22.690	-13.732	-2.874	-0.906
0.082	-28.063	-29.712	-22.768	-13.736	-2.878	-0.905
0.084	-28.425	-28.100	-22.847	-13.738	-2.885	-0.904
0.086	-29.125	-26.279	-22.897	-13.736	-2.888	-0.904
0.088	-29.931	-24.956	-22.913	-13.736	-2.889	-0.905
0.090	-30.127	-24.161	-22.905	-13.734	-2.891	-0.905
0.092	-30.093	-23.869	-22.885	-13.730	-2.894	-0.904
0.094	-30.089	-24.085	-22.864	-13.730	-2.898	-0.903
0.096	-29.975	-24.537	-22.848	-13.727	-2.898	-0.903
0.098	-29.702	-25.050	-22.840	-13.725	-2.897	-0.904
0.100	-29.504	-25.565	-22.836	-13.726	-2.898	-0.904

Figure 34

	Dentary at 49°				
Time	**Kin = 150°**	**Kin = 130°**	**Kin = 120°**	**Kin = 100°**	**Kin = 90°**
0.000	150.000	130.000	120.000	100.000	90.000
0.002	150.028	129.989	119.991	99.993	89.993
0.004	150.062	129.981	119.983	99.985	89.985
0.006	150.122	129.974	119.975	99.977	89.977
0.008	150.162	129.967	119.967	99.969	89.968
0.010	150.174	129.961	119.959	99.959	89.958

0.012	150.163	129.956	119.950	99.949	89.948
0.014	150.134	129.951	119.942	99.937	89.936
0.016	150.088	129.947	119.932	99.923	89.922
0.018	150.029	129.942	119.921	99.908	89.907
0.020	149.963	129.937	119.909	99.891	89.890
0.022	149.895	129.932	119.896	99.871	89.870
0.024	149.835	129.927	119.881	99.848	89.847
0.026	149.782	129.921	119.863	99.822	89.821
0.028	149.695	129.914	119.844	99.792	89.792
0.030	149.561	129.906	119.821	99.758	89.757
0.032	149.440	129.897	119.795	99.718	89.718
0.034	149.387	129.887	119.765	99.673	89.672
0.036	149.475	129.875	119.731	99.621	89.620
0.038	149.624	129.861	119.692	99.561	89.560
0.040	149.721	129.845	119.646	99.492	89.490
0.042	149.755	129.826	119.593	99.412	89.410
0.044	149.753	129.804	119.532	99.320	89.316
0.046	149.740	129.779	119.462	99.214	89.209
0.048	149.721	129.750	119.382	99.091	89.084
0.050	149.709	129.717	119.289	98.949	88.940
0.052	149.729	129.680	119.182	98.786	88.773
0.054	149.775	129.638	119.061	98.597	88.579
0.056	149.818	129.592	118.923	98.381	88.356
0.058	149.843	129.544	118.766	98.132	88.099
0.060	149.849	129.494	118.591	97.847	87.803
0.062	149.837	129.446	118.397	97.523	87.463
0.064	149.809	129.406	118.184	97.155	87.074
0.066	149.771	129.385	117.955	96.740	86.632
0.068	149.727	129.402	117.715	96.276	86.130
0.070	149.691	129.510	117.473	95.764	85.566
0.072	149.681	129.900	117.242	95.204	84.937
0.074	149.703	131.702	117.040	94.606	84.244
0.076	149.739	129.308	116.892	93.985	83.489
0.078	149.767	130.374	116.828	93.371	82.684
0.080	149.777	131.132	116.870	92.817	81.850
0.082	149.770	131.026	117.010	92.427	81.033
0.084	149.750	132.075	117.362	92.417	80.326
0.086	149.725	132.210	114.855	93.301	79.944
0.088	149.701	131.963	114.829	96.400	80.464
0.090	149.692	132.226	115.419	100.903	81.900
0.092	149.705	132.333	116.181	103.293	84.242

0.094	149.732	131.784	117.130	107.674	88.033
0.096	149.759	131.676	117.766	120.068	74.316
0.098	149.775	132.003	117.827	138.805	75.326
0.100	149.776	131.584	117.534	139.423	76.156

3.3 Results

Figure 35

Dent	**53.44°**		
Kin	**90°**		
Time	**10 dynes**	**100 dynes**	**1000 dynes**
0.00	0.00	0.00	0.00
0.00	0.30	3.18	48.45
0.00	1.26	15.57	75.63
0.01	2.92	45.39	79.48
0.01	5.38	56.98	81.17
0.01	8.93	62.20	81.86
0.01	14.00	62.02	82.17
0.01	20.95	62.18	82.29
0.02	29.60	62.30	82.35
0.02	37.29	62.14	82.38
0.02	44.15	62.42	82.39
0.02	51.51	62.21	82.40
0.02	56.07	62.44	82.41
0.03	56.39	62.32	82.41
0.03	53.78	62.38	82.41
0.03	51.77	62.39	82.42
0.03	51.56	62.34	82.42
0.03	52.77	62.41	82.42
0.04	54.54	62.34	82.43
0.04	56.25	62.42	82.43
0.04	57.06	62.34	82.43
0.04	56.42	62.41	82.43
0.04	55.97	62.37	82.43
0.05	55.90	62.38	82.44
0.05	56.42	62.40	82.44
0.05	57.10	62.36	82.44
0.05	57.02	62.40	82.44
0.05	56.57	62.37	82.44
0.06	56.45	62.40	82.44

0.06	56.93	62.37	82.44
0.06	57.23	62.40	82.44
0.06	56.58	62.38	82.45
0.06	56.10	62.38	82.44
0.07	56.21	62.40	82.45
0.07	56.69	62.37	82.45
0.07	57.22	62.40	82.45
0.07	57.27	62.38	82.45
0.07	57.22	62.39	82.45
0.08	57.37	62.38	82.45
0.08	57.33	62.39	82.45
0.08	57.24	62.38	82.45
0.08	57.21	62.39	82.45
0.08	57.28	62.39	82.45
0.09	57.31	62.38	82.45
0.09	57.35	62.39	82.45
0.09	57.37	62.39	82.45
0.09	57.30	62.38	82.45
0.09	57.29	62.39	82.45
0.10	57.34	62.39	82.45
0.10	57.33	62.38	82.45
0.10	57.34	62.39	82.45

Figure 36

dent	**53.44°**		
kin	**120°**		
Time	**10 dynes**	**100 dynes**	**1000 dynes**
0.00	0.00	0.00	0.00
0.00	0.30	3.18	47.64
0.00	1.26	15.54	72.33
0.01	2.92	43.07	75.34
0.01	5.38	58.07	76.77
0.01	8.93	57.37	77.46
0.01	13.94	56.85	77.65
0.01	20.36	56.91	77.71
0.02	26.65	56.62	77.81
0.02	32.01	56.79	77.83
0.02	37.89	56.61	77.77
0.02	44.65	56.65	77.79
0.02	48.63	56.71	77.82
0.03	49.74	56.72	77.82

0.03	48.99	56.69	77.81
0.03	47.66	56.69	77.81
0.03	46.35	56.65	77.82
0.03	45.66	56.69	77.80
0.04	45.39	56.69	77.82
0.04	45.39	56.69	77.82
0.04	44.99	56.68	77.81
0.04	44.88	56.65	77.81
0.04	44.93	56.67	77.81
0.05	45.15	56.69	77.81
0.05	45.25	56.69	77.82
0.05	45.54	56.69	77.82
0.05	45.79	56.70	77.81
0.05	45.71	56.70	77.81
0.06	45.56	56.67	77.81
0.06	45.36	56.66	77.81
0.06	45.31	56.66	77.82
0.06	45.20	56.70	77.82
0.06	45.04	56.70	77.80
0.07	44.93	56.70	77.81
0.07	45.02	56.69	77.81
0.07	45.13	56.69	77.82
0.07	45.23	56.67	77.82
0.07	45.27	56.67	77.82
0.08	45.30	56.68	77.80
0.08	45.43	56.69	77.81
0.08	45.57	56.69	77.82
0.08	45.58	56.69	77.82
0.08	45.47	56.69	77.81
0.09	45.38	56.69	77.81
0.09	45.30	56.69	77.81
0.09	45.26	56.69	77.82
0.09	45.17	56.68	77.82
0.09	45.13	56.69	77.82
0.10	45.16	56.66	77.81
0.10	45.21	56.69	77.80
0.10	45.25	56.68	77.81

Figure 37

dent	53.44°		
kin	150°		
Time	10 dynes	100 dynes	1000 dynes
0.000	0.000	0.000	0.000
0.002	0.278	2.977	47.543
0.004	1.163	14.845	70.060
0.006	2.723	42.259	72.897
0.008	5.047	55.778	74.253
0.010	8.454	53.678	74.548
0.012	13.363	53.566	74.756
0.014	19.918	53.587	74.886
0.016	27.195	53.513	74.944
0.018	33.270	53.295	74.873
0.020	36.635	53.264	74.893
0.022	38.527	53.356	74.958
0.024	37.733	53.368	74.930
0.026	35.765	53.347	74.890
0.028	33.917	53.298	74.916
0.030	32.820	53.296	74.931
0.032	32.910	53.292	74.948
0.034	33.702	53.327	74.926
0.036	34.540	53.317	74.913
0.038	35.035	53.361	74.906
0.040	35.123	53.333	74.916
0.042	34.964	53.331	74.947
0.044	34.757	53.312	74.926
0.046	34.629	53.293	74.914
0.048	34.607	53.318	74.922
0.050	34.656	53.324	74.932
0.052	34.724	53.323	74.914
0.054	34.774	53.345	74.914
0.056	34.795	53.343	74.922
0.058	34.796	53.331	74.923
0.060	34.797	53.321	74.923
0.062	34.816	53.307	74.926
0.064	34.853	53.321	74.925
0.066	34.879	53.323	74.924
0.068	34.871	53.327	74.925
0.070	34.836	53.324	74.926

0.072	34.796	53.321	74.919
0.074	34.767	53.330	74.914
0.076	34.754	53.330	74.918
0.078	34.753	53.330	74.920
0.080	34.757	53.323	74.928
0.082	34.762	53.327	74.930
0.084	34.763	53.325	74.927
0.086	34.761	53.323	74.925
0.088	34.757	53.327	74.923
0.090	34.752	53.313	74.914
0.092	34.747	53.317	74.916
0.094	34.741	53.322	74.921
0.096	34.733	53.321	74.922
0.098	34.716	53.337	74.923
0.100	34.686	53.343	74.922

Figure 38

dent	**50°**		
kin	**90°**		
Time	**10 dynes**	**100 dynes**	**1000 dynes**
0.00	0.00	0.00	0.00
0.00	0.03	0.31	0.58
0.00	0.16	1.55	1.57
0.01	0.38	4.87	2.82
0.01	0.72	13.65	6.50
0.01	1.22	36.39	11.41
0.01	1.94	60.58	-3.89
0.01	2.94	63.46	-36.98
0.02	4.32	64.94	-22.47
0.02	6.22	65.52	-7.46
0.02	8.86	65.65	-15.61
0.02	12.55	65.76	-27.45
0.02	17.68	65.81	-25.05
0.03	24.60	65.76	-17.89
0.03	33.17	65.87	-15.56
0.03	40.57	65.76	-20.52
0.03	47.09	65.89	-23.00
0.03	54.11	65.79	-20.94
0.04	59.77	65.87	-19.63
0.04	59.49	65.83	-18.86

0.04	56.12	65.84	-19.66
0.04	54.68	65.85	-21.19
0.04	53.75	65.82	-21.33
0.05	54.45	65.86	-19.94
0.05	55.98	65.82	-19.51
0.05	57.98	65.86	-20.05
0.05	60.05	65.83	-20.19
0.05	60.43	65.85	-20.41
0.06	59.12	65.83	-20.73
0.06	58.63	65.85	-20.37
0.06	58.96	65.84	-19.82
0.06	60.14	65.84	-19.87
0.06	61.08	65.85	-20.33
0.07	60.37	65.84	-20.52
0.07	59.68	65.85	-20.59
0.07	59.53	65.83	-20.28
0.07	60.11	65.85	-19.69
0.07	60.81	65.84	-20.02
0.08	60.82	65.84	-20.61
0.08	60.31	65.84	-20.47
0.08	60.28	65.84	-20.06
0.08	60.70	65.84	-20.19
0.08	60.85	65.84	-20.33
0.09	60.32	65.84	-20.12
0.09	60.41	65.84	-20.26
0.09	60.84	65.85	-20.38
0.09	60.92	65.84	-20.27
0.09	60.79	65.85	-20.18
0.10	60.83	65.84	-20.23
0.10	60.89	65.84	-20.25
0.10	60.68	65.85	-20.05

Figure 39

dent	**50°**		
kin	**120°**		
Time	**10 dynes**	**100 dynes**	**1000 dynes**
0.00	0.00	0.00	0.00
0.00	0.03	0.31	0.58
0.00	0.16	1.55	1.63
0.01	0.37	4.87	2.76

0.01	0.72	13.65	2.98
0.01	1.22	34.99	0.62
0.01	1.94	60.26	-11.48
0.01	2.94	59.89	-19.83
0.02	4.32	60.13	-22.44
0.02	6.22	60.57	-22.28
0.02	8.86	60.09	-15.13
0.02	12.54	60.41	-16.57
0.02	17.63	60.26	-20.93
0.03	23.98	60.33	-19.17
0.03	29.69	60.31	-17.44
0.03	34.47	60.30	-18.46
0.03	39.26	60.32	-18.42
0.03	45.89	60.30	-18.08
0.04	51.87	60.31	-19.02
0.04	53.45	60.30	-19.00
0.04	52.57	60.30	-18.13
0.04	51.10	60.30	-17.77
0.04	49.68	60.30	-18.45
0.05	49.00	60.29	-18.85
0.05	48.82	60.30	-18.58
0.05	48.97	60.31	-18.63
0.05	49.13	60.31	-18.50
0.05	49.18	60.31	-18.39
0.06	49.20	60.31	-18.07
0.06	49.12	60.31	-18.37
0.06	49.11	60.31	-18.69
0.06	49.06	60.31	-18.56
0.06	49.08	60.31	-18.67
0.07	49.07	60.31	-18.52
0.07	49.07	60.31	-18.39
0.07	49.08	60.30	-18.36
0.07	49.06	60.30	-18.18
0.07	49.08	60.30	-18.47
0.08	49.06	60.30	-18.62
0.08	49.08	60.30	-18.48
0.08	49.06	60.30	-18.66
0.08	49.08	60.30	-18.57
0.08	49.07	60.30	-18.39
0.09	49.07	60.30	-18.44
0.09	49.08	60.30	-18.31

0.09	49.06	60.31	-18.28
0.09	49.08	60.31	-18.54
0.09	49.06	60.31	-18.55
0.10	49.08	60.31	-18.46
0.10	49.07	60.31	-18.63
0.10	49.07	60.31	-18.56

Figure 40

dent	**50°**		
kin	**150°**		
Time	**10 dynes**	**100 dynes**	**1000 dynes**
0.00	0.00	0.00	0.00
0.00	0.01	0.06	0.06
0.00	0.07	0.54	0.27
0.01	0.22	1.86	0.57
0.01	0.47	5.51	0.82
0.01	0.86	15.32	0.62
0.01	1.41	38.76	-1.06
0.01	2.17	56.87	-7.88
0.02	3.22	55.53	-23.58
0.02	4.67	56.52	-18.96
0.02	6.69	57.02	-20.28
0.02	9.53	57.14	-18.65
0.02	13.53	56.80	-16.74
0.03	19.03	57.00	-16.75
0.03	25.81	56.94	-17.42
0.03	33.21	56.92	-17.49
0.03	38.60	56.95	-17.12
0.03	41.17	56.93	-16.98
0.04	42.26	56.94	-17.08
0.04	41.05	56.94	-17.08
0.04	39.10	56.93	-16.91
0.04	37.40	56.92	-16.98
0.04	36.76	56.91	-17.10
0.05	37.23	56.91	-17.11
0.05	38.06	56.93	-17.06
0.05	38.74	56.92	-17.16
0.05	39.02	56.93	-17.23
0.05	38.95	56.94	-17.13
0.06	38.78	56.94	-17.06

0.06	38.61	56.94	-17.08
0.06	38.55	56.93	-17.10
0.06	38.58	56.93	-17.00
0.06	38.63	56.92	-16.92
0.07	38.69	56.92	-17.03
0.07	38.72	56.92	-17.12
0.07	38.74	56.92	-17.10
0.07	38.76	56.93	-17.06
0.07	38.79	56.93	-17.11
0.08	38.81	56.94	-17.20
0.08	38.80	56.93	-17.17
0.08	38.76	56.92	-17.09
0.08	38.72	56.92	-17.08
0.08	38.69	56.93	-17.08
0.09	38.68	56.93	-17.03
0.09	38.69	56.93	-17.01
0.09	38.69	56.93	-17.03
0.09	38.69	56.93	-17.08
0.09	38.69	56.93	-17.13
0.10	38.69	56.93	-17.15
0.10	38.68	56.93	-17.08
0.10	38.68	56.93	-16.97

3.4 Results

Figure 41

A1_alpha	10 dynes	A1_beta	5 dynes

	Dentary Rotation						
Time	A1α_T_0	A1α_T_0.025	A1α_T_0.03	A1α_T_0.035	A1α_T_0.05	A1α_Only	A1β_Only
0.000	0.000	0.000	0.000	0.000	0.000	0.000	0.000
0.002	0.901	-0.020	-0.020	-0.020	-0.020	0.917	-0.020
0.004	3.724	-0.072	-0.072	-0.072	-0.072	3.730	-0.072
0.006	8.621	-0.161	-0.161	-0.161	-0.161	8.438	-0.161
0.008	16.227	-0.292	-0.292	-0.292	-0.292	15.400	-0.292
0.010	26.583	-0.473	-0.473	-0.473	-0.473	24.530	-0.473
0.012	37.162	-0.715	-0.715	-0.715	-0.715	33.589	-0.715
0.014	47.818	-1.031	-1.031	-1.031	-1.031	42.691	-1.031
0.016	53.632	-1.437	-1.437	-1.437	-1.437	48.839	-1.437

0.018	54.243	-1.956	-1.956	-1.956	-1.956	51.126	-1.956
0.020	51.508	-2.615	-2.615	-2.615	-2.615	49.869	-2.615
0.022	49.071	-3.398	-3.447	-3.447	-3.447	47.317	-3.447
0.024	47.928	-3.880	-4.494	-4.494	-4.494	45.481	-4.494
0.026	48.265	-3.434	-5.806	-5.808	-5.808	45.099	-5.808
0.028	49.085	-1.782	-7.285	-7.456	-7.456	45.730	-7.456
0.030	49.582	1.364	-8.539	-9.519	-9.519	46.291	-9.519
0.032	49.710	6.526	-9.402	-12.077	-12.098	46.548	-12.098
0.034	49.592	13.903	-9.981	-15.042	-15.190	46.535	-15.190
0.036	49.540	24.058	-10.372	-17.727	-17.860	46.452	-17.860
0.038	49.653	35.018	-10.642	-19.783	-19.451	46.407	-19.451
0.040	49.759	46.342	-10.837	-21.203	-19.945	46.435	-19.945
0.042	49.720	52.869	-10.992	-22.176	-19.744	46.548	-19.744
0.044	49.615	54.774	-11.135	-22.961	-19.313	46.604	-19.313
0.046	49.561	52.441	-11.289	-23.759	-18.980	46.564	-18.979
0.048	49.534	49.345	-11.483	-24.694	-18.935	46.503	-18.856
0.050	49.539	47.918	-11.750	-25.836	-19.368	46.454	-18.916
0.052	49.503	48.276	-12.136	-27.105	-20.265	46.435	-19.065
0.054	49.384	49.157	-12.705	-26.598	-21.386	46.436	-19.217
0.056	49.322	49.669	-13.556	-24.175	-22.532	46.430	-19.323
0.058	49.390	49.747	-14.835	-22.333	-23.623	46.436	-19.377
0.060	49.479	49.630	-16.727	-21.378	-24.697	46.412	-19.394
0.062	49.535	49.501	-18.881	-21.041	-25.858	46.399	-19.394
0.064	49.548	49.482	-20.758	-20.991	-27.106	46.313	-19.394
0.066	49.545	49.495	-22.164	-20.712	-26.631	46.276	-19.401
0.068	49.557	49.543	-23.203	-20.115	-24.241	46.266	-19.415
0.070	49.641	49.585	-24.096	-19.624	-22.525	46.342	-19.432
0.072	49.742	49.643	-25.050	-19.435	-21.501	46.376	-19.446
0.074	49.718	49.663	-26.204	-19.613	-21.089	46.415	-19.458
0.076	49.635	49.622	-27.312	-20.069	-20.893	46.413	-19.466
0.078	49.571	49.582	-25.991	-20.366	-20.201	46.421	-19.471
0.080	49.547	49.555	-23.547	-20.456	-19.682	46.416	-19.475
0.082	49.549	49.548	-21.884	-20.148	-19.497	46.426	-19.479
0.084	49.551	49.553	-21.101	-19.580	-19.805	46.432	-19.483
0.086	49.544	49.552	-20.911	-19.255	-20.470	46.460	-19.490
0.088	49.512	49.555	-20.944	-19.189	-20.777	46.515	-19.499
0.090	49.434	49.548	-20.884	-19.271	-20.644	46.574	-19.510
0.092	49.379	49.548	-20.434	-19.379	-20.095	46.560	-19.519
0.094	49.412	49.541	-19.845	-19.394	-19.430	46.518	-19.524
0.096	49.481	49.537	-19.397	-19.264	-18.894	46.468	-19.525

0.098	49.530	49.518	-19.394	-19.302	-18.665	46.449	-19.524
0.100	49.547	49.482	-19.599	-19.361	-18.792	46.438	-19.522

Figure 42

Kinethmoid Rotation				
Time	Alp_T_0.03	Alp_T_0.035	Alp_T_0.05	A1β_Only
0.000	130.000	130.000	130.000	130.000
0.002	129.961	129.961	129.961	129.961
0.004	129.942	129.942	129.942	129.942
0.006	129.923	129.923	129.923	129.923
0.008	129.907	129.907	129.907	129.907
0.010	129.891	129.891	129.891	129.891
0.012	129.876	129.876	129.876	129.876
0.014	129.861	129.861	129.861	129.861
0.016	129.844	129.844	129.844	129.844
0.018	129.824	129.824	129.824	129.824
0.020	129.800	129.800	129.800	129.800
0.022	129.769	129.769	129.769	129.769
0.024	129.732	129.732	129.732	129.732
0.026	129.692	129.697	129.697	129.697
0.028	129.572	129.680	129.680	129.680
0.030	129.414	129.724	129.724	129.724
0.032	129.377	129.929	129.989	129.989
0.034	129.413	130.546	129.863	129.863
0.036	129.478	126.841	125.991	125.991
0.038	129.559	124.822	124.826	124.826
0.040	129.646	122.883	124.778	124.778
0.042	129.733	120.679	125.545	125.545
0.044	129.818	118.420	126.577	126.577
0.046	129.901	115.886	127.171	127.166
0.048	129.985	112.783	127.247	127.134
0.050	130.073	108.784	126.818	126.725
0.052	130.171	103.071	125.259	126.251
0.054	130.286	94.845	122.587	125.880
0.056	130.408	89.952	119.547	125.662
0.058	130.486	87.352	116.285	125.564
0.060	130.158	81.114	112.808	125.534
0.062	125.469	79.599	108.724	125.520
0.064	123.053	80.146	103.114	125.495
0.066	120.379	76.123	94.970	125.451

0.068	117.574	78.606	90.340	125.399
0.070	114.782	77.656	87.107	125.347
0.072	111.560	73.456	80.328	125.305
0.074	107.373	75.812	80.380	125.274
0.076	100.955	76.696	79.169	125.252
0.078	93.066	71.805	77.875	125.237
0.080	89.010	73.911	78.746	125.225
0.082	85.769	76.479	75.550	125.215
0.084	80.593	72.569	75.740	125.205
0.086	79.761	73.104	75.637	125.190
0.088	79.534	75.492	72.992	125.168
0.090	75.891	71.721	74.381	125.141
0.092	77.419	72.899	75.733	125.117
0.094	78.503	75.431	72.787	125.103
0.096	73.561	71.531	74.753	125.096
0.098	74.666	72.890	74.893	125.095
0.100	76.545	74.888	71.453	125.094

Figure 43

A1_alpha	A1_beta	Kin	Dent	Alpha_T								
10 dynes	5 dynes	130	49	0.03	Position (mm)							
					Dent			PMX			pal-ncr	
Time	Kin Rot	Dent Rot	Gape	Protrusion	x	y	z	x	y	z	x	y
0.000	130.00	0.00	1.02	2.99	0.836	-5.590	0.000	0.672	-4.583	0.000	-2	-3.25
0.002	129.96	-0.02	1.02	2.99	0.837	-5.592	0.000	0.672	-4.583	0.000		
0.004	129.94	-0.07	1.03	2.99	0.839	-5.596	0.000	0.672	-4.583	0.000		
0.006	129.92	-0.16	1.03	2.99	0.843	-5.603	0.000	0.671	-4.583	0.000		
0.008	129.91	-0.29	1.04	2.99	0.849	-5.613	0.000	0.671	-4.583	0.000		
0.010	129.89	-0.47	1.06	2.99	0.857	-5.627	0.000	0.671	-4.585	0.000		
0.012	129.88	-0.71	1.08	2.99	0.867	-5.646	0.000	0.670	-4.586	0.000		
0.014	129.86	-1.03	1.10	2.99	0.881	-5.671	0.000	0.670	-4.589	0.000		
0.016	129.84	-1.44	1.13	2.99	0.898	-5.703	0.000	0.670	-4.592	0.000		
0.018	129.82	-1.96	1.17	2.99	0.920	-5.744	0.000	0.669	-4.597	0.000		

0.020	129.80	-2.61	1.23	2.99	0.947	-5.796	0.000	0.669	-4.602	0.000
0.022	129.77	-3.45	1.29	3.00	0.980	-5.863	0.000	0.670	-4.608	0.000
0.024	129.73	-4.49	1.38	3.00	1.021	-5.947	0.000	0.672	-4.616	0.000
0.026	129.69	-5.81	1.48	3.01	1.070	-6.054	0.000	0.675	-4.623	0.000
0.028	129.57	-7.29	1.61	3.01	1.122	-6.176	0.000	0.678	-4.631	0.000
0.030	129.41	-8.54	1.71	3.02	1.163	-6.280	0.000	0.679	-4.637	0.000
0.032	129.38	-9.40	1.78	3.02	1.190	-6.353	0.000	0.676	-4.645	0.000
0.034	129.41	-9.98	1.83	3.02	1.208	-6.401	0.000	0.671	-4.652	0.000
0.036	129.48	-10.37	1.86	3.02	1.220	-6.434	0.000	0.665	-4.661	0.000
0.038	129.56	-10.64	1.88	3.01	1.228	-6.457	0.000	0.658	-4.670	0.000
0.040	129.65	-10.84	1.89	3.01	1.233	-6.474	0.000	0.651	-4.680	0.000
0.042	129.73	-10.99	1.89	3.01	1.238	-6.487	0.000	0.644	-4.690	0.000
0.044	129.82	-11.13	1.90	3.01	1.242	-6.499	0.000	0.636	-4.700	0.000
0.046	129.90	-11.29	1.91	3.01	1.246	-6.512	0.000	0.629	-4.710	0.000
0.048	129.98	-11.48	1.92	3.01	1.252	-6.529	0.000	0.623	-4.719	0.000
0.050	130.07	-11.75	1.93	3.01	1.259	-6.551	0.000	0.617	-4.728	0.000
0.052	130.17	-12.14	1.96	3.00	1.270	-6.584	0.000	0.612	-4.736	0.000
0.054	130.29	-12.71	2.01	3.00	1.285	-6.633	0.000	0.609	-4.741	0.000
0.056	130.41	-13.56	2.08	3.01	1.306	-6.706	0.000	0.608	-4.745	0.000
0.058	130.49	-14.84	2.19	3.01	1.337	-6.816	0.000	0.612	-4.746	0.000
0.060	130.16	-16.73	2.35	3.03	1.377	-6.981	0.000	0.628	-4.750	0.000
0.062	125.47	-18.88	2.54	3.04	1.417	-7.170	0.000	0.647	-4.752	0.000
0.064	123.05	-20.76	2.71	3.05	1.446	-7.335	0.000	0.653	-4.749	0.000
0.066	120.38	-22.16	2.83	3.05	1.463	-	0.000	0.654	-	0.000

						7.460			4.746	
0.068	117.57	-23.20	2.92	3.05	1.475	-7.552	0.000	0.652	-4.746	0.000
0.070	114.78	-24.10	3.00	3.04	1.483	-7.632	0.000	0.650	-4.746	0.000
0.072	111.56	-25.05	3.09	3.04	1.491	-7.717	0.000	0.646	-4.746	0.000
0.074	107.37	-26.20	3.19	3.03	1.498	-7.820	0.000	0.641	-4.742	0.000
0.076	100.95	-27.31	3.31	3.01	1.503	-7.919	0.000	0.623	-4.727	0.000
0.078	93.07	-25.99	3.23	2.97	1.497	-7.801	0.000	0.586	-4.705	0.000
0.080	89.01	-23.55	3.07	2.91	1.478	-7.583	0.000	0.544	-4.662	0.000
0.082	85.77	-21.88	3.01	2.90	1.460	-7.435	0.000	0.585	-4.560	0.000
0.084	80.59	-21.10	2.99	2.97	1.450	-7.366	0.000	0.707	-4.473	0.000
0.086	79.76	-20.91	3.08	2.99	1.448	-7.349	0.000	0.777	-4.346	0.000
0.088	79.53	-20.94	3.19	2.99	1.448	-7.352	0.000	0.832	-4.218	0.000
0.090	75.89	-20.88	3.23	3.04	1.447	-7.346	0.000	0.900	-4.161	0.000
0.092	77.42	-20.43	3.17	2.99	1.441	-7.307	0.000	0.831	-4.199	0.001
0.094	78.50	-19.85	3.06	2.95	1.432	-7.255	0.000	0.768	-4.265	0.002
0.096	73.56	-19.40	2.90	3.01	1.425	-7.215	0.000	0.791	-4.389	0.002
0.098	74.67	-19.39	2.85	2.99	1.425	-7.215	0.000	0.735	-4.451	0.003
0.100	76.55	-19.60	2.84	2.95	1.428	-7.233	0.000	0.672	-4.496	0.003

Figure 44

A1_alpha	A1_beta	Kin	Dent				
24 dynes	12 dynes	150	49				
Dentary Rotation							
Time	A1α_T_0	A1α_T_0.03	A1α_T_0.035	A1α_T_0.05	A1α_T_0.06	A1α_Only	A1β_Only
0.00	0.00	0.00	0.00	0.00	0.00	0.00	0.00
0.00	2.04	-0.09	-0.09	-0.09	-0.09	2.10	-0.09

0.00	8.70	-0.28	-0.28	-0.28	-0.28	8.58	-0.28
0.01	21.75	-0.59	-0.59	-0.59	-0.59	20.37	-0.59
0.01	40.05	-1.04	-1.04	-1.04	-1.04	36.10	-1.04
0.01	55.44	-1.69	-1.69	-1.69	-1.69	49.56	-1.69
0.01	55.90	-2.61	-2.61	-2.61	-2.61	55.53	-2.61
0.01	51.87	-3.82	-3.82	-3.82	-3.82	53.70	-3.82
0.02	50.88	-5.26	-5.26	-5.26	-5.26	49.83	-5.26
0.02	52.63	-6.78	-6.78	-6.78	-6.78	47.75	-6.78
0.02	54.32	-8.26	-8.26	-8.26	-8.26	48.04	-8.26
0.02	55.32	-9.58	-9.58	-9.58	-9.58	48.84	-9.58
0.02	55.55	-10.67	-10.67	-10.67	-10.67	49.35	-10.67
0.03	54.44	-11.51	-11.51	-11.51	-11.51	49.64	-11.51
0.03	53.14	-12.01	-12.13	-12.13	-12.13	49.92	-12.13
0.03	52.87	-12.02	-12.56	-12.56	-12.56	50.20	-12.56
0.03	52.86	-11.69	-12.86	-12.88	-12.88	50.01	-12.88
0.03	53.36	-11.26	-12.96	-13.13	-13.13	49.72	-13.13
0.04	53.73	-10.87	-12.89	-13.35	-13.35	49.38	-13.35
0.04	53.97	-10.53	-12.84	-13.56	-13.56	49.19	-13.56
0.04	53.78	-10.21	-12.96	-13.76	-13.76	49.40	-13.76
0.04	53.49	-9.84	-13.34	-13.95	-13.95	49.65	-13.95
0.04	53.25	-9.35	-13.98	-14.12	-14.12	49.79	-14.12
0.05	53.22	-8.55	-14.91	-14.27	-14.27	49.99	-14.27
0.05	53.43	-6.99	-16.15	-14.39	-14.39	50.03	-14.39
0.05	53.60	-4.11	-17.73	-14.56	-14.50	49.87	-14.50
0.05	53.67	1.02	-19.75	-14.96	-14.58	49.71	-14.58
0.05	53.63	10.34	-22.41	-15.75	-14.66	49.66	-14.66
0.06	53.58	25.21	-25.52	-16.99	-14.74	49.60	-14.74
0.06	53.54	45.44	-20.74	-18.73	-14.84	49.44	-14.82
0.06	53.43	57.30	-16.55	-21.05	-15.08	49.47	-14.90
0.06	53.38	56.49	-13.54	-24.26	-15.64	49.62	-14.96
0.06	53.47	55.29	-12.59	-23.25	-16.64	49.72	-15.01
0.07	53.55	55.75	-13.83	-18.18	-18.14	49.75	-15.05
0.07	53.57	54.44	-15.55	-14.65	-20.21	49.81	-15.08
0.07	53.54	52.78	-15.38	-12.70	-23.07	49.91	-15.10
0.07	53.54	52.56	-13.64	-13.01	-25.07	49.86	-15.13
0.07	53.54	53.19	-11.79	-14.89	-19.44	49.76	-15.15
0.08	53.47	53.65	-11.44	-15.80	-14.88	49.70	-15.17
0.08	53.48	53.73	-12.03	-14.56	-12.94	49.65	-15.19
0.08	53.52	53.64	-12.68	-12.52	-12.92	49.59	-15.20
0.08	53.54	53.47	-12.41	-11.42	-14.33	49.58	-15.22
0.08	53.54	53.41	-11.72	-11.70	-15.76	49.62	-15.23
0.09	53.52	53.49	-11.19	-12.48	-15.63	49.68	-15.24

0.09	53.52	53.60	-11.22	-12.61	-14.02	49.72	-15.25
0.09	53.51	53.60	-11.65	-12.01	-12.21	49.77	-15.26
0.09	53.51	53.55	-11.88	-11.40	-11.08	49.76	-15.27
0.09	53.56	53.52	-11.73	-11.19	-10.95	49.71	-15.28
0.10	53.55	53.51	-11.18	-11.51	-11.59	49.65	-15.28
0.10	53.51	53.46	-10.77	-11.85	-12.29	49.66	-15.29
0.10	53.49	53.38	-10.64	-11.71	-12.55	49.74	-15.30

Figure 45

Kinethmoid Rotation				
Time	A1α_T_0.035	A1α_T_0.05	A1α_T_0.06	A1β_Only
0.00	150.00	150.00	150.00	150.00
0.00	150.07	150.07	150.07	150.07
0.00	150.93	150.93	150.93	150.93
0.01	151.75	151.75	151.75	151.75
0.01	152.18	152.18	152.18	152.18
0.01	152.09	152.09	152.09	152.09
0.01	151.29	151.29	151.29	151.29
0.01	148.91	148.91	148.91	148.91
0.02	145.47	145.47	145.47	145.47
0.02	143.49	143.49	143.49	143.49
0.02	141.07	141.07	141.07	141.07
0.02	138.93	138.93	138.93	138.93
0.02	137.04	137.04	137.04	137.04
0.03	135.51	135.51	135.51	135.51
0.03	134.34	134.34	134.34	134.34
0.03	133.46	133.46	133.46	133.46
0.03	132.97	132.78	132.78	132.78
0.03	133.94	132.18	132.18	132.18
0.04	136.16	131.61	131.61	131.61
0.04	137.73	131.05	131.05	131.05
0.04	137.92	130.51	130.51	130.51
0.04	136.97	130.00	130.00	130.00
0.04	134.89	129.54	129.54	129.54
0.05	131.71	129.16	129.15	129.15
0.05	127.68	129.45	128.81	128.81
0.05	122.70	130.74	128.54	128.54
0.05	116.60	130.96	128.30	128.30
0.05	108.54	128.87	128.09	128.09
0.06	94.74	125.11	127.88	127.86
0.06	80.94	119.72	128.22	127.63
0.06	68.95	112.69	129.30	127.42

0.06	73.79	102.61	128.94	127.25
0.06	61.76	84.95	126.14	127.12
0.07	56.85	74.50	121.59	127.01
0.07	62.49	70.40	115.23	126.93
0.07	56.81	69.20	106.45	126.86
0.07	61.48	56.06	89.92	126.79
0.07	55.13	61.58	77.77	126.73
0.08	53.55	57.26	73.32	126.67
0.08	53.99	60.38	66.09	126.62
0.08	52.52	58.28	60.49	126.57
0.08	54.61	52.97	59.80	126.53
0.08	51.46	54.84	59.62	126.49
0.09	53.97	51.33	58.59	126.46
0.09	48.95	55.45	58.86	126.43
0.09	52.39	51.58	57.07	126.41
0.09	49.74	53.93	54.87	126.38
0.09	52.67	50.42	52.40	126.36
0.10	50.36	50.84	52.42	126.33
0.10	51.17	51.13	51.82	126.31
0.10	49.78	51.74	52.05	126.29

Figure 46

A1_alpha	A1_beta	Kin	Dentary	Alpha_T						
24 dynes	12 dynes	150.000	49.000	0.035	Position (mm)					
					Dent			PMX		
Time	Kin Rot	Dent Rot	Gape	Protrusion	x	y	z	x	y	z
0.000	150.000	0.000	1.020	2.986	0.836	-5.590	0.000	0.672	-4.583	0.000
0.002	150.075	-0.086	1.034	2.981	0.840	-5.597	0.000	0.669	-4.577	0.000
0.004	150.927	-0.284	1.058	2.974	0.848	-5.612	0.000	0.665	-4.570	0.000
0.006	151.749	-0.586	1.087	2.970	0.862	-5.636	0.000	0.662	-4.567	0.000
0.008	152.182	-1.036	1.123	2.970	0.881	-5.671	0.000	0.661	-4.570	0.000

0.010	152.088	-1.689	1.169	2.977	0.909	-5.723	0.000	0.664	-4.579	0.000
0.012	151.288	-2.607	1.229	2.992	0.947	-5.796	0.000	0.671	-4.598	0.000
0.014	148.908	-3.818	1.304	3.017	0.995	-5.893	0.000	0.685	-4.626	0.000
0.016	145.472	-5.257	1.409	3.035	1.050	-6.009	0.000	0.695	-4.646	0.000
0.018	143.494	-6.782	1.522	3.053	1.104	-6.134	0.000	0.705	-4.666	0.000
0.020	141.067	-8.257	1.632	3.070	1.154	-6.257	0.000	0.714	-4.685	0.000
0.022	138.925	-9.578	1.731	3.084	1.196	-6.367	0.000	0.720	-4.703	0.000
0.024	137.044	-10.672	1.811	3.095	1.229	-6.460	0.000	0.723	-4.721	0.000
0.026	135.509	-11.515	1.870	3.102	1.253	-6.531	0.000	0.722	-4.738	0.000
0.028	134.337	-12.128	1.910	3.106	1.269	-6.584	0.000	0.717	-4.755	0.000
0.030	133.462	-12.564	1.935	3.108	1.281	-6.621	0.000	0.710	-4.772	0.000
0.032	132.975	-12.862	1.948	3.109	1.289	-6.646	0.000	0.701	-4.789	0.000
0.034	133.938	-12.963	1.950	3.101	1.291	-6.655	0.000	0.685	-4.802	0.000
0.036	136.157	-12.888	1.939	3.089	1.289	-6.649	0.000	0.664	-4.813	0.000
0.038	137.730	-12.837	1.928	3.081	1.288	-6.644	0.000	0.647	-4.826	0.000
0.040	137.921	-12.962	1.929	3.080	1.291	-6.65	0.000	0.637	-4.84	0.000

						5			0	
0.042	136.972	-13.336	1.952	3.082	1.301	-6.687	0.000	0.633	-4.852	0.000
0.044	134.888	-13.981	2.000	3.089	1.317	-6.743	0.000	0.634	-4.863	0.000
0.046	131.706	-14.911	2.072	3.099	1.339	-6.823	0.000	0.641	-4.872	0.000
0.048	127.675	-16.148	2.173	3.112	1.366	-6.930	0.000	0.652	-4.878	0.000
0.050	122.700	-17.730	2.304	3.128	1.397	-7.069	0.000	0.668	-4.883	0.000
0.052	116.598	-19.745	2.474	3.147	1.431	-7.246	0.000	0.689	-4.885	0.000
0.054	108.543	-22.413	2.706	3.171	1.466	-7.482	0.000	0.719	-4.881	0.000
0.056	94.741	-25.519	3.006	3.175	1.494	-7.759	0.000	0.744	-4.848	0.000
0.058	80.944	-20.740	2.801	3.174	1.445	-7.334	0.000	0.877	-4.590	0.000
0.060	68.947	-16.554	2.772	3.260	1.374	-6.966	0.000	1.117	-4.206	0.000
0.062	73.788	-13.537	2.372	3.076	1.306	-6.704	0.000	0.864	-4.374	0.000
0.064	61.756	-12.587	2.032	3.241	1.282	-6.623	0.000	0.937	-4.620	0.001
0.066	56.854	-13.828	2.262	3.347	1.313	-6.729	0.000	1.114	-4.476	0.001
0.068	62.494	-15.548	2.695	3.264	1.353	-6.878	0.000	1.125	-4.193	0.000
0.070	56.814	-15.384	2.526	3.302	1.349	-6.864	0.000	1.114	-4.349	-0.003
0.072	61.484	-13.642	2.242	3.201	1.30	-	0.00	0.94	-	-

					8	6.713	0	7	4.500	0.004
0.074	55.130	-11.794	1.972	3.291	1.260	-6.555	0.000	1.001	-4.601	-0.002
0.076	53.548	-11.435	2.121	3.318	1.250	-6.525	0.000	1.109	-4.408	-0.007
0.078	53.994	-12.028	2.384	3.306	1.267	-6.575	0.000	1.169	-4.193	-0.008
0.080	52.524	-12.683	2.432	3.285	1.284	-6.631	0.000	1.143	-4.204	0.031
0.082	54.612	-12.406	2.250	3.247	1.277	-6.607	0.000	1.047	-4.370	0.061
0.084	51.463	-11.718	2.005	3.288	1.258	-6.549	0.000	1.016	-4.559	0.073
0.086	53.971	-11.188	1.970	3.267	1.243	-6.504	0.000	0.997	-4.550	0.054
0.088	48.954	-11.224	2.039	3.358	1.244	-6.507	0.000	1.128	-4.472	0.070
0.090	52.392	-11.648	2.243	3.311	1.256	-6.543	0.000	1.138	-4.304	0.082
0.092	49.735	-11.877	2.342	3.331	1.263	-6.562	0.000	1.186	-4.221	0.039
0.094	52.669	-11.732	2.387	3.266	1.259	-6.550	0.000	1.134	-4.169	-0.109
0.096	50.361	-11.177	2.252	3.282	1.243	-6.503	0.000	1.122	-4.263	-0.199
0.098	51.171	-10.768	2.147	3.257	1.231	-6.468	0.000	1.069	-4.340	-0.230
0.100	49.775	-10.643	2.078	3.250	1.228	-6.457	0.000	1.040	-4.402	-0.237

Appendix E (See CD for Simulations Videos)

1. Matlab Double Pendulum Simulation Video in reference to Figure 50 (Angular displacement for links 1and 2 from Matlab and AdamsView).
2. This video specifically shows the kinethmoid's static equilibrium state at com (-1.09mm, -3.64mm) and an orientation of 120° in reference to Figure 26 (The effect of varying initial kin (θz) positions on its static equilibrium).
3. Figure 46 - Gape, protrusion, kinethmoid rotation and dentary rotation when A1α acts upon the maxilla at 0.035 seconds after A1β acts.
4. Figure 48 - Simulation showing the effect of a fictitious force F alone.
5. Figure 49 – Simulation showing the effect of a fictitious force F and maxillary forces.
6. Figure 50 – Simulation showing the effect of changing ligament 2 to a spring joint

Appendix F (Guidelines to using AdamsView for this model)

1) Importing CAD models from Solidworks into AdamsView

   i) Save Cad models as parasolid files

   ii) In AdamsView, click on File >> Import >> select Parasolid under File Type >> Choose your file >> select Part Name >> Name your part >> select or specify the Location, Orientation and Relative To coordinates >> click OK

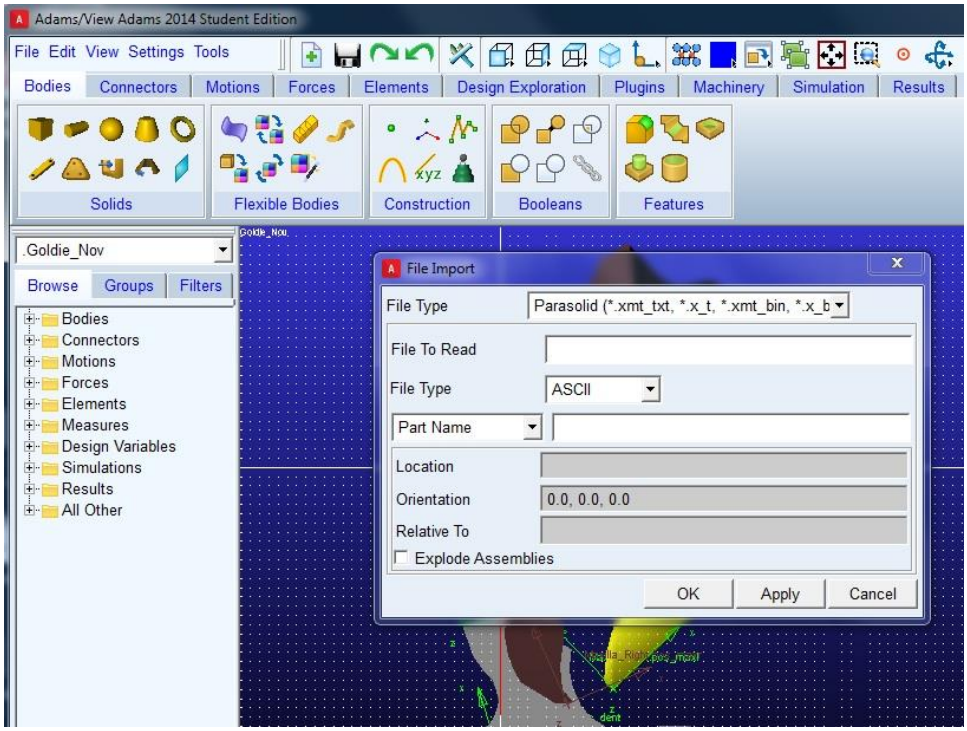

2) Settings in AdamsView

   i) For Coordinate System, I selected ‘Cartesian’. For Rotation Sequence, I selected 123 and Space Fixed. Space fixed means the coordinates are relative to the global x, y, z axes. 123 sequence means the part rotates about its x axis first, then y axis followed by z axis.

   ii) For Working Grid, specify the size of the field you wish to work on and the spacing.

iii) For Units, select millimeter for Length, gram for Mass, dyne for Force, second for Time, degree for Angle and rad/s for Frequency.

iv) For Gravity, select Gravity, and click on –Y and it will automatically specify the value in the appropriate units.

v) For Solver settings, select

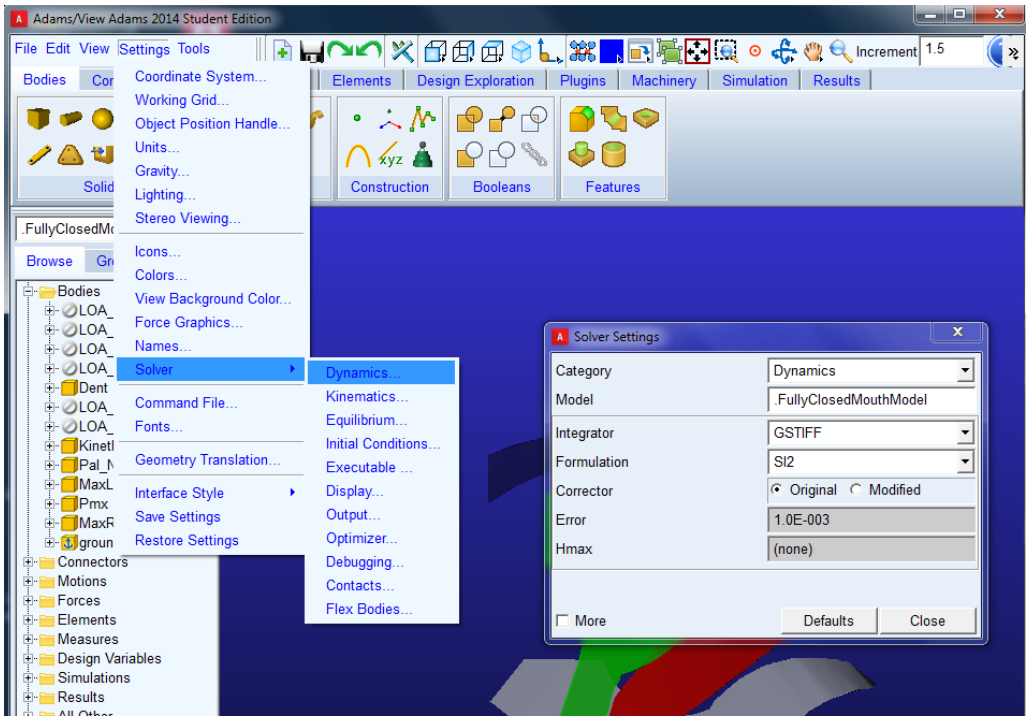

vi) The rest of the settings is for personal preference and will not affect your kinematic results.

3) Adding joints and springs to complete the 3D model

i) To add pin joints, go to Connectors >> Joints >> Create a Revolute Joint >> select the first body >> select the second body >> select the point of connection

ii) To add fixed joints, go to Connectors >> Joints >> Create a Fixed Joint >> select the first body >> select the second body >> select the point of connection

iii) To create springs, click on Forces. Under Flexible Connections, click on Create a Translational Spring Damper. Check K and C and add in the appropriate values. Next, click on the first point of attachment in the model followed by the second point of attachment.

4) Adding A1α and A1β maxillary forces

i) In order to add forces, we must first define lines of action, for which we use polylines. Under Bodies, go to Construction >> Construction Geometry: Polyline >> New Part >> One Line >> check Line and Angle >> Add appropriate values >> Pick a point of insertion on the maxilla for A1α first and repeat this procedure again for A1β. Do not forget to add forces on both sides of the mouth.

ii) Click on Forces. Under Applied Forces, click on Create a Force (Single component) Applied Force. For Run-time direction, pick Space Fixed. For Construction, pick Feature. For Characteristic, pick Constant, then select Force and enter a constant value. Repeat this for both forces on both sides of the mouth.

iii) Once the forces have been created, you can click on them under the tree and modify the force values accordingly. Below is an example to create step functions for A1α.

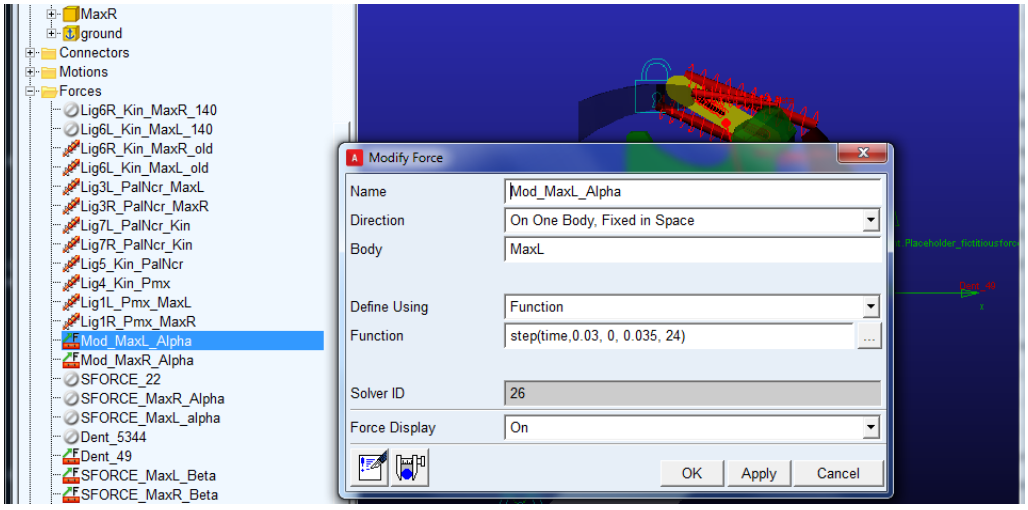

5) Creating Measures

    i) In order to measure angles of the kinethmoid and the dentary relative to the horizontal axis, we have to create angle measures. Go to Design Exploration >> Measures >> Create a New Angle Measure >> Pick the tip of the first vector >> Pick the vertex of the angle >> Pick the third tip. Do this for the kinethmoid and the dentary.

6) Running Simulations

    i) Go to Simulations >> Simulate >> Run an Interactive Simulation. Specify the End Time and Steps. Click on Play. After the simulation is completed, always click on Reset to Input Configuration ⏮.

7) Using Post Processor to collect and analyze results

    i) Once a simulation is completed running, click on Plotting in the bottom right corner of the Simulation Control box. This opens up Adams Post Processor. In the scroll box, select Plotting. Now you can pick the graphs from the Source. The source provides options such as Measures, Objects and Result Sets. Read the Manual for more help on this.

8) How to capture animations

    i) In the Post Processor's scroll box, pick Animation. Then right click on the viewport background and select Load Animation. Under Record tab, give it a File Name, Format and Frame Size. Uncheck compression to improve the quality of the images and set the interval to 10 frames per second. Click on Record button >> click on Play. Once you're done recording, click on Record button again. The video gets saved in the respective directory.